The spatial biodistribution and dosimetry of holmium loaded microspheres after intratumoral injection

A study on the utility of different imaging techniques in this new microbrachytherapy treatment

Nicole C. B. Reijniers

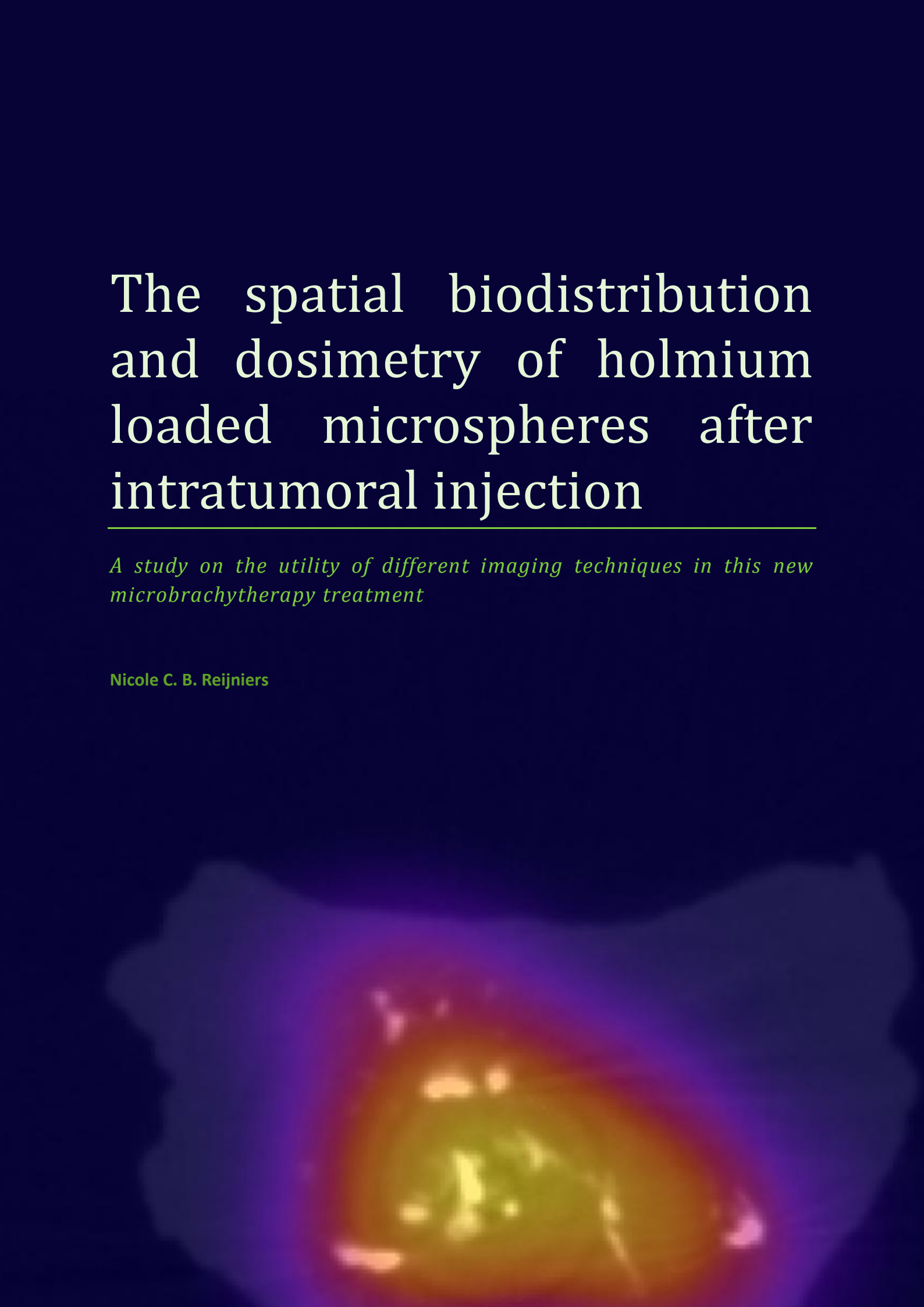

The spatial biodistribution and dosimetry of holmium loaded microspheres after intratumoral injection-

Honors Program Report

2013-2014

Nicole C.B. Reijniers

Department of Clinical Sciences of Companion Animals, Utrecht University

In collaboration with the department of Radiology and Nuclear Medicine, University Medical Centre Utrecht

Supervisors: Dr. Sebastiaan A. Van Nimwegen

Prof. Dr. J. Frank W. Nijsen

Prof. Dr. Jolle Kirpensteijn

Drs. Bo S. van Leeuwen

Table of contents

List of abbreviations

Ho= Holmium
^{165}Ho= the naturally occurring, non-radioactive form of holmium
^{166}Ho= the radioactive form of holmium, obtained after neutron bombardment of ^{165}Ho.
HoMS= Holmium microspheres
HoPLLA-MS= Holmium poly(L-lactic acid) microspheres
HoAcAc-MS= Holmium acetylacetonate microspheres
Y= yttrium
Re=rhenium
P= phosphor
E_{max}= maximum energy decay product
$T_{1/2}$= half-life of radionuclide
Bq= Becquerel
Gy=Gray
TIFP=tumor interstitial fluid pressure
EBRT= external beam radiation therapy
NZW= New Zealand White
SPECT=single-photon emission computed tomography
PET= Positron emission tomography
CT= computed tomography
µCT= micro computed tomography
HU= Houndsfield Unit
MRI= magnetic resonance imaging
TSE= turbo spin echo scan
GE= gradient echo scan
FFE= fast field echo/ gradient echo
UTE= ultrashort echo time scan
mFFE= multi-echo fast field echo, used for the determination of the R_2* value of a tissue
FOV= field of view
ROI= region of interest
VOI= volume of interest
s.c.= subcutaneous(ly)
i.v.=intravenous(ly)
i.m.=intramuscular(y)

Chapter 1. General introduction

More than 14 million adults were diagnosed with cancer in 2012 and over 8 million cancer-related deaths occurred in the same year.[1] The incidence of cancer in dogs is probably even higher than in human patients: 180 humans per 100.000 inhabitants a year were diagnosed in 2012,[1] compared to 270 dogs per 100.000 dogs a year during a study from 1985-2002.[2]

Many different kinds of malignancies exist and not all of them are easily treated. Sometimes excision is impossible due to location and tumor size and/or the presence of metastases makes tumor control very complex. Finding better treatment options have been a research goal for many years.[3] At the moment a focus to more local therapy strategies can be observed. Local treatments aim to reduce the adverse side effects of systemic cancer treatment, like systemic chemotherapy, and less precise or targeted local treatments such as external beam radiation and hormone therapy. Examples of targeted local cancer treatments are immunotherapy, HIFU, (micro)brachytherapy, radioembolization and chemoembolization.[4]

The focus of this thesis will be on radioactive particles, which can be used for microbrachytherapy as well as for radioembolization of solid tumors. A few β-emitting radio-isotopes are considered to be suitable for local radiotherapy, including ^{90}Y, ^{186}Re, ^{188}Re, ^{166}Ho, ^{32}P, ^{198}Au, ^{64}Cu and ^{177}Lu.

1.1 Overview of internal radiotherapy

Nuclear decay and ionizing radiation

Radionuclides are isotopes with an unfavorable amount of neutrons compared to protons in its nucleus. This results in an unstable situation and the radionuclide will decay to a lower and more stable energy state and emit high energy radiation. Depending on the type of decay of the nucleus, different types of radiation occur.[5]

α-decay will arise when the nucleus is too heavy and contains too much protons, in this cause the nucleus will emit 2 protons and 2 neutrons, the α-particle. α-particles are relatively heavy and positively charged. Therefore, α-radiation has a tissue penetration depth of only a few micrometers and for that reason they are seldom used in cancer treatment. Although tissue penetration is only shallow, it is considered to be the more radiotoxic than β and γ radiation due to its large energy deposition over relatively short distance in tissue, causing many ionizations over a short distance leading to damage that is difficult to repair. Furthermore, α-sources have a considerable recoil effect, due to the large mass of an α-particle, with the risk of spontaneous dispersion, increasing the risk of internal contamination. For these reason α-emitters are more dangerous compared to β- and γ-emitters and are seldom used.[5, 6]

β^--decay will occur when there are too many neutrons inside the nucleus, compared to protons. In this case a neutron changes into a proton, resulting in a nucleus with a proton

more and a neutron less, with the surplus negative charge being emitted from the nucleus as a β^--particle. β^--radiation is relatively light and is negatively charged. β^--radiation has a tissue penetration depth of a few millimeters. β^+-decay (positron-emission) will occur when the nucleus has a proton excess and a neutron shortage. In this case a β^+-particle can be emitted, or a nucleus can capture an electron from the nearest electron shell. Electron capture will cause characteristic X-ray. β^+-particles are positively charged and are relatively light. After transferring some of its energy to its surroundings, β^+-particles will combine with an electron. This process is called annihilation and will create two annihilation photons of 512 keV travelling in opposite direction. These annihilation photons are used by PET-scanners (positron emission tomography) to create an image.[5, 6]

γ-decay will occur when the nucleus contains too much energy. In this case a high energetic photon will arise from the nucleus. This photon has only a lot of energy and no mass and no charge. Because γ-radiation has no mass and no charge, it has a large penetration depth and will partly travel through the body. This principle is used in gamma-cameras and SPECT-scanners (Single-photon emission computed tomography), which detect the escaping photons to create an image.[5, 6]

All kinds of radiation have in common that they contain a specific amount of energy. This energy is transmitted to other molecules causing ionizations in these molecules. These ionizations cause the well-known dangerous effect of ionizing-radiation. The most important damage mechanisms of ionizing radiation is damage to the DNA and cell membranes. DNA damage is due to chromosome damage and breakage and point mutations; furthermore the DNA may become more 'sticky', resulting in unequally division of DNA over daughter cells. The effects on a cellular level include cell death, which can occur in different ways (pyknosis, kayolysis, protoplasmic coagulation, karyorrhexis and cytolysis), and changes in cell function like: delayed or inhibited mitotic cell cycle, disruptions in cell growth, changes in permeability and metabolic equilibrium and changes in motility. Actively proliferating cells are most prone to radiation damage because their DNA is more exposed. This causes differences in organ sensitivity to radiation. Bone marrow, lymphoid organs, ovaries, testes and small intestines are most prone to radiation damage. All the afore mentioned effects cause tissue damage and result in the death of the radiated cancer cells, this is the aimed effect of radiation therapy. Radiation-induced changes in cell function may also lead to neoplastic transformation.[6, 7]

Radio-isotopes for therapeutic purposes

^{90}Yttrium

^{90}Yttrium microspheres (β E_{max} = 2.28 MeV, t1/2 =64.1 h) are among other things used for the treatment of liver malignancies. Y-90 microspheres are commercially available as glass-microspheres and as resin-microspheres. Radioembolization using ^{90}Y microspheres has shown to have a good response rate and improved patient survival, however tissue shunting of microspheres to the lungs also occurred, resulting in a radiation pneumonitis. Due to the

large weight of ^{90}Y microspheres, they have a tendency to sag back into the blood flow, towards the intestines and stomach, with the risk of gastrointestinal side effects.[8] The effect of ^{90}Y microsphere radioembolization was elaborated by Vente et al. in a meta-analysis.[9] This literature study shows that patients with liver malignancies receiving ^{90}Y microspheres in addition to chemotherapy will have a higher response rate. Resin microspheres seemed more effective for hepatocellular carcinomas than glass microspheres. This may be due to the amount of microspheres administered per treatment, due to the amount of radioactivity which can be contained per microsphere, glass spheres 1250-2500 Bq, while resin microspheres can only obtain 50 Bq per sphere. ^{90}Y containing particles are also used for intratumoral injection.[10] The intratumoral injected glass-^{90}Y-microspheres caused a decrease in tumor volume and an increase in patient survival and patient wellbeing. Compared to intra-arterial injections, intratumoral injection also seems to have a better and more homogenously distributed tumor response. In order to visualize the ^{90}Y distribution after radioembolization, a γ-emitting tracer is often added to the injected solution, because ^{90}Y is difficult to visualize after injection due to the exclusive emission of β-particles, making ^{90}Y unsuitable for SPECT imaging, because Bremstrahlung SPECT is very inaccurate, and its invisibility on MRI and CT. Nowadays this imaging difficulty is reduced due to the ability for high resolution PET/CT. PET/CT is possible, due to a minor decay branch to the 0^+ first excited state of ^{90}zirconium followed by $\beta^-\beta^+$ internal pair production at a very low branching ratio of $31.86 \pm 0.47 \times 10^{-6}$. The detection of this positron emission is possible even though the background scatter in standard ^{176}Lu time-of-flight scanners is high, due to improved imaging protocols.[11-14] Predictive dosimetry for ^{90}Y resin microspheres is possible at the moment using integrated PET/CT.[15] Leaving two other disadvantage of ^{90}Y open: ^{90}Y has a tendency to accumulate in bone, which may be limiting factor for radioembolization of the liver, because the bone marrow is very radiosensitive[16]and the long neutron activation times, over 2 weeks.[17]

^{32}Phosphor

Like ^{90}Y, ^{32}phosphor is a pure β-emitter (E_{max}=1.711 MeV, T1/2=14.28 days). ^{32}Phosphor is used in glass-microsphere or chromic phosphate-colloid form. The former is used for intra-arterial interventional treatment. The latter is used for intratumoral interventional treatment for refractory solid tumors and allows a much higher dose rate locally.[18] In a patient study, both therapies showed an increased quality of life and complete response in 52% of the cases, partial response in 42% and no effect in under 7% of the cases. In general, radioactive count in blood was low, indicating almost no tissue leakage. However, in one patient ^{32}P colloid leaked during the injection procedure and this patient died of multiple organ failure the next day.[18] Direct intratumoral injection of ^{32}P in the center of the tumor, in a large amount of fluid is stated to increase tumor interstitial fluid pressure (TIFP). Increased TIFP would cause an artificial pressure gradient, which, as the drug spreads by convection from the core of the tumor to the tumor periphery, allows good tumor coverage. After a day, the TIFP would be reduced compared with the start situation.[19] ^{32}P colloid was shown to be effective in an animal model for pancreatic carcinomas in nude mice, with higher dose

groups showing better tumor inhibition rates, lower proliferation indexes and lower microvasculature density. However in the higher dose groups, some side effects, like coagulation disorders and weight loss were also revealed. Moreover, these high dose classes also show greater radioactivity concentrations in the liver, spleen and other organs, possibly leading to toxicity to these organs. Moreover in organs adjacent to the tumor, some dedifferentiation was seen, possibly as a consequence of irradiation of these organs. Another disadvantage is that ^{32}P, like ^{90}Y, shows bone marrow depression at high doses. The mentioned side effects advocate for an optimal dose, which was established at 444-558 Gy.[20] Other disadvantages of ^{32}P are its long half-life, more than 2 weeks and its poor imaging abilities due to its lack of γ-radiation, making it invisible on SPECT.

^{186}Rhenium and ^{188}Rhenium

Radioactive rhenium, as a therapeutic β-emitter, is available in two forms: ^{186}Re (β E_{max}= 1.07 MeV, t1/2=3.78 days, γ-emission E=137 keV) and ^{188}Re (β E_{max}= 2.12 MeV, t1/2=16.9h, γ-emission E=155 keV, 15%). The γ-emission of radioactive Re allows for SPECT imaging, an advantage compared to the afore mentioned ^{90}Y and ^{32}P. ^{188}Re has a higher β-energy and is therefore more favorable for antitumor-treatment of these two. Moreover ^{188}Re can be produced using a ^{188}W/^{188}Re generator system and is therefore cost effective.[21, 22]

Radioactive Re is used in different ways. ^{188}Re-sulfide suspension contains very small particles of rhenium-sulfide, diameter 1-10 µm. This suspension is injected directly into the tumor. These injections show tumor inhibiting rates ranging from 21% to 89%, depending on the injected dose, 3.7 MBq and 29.6 MBq respectively. [21] 90% of the injected suspension remains local for at least 3 days, with smaller particles having a higher tendency to leak to other organs.[21] Radioactive rhenium is also used as ^{186}Re and ^{188}Re encapsulated liposomes.[23, 24] Compared to ^{186}Re liposome intermediates, encapsulation strongly increases tumor retention. As a consequence, the tumor reaction in the liposome group was much better, showing controlled tumor growth, whereas in the three control groups, a strong increase in tumor size was seen.[23] The same Re-liposomes were used in order to calculate the effects of a non-uniform intratumoral dose distribution. These calculations show that a more homogeneous dose distribution, i.e. more injections, will increase the tumor control probability.[24] Other uses of ^{188}Re are linkage to antibodies against HER2/neu in a mouse model for nasopharyngeal carcinoma,[25] commercially available microspheres for tumoral injection,[22] and a ^{188}Re-ECD/lipiodol complex for intratumoral injection.[26] These last three methods all showed a decreased tumor growth after intratumoral injection in the treated group compared to the control group and the latter two uses also showed an increased survival time.

^{166}Holmium

^{166}Ho (E_{max}=1.86 MeV, t1/2=26.8 h, γ-emission= 80 keV 6.7%) has a few advantages compared to ^{90}Y and ^{32}P: besides β-radiation, it also emits a small fraction of γ-radiation, which makes it detectable on SPECT. Moreover, ^{166}Ho is highly paramagnetic and has a high

mass attenuation coefficient, making holmium visible on MRI and CT, respectively.[27, 28] These imaging possibilities allow for post treatment localization of the microspheres and dosimetry. Compared to ^{188}Re, it could be suggested that ^{166}Ho emits fewer γ-radiation and has therefore more therapeutic β-radiation at the tumor location and fewer γ-radiation reaching vital organs. However, the higher β E_{max} of ^{188}Re, compared to ^{166}Ho, gives ^{188}Re a slightly higher tissue penetration. ^{186}Re emits β-radiation with a lower maximal energy compared to holmium and therefore has a lower tissue penetration and is therefore less favorable compared to ^{166}Ho.

^{166}Ho may be used for intratumoral injection and radioembolization in different forms. ^{166}Ho as a free radionuclide has been injected intratumorally into a B16 melanoma model in C57BL/6 mice.[29] These injections increased both median survival time and survival rate. One effect of the injections was central necrosis at the injection sites. This necrosis remained local, because the ^{166}Ho remained around the injection site and complete tumor volume coverage was not achieved. This may lead to tumor re-growth or marginal failure and although the survival times were increased, almost all of the treated animals died of tumor recurrence. Furthermore, free ^{166}Ho was used in the same melanoma model in mice to enhance the effect of dentritic cell based immunotherapy. ^{166}Ho and immature dendritic cells, injected 7 days after ^{166}Ho injection, showed a synergic effect at the anti-tumor probability of both agents and showed an improved survival rate and less tumor size increment.[30] A side effect seen in both studies was skin ulceration.

Another available form of ^{166}Ho, ^{166}Ho chitosan complex, has been used in a prostate cancer model in rats. Tumors treated with ^{186}Ho chitosan showed a lower tumor mass with wide central necrosis in areas matching the ^{166}Ho deposition. Histopathological examination of adjacent organs, showed no adverse injury.[31] ^{166}Ho-chitosan complex has also been used in a phase IIb clinical trial of hepatocellular carcinomas. In this study, hepatocellular carcinomas were treated with ^{166}Ho-chitosan complex per percutaneous injection. Treated tumors showed complete tumor necrosis after two months in 42 out of 52 cases. However, some patients showed decreases in leukocyte and platelet counts, in addition to an allergic reaction to the chitosan component. Moreover, in about 50% of the cases, blood radioactivity count had a correlation to bone marrow suppression, indicating that some ^{166}Ho was released from the chitosan complex and accumulated in the bones.[32] This is in agreement with a previous research after the biodistribution and kinetics of ^{166}Ho chitosan complex after injection in the caudal vein in mice, showing some excretion of ^{166}Ho in the urine and feaces and some activity in the lungs, liver, bones and spleen.[33]

A more advanced method of therapeutic ^{166}Ho delivery is by means of polymeric microspheres in which ^{166}Ho is incorporated into polymers like poly-L-lactid acid (PLLA) and acetylacetonate (AcAc). Polymeric spheres, like PLLA, have a density which equals plasma, which is an advantage compared to carriers of ^{90}Y, resin and glass microspheres, which have a much higher density. Unlike glass and resin microspheres, polymers like PLLA degrade,

which can cause a tissue reaction. During the degration, simple PLLA microspheres <300µm in diameter undergo a homogeneous hydrolytic degeneration *in vivo*, with micropores allowing for the release of small degradation products. After release of these products the microspheres become more crystallized and become more stable.[17] The ^{166}HoPLLAMS however show a high stability and a high retention of more than 98% of ^{166}Ho in the microspheres after 8 days incubation in 37°C in several physiological media. This indicates that, although PLLA microspheres often show a hydrolytic degeneration and release of small particles, the Ho remain relatively fixed to the microspheres. This high stability of Ho-loaded microspheres is most probably due to carbonyl groups of PLLA interacting with the holmium ion in the HoAcAc complex, leading to an immobilized complex in the PLLA matrix. The final Ho-PLLA-microspheres have a diameter between 20-50 µm and a holmium content of 18.5%±0.6% (*w/w*).[17, 34, 53]

Holmium acetylacetonate microspheres (HoAcAcMS) have a holmiumcontent of 45% (*w/w*). Because the holmiumcontent of these microspheres is higher than that of HoPLLAMS (17% (*w/w*), the maximum radioactivity per sphere increases a 2.6 fold (29MBq/mg for HoPLLAMS, compared to 76 MBq/mg for HoAcAcMS). Furthermore, the increased holmium content increases the sensitivity for MRI and CT.[35] Like the HoPLLAMS, these microspheres were tested for *in vitro* and *in vivo* stability. During 6 months of in vitro measurements in a 2% pluronic phosphate buffer, less than 0.5% of the holmium was released, irrespective of radiation time. This is comparable to the holmium release from HoPLLAMS.[36, 37] After 6 months of incubation, the surface of the HoAcAcMS was still smooth, unlike the HoPLLAMS, which show a rough surface after 24 weeks of incubation due to hydrolysis of the poly(L-lactic acid).[36, 37] *In vivo* stability was tested through intratumoral administration of HoAcAcMS in hepatic Vx2 carcinoma-bearing rabbits. Blood, urine and faeces samples were taken and Ho-content was determined. In all samples, holmium content was below detection limits and histological examination of the liver showed intact microspheres. It was concluded that the microspheres retain their integrity for over one month *in vivo*.[36]

Holmium-166 radioembolization

Initially, HoPLLAMS particles were developed for the radioembolization of primary and secondary liver malignancies.[17, 38] During this treatment, the radioactive microspheres are injected into the hepatic artery, by means of intra-arterial catheterization under angiography-guidance. After intra-arterial injection, the microspheres get stuck into the smaller vessels, spreading their β-radiation within a range of 8 mm around the microsphere. Radioembolization of liver malignancies has the advantage that the blood supply to liver tumors and metastases is mainly covered by tributaries of hepatic arteries, causing most microspheres to get stuck around the tumors. This allows for targeted therapy, because the rest of the liver is mainly supplied by the portal vein and receives less blood from the hepatic artery. The maximal radiation dose to liver tumors is 30-35 Gy by external beam radiation (EBR), because higher doses will cause radiation hepatitis.[17, 39] Much higher local doses can be achieved without increased side effects using a more localized radiation method, like

radioembolization.[17] The maximum tolerated radiation dose of ^{166}Ho-radioembolization in human patients with liver malignancies was identified in the Holmium Embolization Particles for Arterial Radiotherapy (HEPAR) trial, as 60 Gy over the whole liver. However this dose is non-homogenously distributed through the liver, which implicates that the tumors receive a much higher dose than the surrounding liver tissue. Over different dose groups, tumor response was observed in 14/15 patients at 6 weeks after treatment and in 9/14 patients after 12 weeks. Side effects were lymphocytopenia, hypoalbuminemia, and increased plasma liver-enzyme concentrations in 12/15 patients. Moreover, hypersplenism was observed in 10/15 patients, something also seen after Y-90 radioembolization. Leucopenia and thrombocytopenia were found in 1 patient in the 80 Gy cohort, however this patient showed no signs of typical radiation induced pathological changes on autopsy. Biochemical and hematological side effects were most severe in patients with progressive liver disease and were therefore probably not due to radiation toxicity.[40]

Holmium-166 microbrachytherapy

Direct intratumoral injection of ^{166}Ho microspheres is a new treatment approach that is currently under investigation and is the main topic of this thesis. During this microbrachytherapy, the holmium microspheres are suspended in injection fluid and injected directly into the tumor through a hypodermic needle, delivering the microspheres with their treatment effect directly at the required location, the tumor interstitium, allowing very high local radiation doses. Efficacy of intratumoral injections of HoAcAcMS was tested in 24 Renca tumor bearing Balb/c mice, a renal carcinoma model. In 62 ±47 mm^3 measuring renal tumors, 2.7 MBq ± 1.2 MBq (270 ±120 µg of microspheres) were injected. The absorbed dose of the treated tumors was calculated to be 2200Gy. The control group consisted of 36 mice and showed a huge increase in tumor volume while the treatment group showed constant tumor volumes. 4 mice from the treatment group showed some radioactivity in the lungs, most probably due to the unintentional delivery of microspheres in a vessel during injection. As for the rest, no activity was found on µSPECT in other organs. Only a very small percentage, 0.12%±0.2%, of injected dose was found in the femora, using inductively coupled plasma mass spectrometry. Histopathological examination of the tumors showed a kidney completely engulfed with tumor in the control group, while the kidney in the treatment group contained only a small tumor, which remained the same size.[41] Moreover HoAcAcMS have been used to experimentally treat 3 cats with non-resectable liver tumors of different histotypes. Intratumoral ^{166}HoAcAcMS were administered percutaneously under ultrasound guidance. The treatment was well tolerated and all cats showed an extension of life and an increase in quality of life after treatment.[42] Moreover, the intratumoral injection of HoMS is investigated as an experimental treatment in veterinary patients with non-resectable tumors.[43]

1.2 Imaging techniques suitable for HoMS visualisation

In this thesis, different imaging techniques are described for HoMS visualization. The basic concepts of these techniques, the effect of holmium on these images en the (dis)advantages per technique are shortly explained in this section.

Single photon emission computed tomography (SPECT)

Single photon emission computed tomography uses γ-cameras, which rotate 180-360 degrees around the object, to take images at multiple positions. These images are reconstructed in a 3-dimensional distribution of the radionuclides in the object. SPECT requires physical collimation to line up the photons. This results in the loss of many available photons and therefore degrades the image.[44,45] In a SPECT scanner the γ-camera is often linked to a CT or an MRI scanner, in order to provide some anatomical reference for the radioactivity distribution.

^{166}Ho can be visualized by a scintigrapy/γ- camera, because ^{166}Ho also emits γ-photons (photopeak 81 keV). Quantification of ^{166}Ho using SPECT is difficult, because ^{166}Ho also emits some other photons (range 0.184–1.830 MeV) and the β-radiation induces bremsstrahlung (range 0–1.850 MeV).This problem was overcome by Elschot et al.,[46] who developed and validated a new reconstruction algorithm for quantitative ^{166}Ho SPECT. This reconstruction algorithm allows for a more exact quantitative evaluation of the SPECT images than before and allows for individual patient dosimetry.[46, 47] SPECT is the most sensitive for the detection of radioactive microspheres of the three mentioned imaging acquisition techniques described here, however the resolution of conventional SPECT images is low and it is not possible to image microsphere distribution of non-radioactive microspheres.[27]

X-ray Computed tomography (CT)

Computed tomography uses Rontgen radiation to create projections. Because different tissues have different X-ray densities, they have different tissue attenuation coefficients. This allows differentiation between tissues with different densities. Different projection intensities at different sites around the object are detected by a collimator in CT scanners. Combining these different projections results into 2-dimensional slices through the object. These data can be reconstructed by software programs into a 3-dimensional image of the object.[27, 48] The afore mentioned attenuation coefficient of a tissue is linked to a CT value in Houndsfield Units.[27] Tissues and holmium have their own Houndsfield Unit value. This allows for linkage between the holmium distribution, white areas, and anatomical reference points, allowing for the qualitative analysis of the HoMS distribution inside the tumor model. Moreover, CT does not require radioactive microspheres to be able to visualize them. However, CT is not very sensitive for the small HoMS and therefore only high concentrations can be properly visualized.[27]

Magnetic Resonance Imaging (MRI)

Magnetic resonance imaging uses the differences in paramagnetic properties of different molecules to visualize different tissue structures. MRI is based on the principle that atomic

nuclei in a strong magnetic field absorb pulses of radiofrequency energy and emit them as radiowaves, that can be detected by radiofrequency coils and reconstructed into computerized images.[49] Magnetic field imhomogeneities caused by the highly paramagnetic element holmium influence the signal formation.[27] In this way, MRI is able to detect HoMs and to show it in relation to the surrounding tissues and the tumor tissue, as dark areas. This enables the qualitative analysis of the distribution.[50] An advantage of MRI compared to SPECT is that it can visualize radioactive HoMS as well as non-radioactive HoMS, which makes evaluation of the HoMS distribution over a longer period of time possible. Compared to CT, MRI is more sensitive for holmium. Furthermore, considerable research on the quantification of HoMS using MRI has been conducted and has led to the development of a method to quantify the HoMS concentration per voxel, based on the R2* value of a voxel. Using dose kernels based on Monte Carlo simulations, the concentration maps can be converted into a dose map, allowing for MRI dosimetry.[27, 50-53] These advantages make MRI a very useful imaging acquisition technique for the HoMS visualization and dosimetry.

1.3 Introduction to the Vx2 tumor model

The Vx2 rabbit carcinoma cell line was created in 1936 by inoculation of Shope-papilloma virus extracts at scarified skin spots of rabbits.[54,55] At that time, carcinomas arose at 10 months, it was called the V1 cell line. In 1940 a continuation of the cell line, V2, resulted in 21% of the inoculated rabbits in a carcinoma, which lacked the morphological features of the original virus induced papilloma.[54,56] After the second world war, the V2 carcinoma was not able anymore to create an immune response against the papilloma virus.[57] Around 1950, this cell line got an anaplastic appearance and seemed to be able to induce tumors even in other species besides rabbits.[54,58] Slowly, different stocks of the cell line arose and the cell line was called Vx2. The Vx2 cell line is used to study carcinogenesis and to study new anti-cancer treatments.[54]

The Vx2 carcinoma model has already been used in combination with holmium microspheres before. The Vx2 auricle carcinoma has been used as a model for head and neck squamous cell carcinomas. In this model the feasibility of different treatment options, like immunotherapy and different particles for embolization as well as the combination of embolization and radiotherapy, using radioactive holmium microspheres, were elaborated.[54,59-63] Moreover, the distribution of holmium microspheres after embolization through intra-arterial injection was elaborated in Vx2 carcinomas in rabbit livers.[64, 65]

1.4 Embedding in the faculty research programs

The present research falls under the Advances in Veterinary Medicine (AVM) program of the department of Clinical Sciences of Companion Animals, Faculty of Veterinary Medicine, Utrecht University. The research is conducted in collaboration with the Department of Radiology and Nuclear Medicine of the University Medical Centre Utrecht, where the holmium microspheres were developed and are used for radioembolization of liver malignancies in humans. The ultimate goal of this ongoing research is to develop a

treatment method for non-resectable tumors by intratumoral injection of radioactive holmium microspheres in humans. In order to achieve this, more knowledge is required about the distribution of the microspheres after injection in solid tumors and the clinical effect in veterinary patients as a pre-clinical natural tumor modal for human patients.

Chapter 2. Holmium microsphere distribution and dosimetry after intratumoral injection: general methods and experimental design

2.1 Background and aims of the study

Cancer is a very common disease nowadays, with more than 14 million new cases diagnosed in adults in 2012 and over 8 million cancer related deaths the same year[1]. Not all tumors can be treated easily and, due to tumor location and size, excision is not always possible. Therefore, other local treatment modalities are investigated. External beam radiation therapy (EBRT) is a possible alternative but has several major disadvantages: the total local radiation dose is limited (typically 40-80 Gy), because the surrounding healthy tissues also receive a certain part of the inflicted radiation dose, causing radiation-induced side effects. To further reduce side effects, the radiation dose is typically divided in several smaller fractions given over time. As a consequence, the radiosensitivity of a specific tumor type greatly influences the therapeutic effect, which is poor in most cases of macroscopic tumor disease. To increase local radiation dose on the tumor and to avoid dose-limiting side effects in surrounding healthy tissues, several methods of local radiotherapy are developed.[66] One of these methods is holmium microbrachytherapy by direct intratumoral injection of holmium microspheres ($E_{\beta,max}$=1.84 MeV, $t_{1/2}$=26.8 hrs, maximal tissue penetration 8 mm). The advantage of holmium therapy, compared to EBRT, is the limited tissue penetration of the β-particles, maximal 8 mm. This allows for a much higher local radiation dose (typically 200 up to >1000 Gy), because radiation of the surrounding tissues is minimal. Another advantage of holmium therapy is that it does not necessarily require multiple treatment sessions, like EBRT. Moreover the half-life of holmium is around a day, meaning that within 4 days the activity levels in the patient are already less than 10% of the original administered activity and that after a week the activity level is only 1% of the original administered activity. This limits the hospitalization period compared to many other radionuclide therapies.

Holmium microbrachytherapy is currently investigated as an experimental treatment for non-resectable tumors in dogs and cats at the Department of Clinical Sciences of Companion Animals at the faculty of Veterinary Medicine of the Utrecht University. Here, veterinary patients with non-resectable solid tumors, accessible for needle injection, without metastases are treated by multiple free hand intratumoral needle-injections with radioactive holmium microspheres. The holmium therapy is sometimes used as a complementary therapy in addition to laser debulking, surgery and/or external beam radiation. At the moment, 35 veterinary patients have been treated with holmium microspheres (unpublished data). A subclass of veterinary patients treated with Ho-166 microspheres are patients with oral sqaumous cell carcinoma. In this subclass, 6 out of 12 patients showed complete remission with a median survival time of 380 days, compared to an overall median survival time of 252 days.[67] Among the veterinary patients, a large variation in treatment outcome was observed. These differences are suspected to be due to differences in microsphere distribution patterns in the tumor tissue. It is expected that the tumor response depends

greatly on the radioactive dose distribution, which depends on the spatial distribution of the holmium microspheres. A non-uniform HoMS distribution might cause local areas of tumor tissue to receive not enough radioactive dose and to survive HoMS treatment. However, at the moment, little is known about the distribution patterns of microspheres after intratumoral needle injection and it is not clear how the microspheres distribute after intratumoral injection and how this is linked to tumor response.

For this reason a study of HoMS distribution and dosimetry for intratumoral injection has been designed using a Vx2 rabbit carcinoma model. The previously described effectiveness of intratumoral HoMS injections in mice renal carcinomas may have been affected by the small tumor size and therefore the relative ease of complete tumor coverage with HoMS in that study.[41] In the present study, the Vx2 tumor model was chosen, because it is a larger tumor model and it can be induced in a location suitable for manual needle injection, comparable to the situation in veterinary patients. In this way the distribution of the holmium microspheres can be studied in a more clinically relevant tumor model. This tumor model has previously been used for the 2D histopathological examination of the HoMS distribution. However, histopathology of 2D slices appeared only limited suitable for the qualitative investigation of the spatial microsphere distribution and not suitable for quantitative dosimetry.[68] Another disadvantage of the investigation of the microsphere distribution based on histology is that it is not possible to use this technique for real-time distribution estimations during treatment. 9 Vx2 tumors were treated with holmium microspheres intratumorally and the microsphere and dose distribution of the microspheres was investigated using different 3D imaging techniques (**chapters 3 to 5**). In addition, distribution of holmium microspheres was also investigated in two feline lingual squamous cell carcinomas treated with holmium microbrachytherapy (**chapter 7**). This was all done in order to increase our understanding of the microsphere biodistribution after intratumoral injection. Increased knowledge of the *in vivo* biodistribution, combined with more data on the clinical effect in veterinary patients as a pre-clinical natural tumor model for human patients, has the ultimate goal of using the holmium microspheres for the treatment of non-resectable tumors in humans by intratumoral injection.

The research questions of the present study are:

- Is it possible to detect a general pattern in the microsphere distribution?
- How does the number of injection sites affect the distribution (volume) of the holmium microspheres?
- Do the holmium microspheres leak or shunt to other organs besides the tumor, after *in vivo* intratumoral injection?
- Which imaging technique is most appropriate for investigating the holmium distribution inside the tumor?
- Can CT-imaging be used to model dose distribution after intratumoral HoMS injection?

- Is image guided microsphere administration possible in order to improve the administration method and dose distribution over the tumor?
- Is it possible to image the HoMS distribution in veterinary patients?
- How do the HoMS distribute after intratumoral holmium treatment in clinically occurring tumors in (veterinary) patients?

Specific aims:

- To set up an in-vivo model for intratumoral HoMS treatment
- To evaluate MRI, CT, SPECT, and μCT as imaging possibilities for intratumoral holmium distribution investigation
- To develop a novel dosimetry model for intratumoral HoMS treatment based on (μ)CT imaging
- To evaluate MRI-guided intratumoral HoMS treatment and the possibilities of CT-guided administration
- To formulate a novel intratumoral HoMS treatment method in order to improve clinical outcome in veterinary and human patients

2.2 General methods

Animal tumor model

All experiments in this thesis were conducted in compliance with The Dutch Experiments on Animals Act "Wet op de dierproeven" (1977), and the European Convention for the Protection of Vertebrate Animals used for Experimental Purposes (1986). The experiments were approved by the ethical committee for animal experiments from the University Animal Experiments Committee (DEC-ABC no. 2011.III.08.080). The experiments were performed using 8 adult female, 3-6 kg weighing, specific pathogen free, New Zealand White out bred rabbits (CRL:KBL (NZW), Charles River, Someren, the Netherlands). Rabbits were housed in accordance with the guidelines of the Central Laboratory Animal Institute "Gemeenschappelijk Dier Laboratorium" (GDL, Utrecht, the Netherlands). Rabbits were fed with standard pelleted food for rabbits and hay, and acidified water ad libitum. After a acclimatization period of at least one week, the rabbits were injected subcutaneously with frozen Vx2 cell suspension, or vital tumor pieces from donor rabbits in both hind limbs after analgesia with 4 mg/kg carprofen s.c. (Carporal®). During the experiments, three different original Vx2 cell suspensions were used for the raise of a tumor donor line and the inoculation of the treatment rabbits over time. Rabbits were checked on a regular base and once to thrice a week the tumor growth was measured with a caliper. After 3-5 weeks the tumors had a sufficient size, 1-4 cm in diameter, for holmium treatment or for the transfer of vital tumor pieces to other rabbits. During microsphere injection and imaging, the rabbits were anesthetized using 0.125 mg/kg dexmedetomidine (Dexdormitor®), 15 mg/kg ketamine (Narketan®) and 0.1 mg/kg glycopyrulate (Ribonul®). After the experiments the rabbits were euthanized using an overdose pentobarbital.

Holmium microsphere preparation

During the experiments 2 types of microspheres were used HoPLLA and HoAcAc microspheres. HoPLLA-MS were prepared using a solvent evaporation process. Holmium acetylacetonate crystals were prepared as described by Nijsen et al[34], by adding holmiumchloride to a water and acetylacetone solution. The formed HoAcAc crystals and PLLA were added to continuously stirred chloroform. This chloroform solution was added to a polyvinylalcohol solution and continuously stirred at 800 rotations per minute, under a constant nitrogen flow (12 L/min) and kept at 25°C, until all the chloroform had evaporated. The residual PVA and HoAcAc were washed out, using water and 0,1M hydrochloric acid. The microspheres were sieved on a 10 µm sieve and dried at room temperature for 3 days and at 50 degrees for 2 days, resulting in microspheres with a holmium content of ±18.5% (*w/w*) and a size varying between 10-20µm. For tumors 4 to 7, non-radioactive HoPLLA-MS were used. For tumors 8 and 9, the microspheres were weighed and packed for neutron activation at the same research reactor facility. The microspheres were irradiated at a research reactor facility, (Department of Radiation, Radionuclides and Reactors, Delft University of Technology, Delft, The Netherlands), with a thermal neutron flux of $5x10^{12}$ n $cm^{-2}s^{-1}$, finally resulting in an activity of 10 MBq per 25 mg, at injection time for every tumor.

HoAcAc-MS were prepared according to the protocol described by Bult et al [35]. HoAcAc crystals were dissolved in chloroform and emulsified in an aqueous PVA solution, no PLLA was added to this solution. The chloroform/water emulsion was continuously stirred at 500 rpm, thermostated at 25°C and applied with a constant nitrogen flow (12 L/min). The formed microspheres were centrifuged and washed with water. Microspheres were sieved as described by Zielhuis et al.[69] and dried at room temperature for one day and dried at 50°C for 2 days. The resulting microspheres varied in diameter between 10-20 µm, and had a holmium content of ±45.0% (*w/w*). These microspheres were irradiated with thermal neutron flux of $5x10^{12}$ n $cm^{-2}s^{-1}$, for 49 minutes, resulting in a specific activity of 500 MBq per 98 mg.

Holmium microsphere injection

Prior to HoMS injection, the HoMS are suspended in 2% Pluronic® F-68 phosphate buffer. The amount of suspension fluid varied over time. The HoMS suspension is sucked into a syringe, using a hypodermic needle. The needle is again covered with the needle shaft and stored in a radio-safety box. At the time of injection, the syringe is covered with a Perspex shaft and the microspheres are suspended again by vigorous agitation of the syringe. The needle shaft is removed and the microspheres are injected at the indicated location. (**Figure 1**)

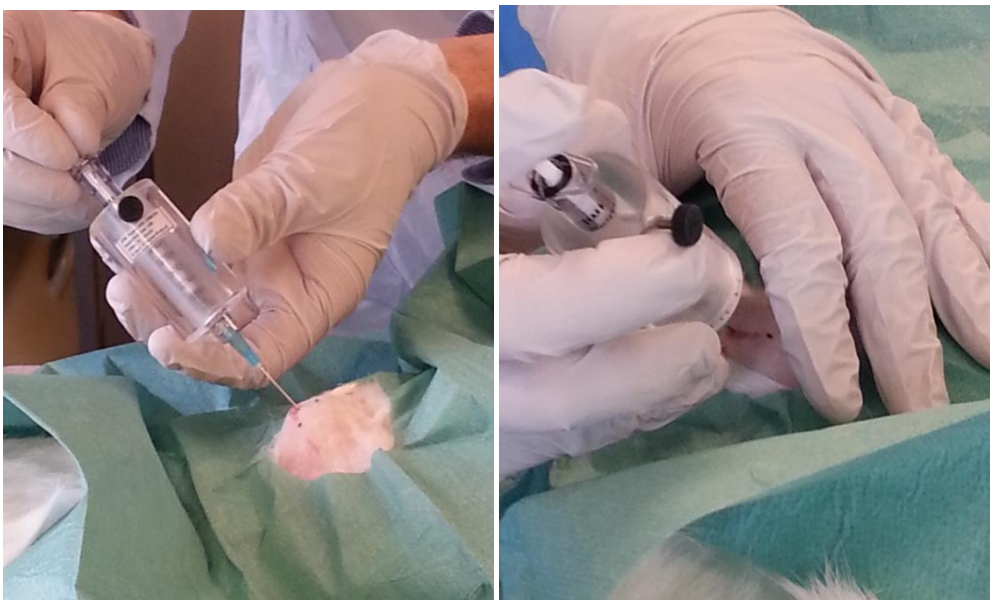

Figure 1: HoMS injection in a Vx2 rabbit carcinoma

2.3 Study design

The study of holmium microsphere spatial distribution and dosimetry was conducted over a time span of 2 years and was comprised of 3 sub studies. An overview of the specific data of HoMS injection and applied measurement techniques of each VX2 tumor in the study is given in **Table 1**.

The first sub study in 2012, was a feasibility and survival study of holmium microsphere distribution after manual intratumoral injection in 3 rabbits carrying a total of 4 tumors. Prior to intratumoral microsphere injection, imaging of the rabbits was performed by means of conventional MRI in order to estimate the tumor size and to calculate the required microsphere activity, to reach a 200 Gy overall tumor dose. 4 tumors were injected with microsphere suspension. One tumor was removed directly after injection, tumor 0. Tumors 1 to 3, were scanned by means of conventional MRI, directly after injection. One day after treatment, the rabbits were scanned by means of conventional SPECT/CT. 5 and 9 days after treatment the rabbits were again scanned by means of conventional MRI. After euthanasia of the rabbits, 9 days after treatment, the tumors were excised and investigated by means of histopathology.[68]

In the second sub study, performed in 2013, HoMS distribution experiments were combined with a pilot study of MR guided microsphere injections. *In vitro* and *in vivo* experiments were conducted for this purpose and varying injection protocols were developed, inter alia with an agarose mold and a Perspex device for holding the needles and tumor in the same position[70] (**chapter 6**). During these experiments 4 Vx2 tumors, tumors 4 to 7, were injected under MR guidance with non-radioactive microspheres. Therefore pre-, peri- and post-treatment MR images are available of these tumors. After treatment the tumors were excised and imaged by means of *ex vivo* MRI, CT and µCT.

The third sub study, performed in 2014, consisted of further data accrual for the investigation of the spatial microsphere and dose distribution directly after intratumoral microsphere injection in the same rabbit VX2 model. The number of injection sites were divided over three groups, the first group would receive one injection in the middle of the tumor, the second group would receive three injections in a line at 0,8cm distance from each other and the third group would receive five injections (**Figure 2**). During these experiments low-radioactive microspheres were used for the investigation of *in vivo* biodistribution, including SPECT analysis, and the detection of possible radioactive contamination of the working area with a NaI(Tl)-crystal contamination detector after the treatment procedure. The tumors, 8 and 9, were injected intratumorally and the rabbits were scanned by means of MRI immediate after injection. After *in vivo* MR imaging, the rabbits were euthanized and scanned by means of *in situ* whole body SPECT/CT. After the SPECT/CT scans, the tumors were excised and of the last rabbit, the one with tumor 9, the intern organs were also removed and measured on a twin crystal scintillation counter (**chapter 4**). The excised tumors were used for *ex vivo* MR, CT and µCT imaging.

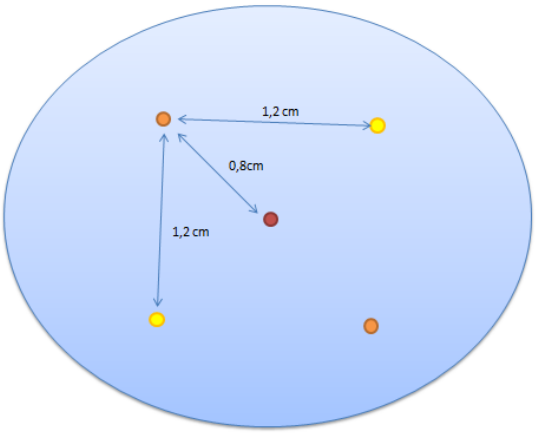

Figure 2: Location of the injection sites inside the tumor. The red location will be used in every group, the orange locations will be used in the group 3 and 5 injections and the yellow sites will only be used in the 5 injections group. Distance between the outer sites is 1.2 cm and 0.8 cm between the middle one and the outer ones.

Table 1: Overview of the different tumors, with their characteristics and treatment variables. (-) means not available data. Y/N of the organ shunting means that only SPECT has been performed

Tumor nr.	experiment	Nr injections	Tumor volume (mm^3)	HoAcAc/HoPLLA	Radioactive microspheres Y/N	Administered HoMS (mg)	Administered activity (MBq)	Administered dose (Gy)	Time euthanasia /excision after injection (h)
0	Holmium pilot	1	1666	HoAcAc	Y	5.4	27.7	264	2
1	Holmium pilot	1	1844	HoAcAc	Y	8.5	43.3	373	216
2	holmium pilot	3	565	HoAcAc	Y	2.3	11.7	329	216
3	Holmium pilot	6	3436	HoAcAc	Y	6.7	34.1	157	216
4	MRG pilot	1	9616	HoPLLA	N	-	-	-	2
5	MRG pilot	2	1555	HoPLLA	N	-	-	-	0
6	MRG pilot	3	2151	HoPLLA	N	-	-	-	0
7	MRG pilot	5	4500	HoPLLA	N	±25	-	-	0
8	Continued distribution study	1	336	HoPLLA	Y	low	low	-	2
9	Continued distribution study	3	9890	HoPLLA	Y	20.9	6.7	11	2

Tumor nr.	MR guided? Y/N	Organ shunting determination Y/N	*In vivo* MRI? Y/N	*In vivo* MRI dosimetry? Y/N	*In situ SPECT/CT? Y/N*	2D Histopathology? Y/N	*Ex vivo* MRI? Y/N	*Ex vivo* CT? Y/N	*Ex vivo* µCT imaging? Y/N
0	N	Y/N	Y	N	N	Y, Directly after injection	N	N	N
1	N	Y/N	Y	N	Y	Y, After 9 days	N	N	N
2	N	Y/N	Y	N	Y	Y, After 9 days	N	N	N
3	N	Y/N	Y	N	Y	Y, After 9 days	N	N	N
4	Y	N	Y	N	N	N	Y	Y	Y
5	Y	N	Y	N	N	N	Y	Y	Y
6	Y	N	Y	N	N	N	Y	Y	Y
7	Y	N	Y	Y	N	N	Y	Y	Y
8	N	Y/N	Y	N	Y	N	Y	Y	Y
9	N	Y	Y	Y	Y	N	Y	Y	Y

2.4 Outline of this thesis

In **chapter 3,** the MRI data of all tumors are analyzed. In this chapter, validated MRI based dosimetry[51] will be conducted on two tumors. Moreover, an estimation of the microsphere distribution volume in all tumors will be given based on surface determination of manually determined regions of interest (ROI). In **chapter 4**, data of CT imaging of intratumoral holmium distribution will be evaluated. Here a new, CT-based dosimetry method for holmium is developed, based on *in situ* and *ex vivo* CT images. In **chapter 5**, the results of

µCT imaging of intratumoral microsphere distribution are evaluated, a qualitative description of the distribution is given and, like for the CT images, a method for dosimetry calculations using µCT images is developed. In **chapter 6,** a novel image-guided administration procedure will be evaluated in a pilot setting, investigating MRI and CT as possible near-real-time treatment targeting and monitoring options. In **chapter 7,** the distribution of holmium microspheres in spontaneous occurring tumors in veterinary patients will be briefly discussed, evaluating HoMS distributions in two feline oral squamous cell carcinomas. This thesis will end with a comparison of the used imaging techniques and a general discussion (**chapter 8**), a summary in Dutch (**chapter 9**), acknowledgements (**chapter 10**), and a bibliography (**chapter 11**).

Chapter 3. Magnetic resonance imaging in the investigation after the holmium microsphere distribution and dosimetry after intratumoral injection on *in vivo* and *ex vivo* tumors.

Summary

Background Intratumoral injection of radioactive holmium microspheres is a promising new treatment option for solid tumors. However, little is known about the distribution patterns of holmium after intratumoral injection. Therefore a distribution study was conducted to elaborate these distribution patterns and to investigate the best injection method.

Methods This chapter will present the MRI data of intratumoral HoMS distribution after injection using different numbers of injection sites. Due to the highly paramagnetic properties of holmium, holmium microspheres can be easily detected on MRI. TSE and 3D UTE scans were made after intratumoral injection. Holmium distribution volumes were calculated using the manual enclosure of the visual microsphere distribution on the 3D UTE scans and were compared to the tumor volumes, in order to estimate the tumor coverage with microspheres. In order to investigate the reliability of this method, the intra-observer variability was calculated as the standard deviation of the mean distribution volume, after 6 manual enclosures of one tumor. Moreover, radiation dose maps were modeled using the difference in R2* values for selected tumors.

Results Mean tumor volume was 3.7±3.6 cm^3. MRI-based intratumoral HoMS distribution volume covered 24.0±20.1% of the total tumor volume. The intra-observer variability of the manual enclosure method was 6%. Intratumoral HoMS distribution volume varied largely for the different tumors, independent of the number of injection sites, tumor volume, microsphere type and scan type, in or *ex vivo*. The 100 Gy mean dose coverage was 37±9% of tumor volume.

Discussion The microsphere coverage data are available for 9 tumors. However, the manual enclosure method disregards differences in holmium concentration and therefore gives only a rough indication of distribution over the tumor. The most reliable method to describe HoMS distribution is to model a HoMS induced dose-map, which was only possible for 2 tumors. The low number of samples and minor differences in injection methods may have contributed to not finding a relation between the number of injection sites and the resulting HoMS distribution volume. On the other hand, considering the wide variation in HoMS distributions, the number of injection sites may not be a suitable predictor of HoMS distribution volume. This is probably due to differences in tumor tissue characteristics, varying per tumor.

Conclusion MR imaging is a useful method for the visualization of the HoMS distribution, because different scan settings have the possibility to change the focus of the scans to different structures, allowing for both HoMS visualization and high tissue contrast. More Vx2 tumors may be needed, all using the same injection method, same amount and type of

microspheres, and the same scan settings, to be able to link the holmium distribution volumes or the tumor coverage to the amount of injection sites. However, the amount of injections might only give a rough prediction of the intratumoral HoMS distribution and other methods, such as MRI-guided treatment, may be needed for reliable tumor dose-coverage evaluation in a clinical situation.

Keywords: Holmium, microspheres, magnetic resonance imaging, dosimetry, distribution, intratumoral injection, internal radiotherapy

Introduction

Intratumoral injections of radioisotopes are a promising new method for the treatment of non-resectable solid tumors. One of these isotopes is ^{166}Holmium. Holmium containing microspheres are already used for the radioembolization of liver tumors, which has recently been investigated in a phase I clinical trial.[40] Moreover holmium microspheres are currently used for intratumoral injections as an experimental treatment of non-resectable solid tumors in veterinary patients, with varying results.[67] Holmium has high paramagnetic properties, making MRI very suitable for the detection of holmium microspheres after injection, allowing the qualification and quantification of the holmium distribution.[50, 51, 53]

MRI-based qualification and quantification of HoPLLAMS distribution after radioembolization of the liver have been proven to be possible, using the change in MRI determined R2* values of liver tissue before and after liver embolization and to have a higher resolution compared to SPECT images.[51, 53, 64] The quantitative R2* based HoMS concentration map can then be converted into a three dimensional dose distribution map over the liver tissue, using a Monte Carlo simulation based dose point kernel for holmium.[51, 53] The afore mentioned qualification and quantification methods were all developed for liver radioembolization, but for the intratumoral injection of the same microspheres, these methods have not been described so far. It is however interesting to use these methods for the investigation of the HoMS and dose distribution after intratumoral injection, because it is unclear which parameters influence the intratumoral HoMS and dose distribution and these methods are already validated.

Therefore, tumors with intratumoral injected HoMS were analyzed using several MRI scan techniques in this study, to develop a scan protocol and to describe the distribution of the microspheres (semi-)quantitatively, using distribution volumes and dose-estimation volumes. Moreover, the difference between *in vivo* and *ex vivo* MR images was elaborated, to investigate the effect of formalin fixation on the tumor visibility and size and the spatial holmium distribution.

Material and Methods

The animals and injection procedures of this study are described in **chapter 2, Table 1**. Four Vx2 rabbit carcinomas were injected with radioactive HoAcAc microspheres (45% w/w), of which three tumors, tumors 1 to 3, were used for *in vivo* MRI imaging directly after injection,

four Vx2 rabbit carcinomas, tumors 4 to 7, were injected with non-radioactive HoPLLA microspheres (18.5% w/w) under MRI guidance and two tumors, tumors 8 and 9, were injected with low-radioactive HoPLLA microspheres (18.5% w/w) and were MR scanned immediately after injection. The number of injection sites and distribution characteristics per tumor are noted in **Table 3**. On the treatment day tumor sizes were measured using a caliper and the tumor volume was calculated using the volume formula of an ellipsoid, (π/6)*Length*Width*Depth.

In vivo MR imaging

All rabbits were scanned on a clinical 1.5T whole body MR scanner (Achieva; Philips Healthcare, Best, The Netherlands) after microsphere injection. For the *in vivo* imaging a Philips SENSE-Flex-M coil was used as a receiving coil and a B coil, as a transmitting coil. Over time the following scan parameters were used. For tumors 1 to 3, scan settings for the anatomical reference, T2_TSE, scans were: FOV 128x34x128 mm, matrix 160x112, slice thickness 2.0 mm, repetition time 2000.00 ms and echo time: 40.00 ms; for the holmium distribution determination, UTE_3D scans, the scan settings were: FOV 128x128x128 mm, matrix 160x160, slice thickness 0.8 mm, repetition time 6.6 ms and echo time 0.34 ms; and mFFE scans with 16 echoes were made of all three rabbits with settings: FOV 128x34x128 mm, matrix 160x160, slice thickness 2.0 mm, repetition time 963.5 ms and echo times starting at 2.53 ms, with the consequent adding of 2.3 ms till 37.0 ms. For tumors 4 to 6, T2_TSE scans were made with settings: FOV 128x128x39.5 mm, matrix 128x120, slice thickness 1.5 mm, repetition time 1573.7 ms and echo time 78.6 ms. The 3D_UTE_koosh_FFE scans had the following parameters: FOV 128x128x128 mm, matrix 128x128, slice thickness 1.0 mm, repetition time 4.4 ms and echo time 0.34 ms. Moreover needle tracking occurred on real time 2D_DUAL_UTE_8mm scans, settings: FOV 8x192x192 mm, matrix 128x128, slice thickness 8 mm, repetition time 3.5 ms ,echo time 0.83 ms. For tumors 7 to 9, scans with the following parameters were made: a 3D_UTE_mFFE, settings: FOV 128x128x128 mm, matrix128x128, slice thickness 1.0 mm, repetition time 19.3 ms and 5 echo times 0.41 ms, 2.04 ms, 3.66 ms, 5.29 ms, and 6.91 ms; a T2w_TSE _linear scan, settings: FOV 160x48x160 mm, matrix 160x154, slice thickness 2.0 mm, repetition time 2177 ms and echo time 90.6 ms; a T2w_TSE_lowhigh scan, settings: FOV 160x48x160 mm, matrix 160x154, slice thickness 2.0 mm, repetition time 2238 ms, echo time 8.1 ms; a T1_TSE_lowhigh, settings: FOV 160x48x160 mm, matrix 160x158, slice thickness 2.0 mm, repetition time 585 ms, echo time 8,1 ms; and a DWI scan, settings: FOV 128x48x128 mm, matrix 64x63, slice thickness 4.0 mm, repetition time 2438 ms, echo time 81.8 ms. The different scan types of the experiments of 2013-2014 will be compared with each other for usefulness. Moreover of tumor 7, a T2w_TSE scan, settings as described before, and a 3D_UTE_mFFE scan, settings: FOV 128x128x128 mm, matrix128x128, slice thickness 1.0 mm, repetition time 19.3 ms and 5 echo times 0.41 ms, 2.04 ms, 3.66 ms, 5.29 ms, and 6.91 ms; were made *pre*-injection, allowing for tumor volume determination without holmium disturbances and the determination of the basic R_2* value of the tumor, required for holmium quantification.

In vivo image processing

R2* tumor values were calculated as described previously.[64] The base R2* value of Vx2 tumors was determined on tumor 7, because of this tumor pre-treatment gradient echo MR scans were available. The post-treatment R2* value could be calculated, for tumors 7 and 9. The change in R2* values before and after treatment were transformed into holmium concentrations with the relationship [HoMS]=ΔR2*/r2* as previously described.[50, 53, 71] An estimation of high local holmium concentrations was made, using S0-fitting.[52, 72] The tumor areas were indicated as volume of interest (VOI). The local holmium concentrations were transformed into local radiation dose, considering a specific HoMS activity of 13.6 MBq/mg, using a Monte Carlo simulation based tissue dose point kernel for holmium.[53, 73] Cumulative dose volume histograms were made for the tumor areas, using MATLAB (MathWorks, Natick, MA, USA). Moreover iso-dose curves were drawn over the radiated areas, displaying the local radiation dose linked to the location in the tumor. (**Figure 7**)

Because DiCom files are required in the present available dose calibration model, dose calibration was only possible for tumors 7 and 9. Therefor all other tumors, as well as these two tumors, were alsof processed for visible HoMS distribution volume measurement. The tumor volume was estimated on T2w_TSE images. On these images the tumor area was visually indicated as ROI per slice and the volume of the tumor was calculated by multiplying the surface of every ROI with the slice thickness, as previously described,[74] using ImageJ® software. The holmium distribution volume on the first echo series of the 3D_UTE scans was estimated in the same way the tumor volume was calculated. On every slice, areas visibly containing holmium were enclosed by manually depicting the visible borders of Ho distribution and indicated as ROI (**Figure 3**). The area of the enclosed ROI was calculated and multiplied with the slice thickness, resulting in a volume optically containing holmium.

All the manual enclosing was done by one person on one day and intra-observer variability was investigated by enclosing the microsphere distribution of one tumor, tumor 9, six times. The variability is expressed as the standard deviation as a percentage of the mean total microsphere distribution volume.

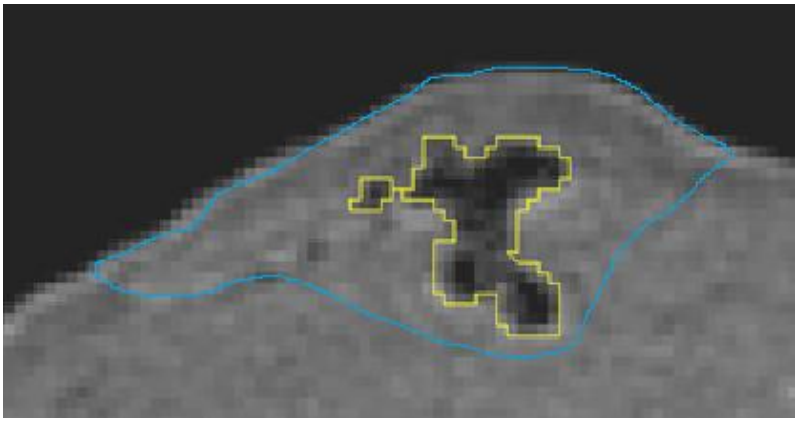

Figure 3: The manual enclosing of holmium microsphere clusters on the MR images in ImageJ® (yellow line), in order to obtain the visible distribution volume of the holmium microspheres using the 3D_UTE MRI scans. (Tumor area indicated by blue line)

Ex vivo MRI image acquisition

Prior to the *ex vivo* MRI scans, tumors were taken out of the formaldehyde solution and washed with water and put into a 3% manganese chloride solution. Small plastic boxes, containing the manganese chloride solution and the tumors, were placed in the SENSE-Head-8 receiving coil of a clinical 1.5T whole body MR scanner (Achieva, Philips Healthcare, Best, The Netherlands). Different scans of the *ex vivo* tumors were made: a UTE_koosh_mFFE, settings: FOV 128x128x128 mm, matrix160x160, slice thickness 1.0 mm, repetition time 19.3 ms and 5 echo times 0.23 ms; a T2 TSE_proflin, settings: FOV 160x160x100 mm, matrix 160x160, slice thickness 2.0 mm, repetition time 52.14 ms, echo time 91 ms; a T2 TSE_lowhigh, settings: FOV 160x160x100 mm, matrix 160x160, slice thickness 2.0 mm, repetition time 52.18 ms, echo 8.1 ms; a T1 TSE_lowhigh, settings: FOV 160x160x100 mm, matrix 160x160, slice thickness 2.0 mm, repetition time 6 ms, echo 8.1 ms; and a T1 FFE, settings: FOV 160x160x100 mm, matrix 160x160, slice thickness 2.0 mm, repetition time 11 ms, and echo time 6.1ms. The data were exported in DiCom format and in Rec/PAR format.

Ex vivo MR image analysis

The DiCom-files of the ex-vivo MRI scans were analyzed using ImageJ® software. The different scans were compared for usefulness. Based on holmium visibility and tissue contrast it was decided to use the T2w_TSE_proflinear images for the determination of the tumor volumes and the 3D_UTE images for the holmium distribution determination, the same settings as for the last *in vivo* scans. The parts of the scans containing tumor were cut out from the whole stack and saved as separate tiff-files for further analysis. The tumor volume and holmium distribution volumes were determined as described for the *in vivo* MR images, by enclosing the desired areas in the ROI and by multiplying the total summed surface of the ROI with the slice thickness.

Results

Figure 4 displays the effect of different scan settings and the effect of *in vivo* scans versus *ex vivo* scans on the visibility of the tumor and the holmium distribution, displayed here is tumor 9. The 3D_UTE scans (**4A and 4F**) show the clearest visibly distinguishable holmium distribution on the MR images and are also used for the holmium quantification in the *in vivo* scans, using the R2* values. For these reasons the 3D_UTE scans were chosen for the holmium distribution volume determination on *in vivo* and *ex vivo* MR images. On the *in vivo* T2W_TSE_proflinear images (**Figure 4B**), the tumor tissue is clearly distinguishable from the surrounding tissue, due to the high contrast between tumor and muscle tissue. On the T2W_TSE_proflowhigh images (**Figure 4C**) this contrast is less evident, because the muscle tissue is brighter. On the T1W_TSE_proflowhigh images (**Figure 4D**) this contrast is comparable to the contrast on the T2W_TSE_proflowhigh images. The tumor contours were less clear on the T1W images. **Figure 4E** shows an example of an *in vivo* DWI image. On this image the tumor is clearly visible, but the resolution of this scan is very low and it is difficult to distinguish the surrounding tissue. Because the contrast between tumor and surrounding tissue, in relation to the resolution, of the *in vivo* images was most optimal for the

T2W_TSE_proflinear images (**Figure 4B**), this scan setting was chosen for tumor size determination on the *in vivo* images. On the *ex vivo* T2W images (**Figure 4G and Figure 4H**) the muscle tissue is very dark, and the tumor is dark gray, not providing much contrast. On the *ex vivo* T1W images (**Figure 4I and Figure 4J**), the muscle tissue and the tumor are lighter, but also some white areas are present around the tumor, making the differentiation between tumor and surrounding very difficult. Moreover on the T1W_GE images the holmium causes a lot of field disturbances. Based on these subjective observations and to make *ex vivo* and *in vivo* data more comparable, the *ex vivo* T2W_TSE_proflinear images were chosen as the best scan setting for the distinction between normal and tumor tissue, and used for the *ex vivo* tumor size determinations. However, the ex vivo scans were in general less clear than the in vivo scans.

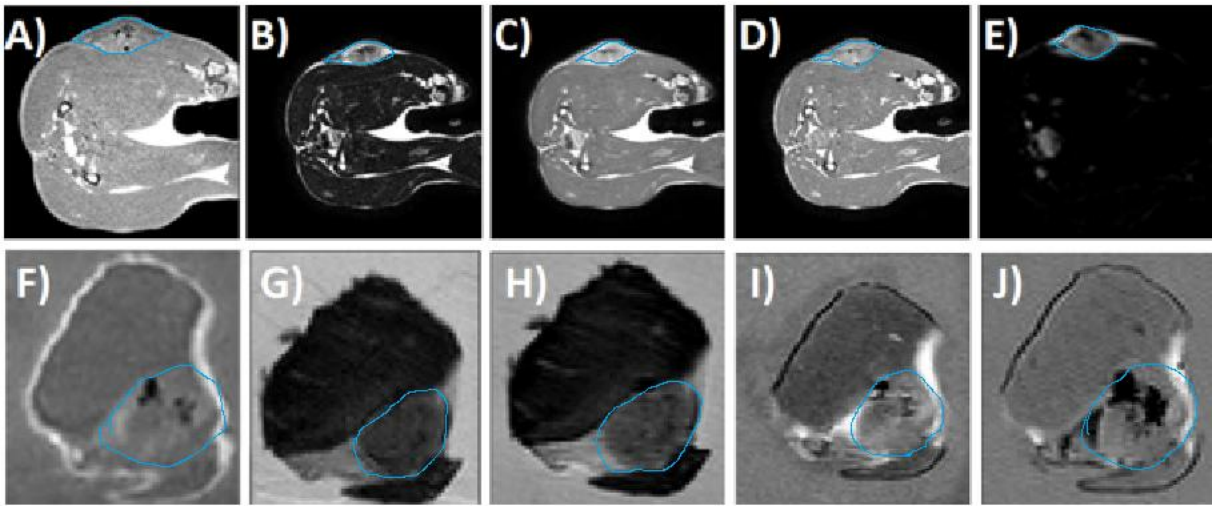

Figure 4: Different *in vivo* and *ex vivo* MRI scans of a tumor next to each other. *In vivo* A) 3D_UTE_koosh B) T2W_TSE_proflinear. C) T2W_TSE_proflowhigh. D) T1W_TSE_proflowhigh. E) DWI. *Ex vivo* F) 3D_UTE_koosh. G)T2W_TSE_proflinear. H)T2W_TSE_proflowhigh. I)T1W_TSE_proflowhigh. J)T1W_GE (Tumor area indicated by blue line)

The measured tumor volumes based on the *in vivo* MRI images varied between 0.3 cm^3 and 9.9 cm^3 for tumors 1 to 9 with a mean tumor volume of 4.7 cm^3 ± 4.2 cm^3. Tumor volumes measured and calculated using a caliper on the living animal and the volume formula of an ellipsoid, were in general smaller for the larger tumors, but larger for the smaller tumors, mean 3.2 cm^3 ±2.3 cm^3, and varying between 0.4 cm^3 and 6.3 cm^3, no significant difference could be found in a paired t-test, P=0.15. The tumor volumes measured on the *ex vivo* images were in general smaller compared to the *in vivo* images, mean tumor volume was 3.7 cm^3 ± 3.0 cm^3, varying between 0.8 cm^3 and 8.9 cm^3, but this difference was not significant in a paired t-test (P=0.23). (**Table 2**)

Table 2: Tumor volumes, calculated in different ways, using a caliper and the formula: (π/6)*LxDxH , based on the *in vivo* MRI scans and based on the *ex vivo* MR images

Tumor	Volume in mm^3 measured with a caliper	Volume in mm^3 measured on the *in vivo* MRI	Volume in mm^3 measured on the *ex vivo* MRI
4	3927	9616	5439
5	1676	1555	1395
6	-	2151	2334
7	3626	4500	3637
8	367	336	756
9	6283	9890	8907

The mean microsphere distribution volume of tumor 9, after 6 volume measurements, was 1293 ± 77 mm^3, range 1170 mm^3 to 1385 mm^3. The calculated intra-observer variability, given as standard deviation, was 5.9%. The available HoMS distribution data for *in* and *ex vivo* MRI for all tumors are summarized in **Table 3**. Neither a significant difference in distribution volume nor in tumor coverage could be found between the *in* and *ex vivo* data in a paired t-test, P=0.20 and P=0.28, respectively. Furthermore, no difference in distribution volume between the tumors treated with HoAcAc or HoPLLA could be observed on the *in vivo* MRI data (P=0.18), nor could a difference in tumor coverage be found between the two different microsphere types (P=0.78).

Table 3: Holmium distributions based on the MRI images. * of tumor 6, *in vivo* MRI is only available for one injection. See Table 1 for treatment overview. MRI dosimetry was only possible for tumors with DiCom files available, 7 and 9.

Tumor	Number of injection sites	HoAcAc/ HoPLLA	Tumor volume in mm^3 measured on the *in vivo* MRI	Volume holmium distribution mm^3 based on the *in vivo* MRI	Microsphere coverage of the tumor (based on *in vivo* MRI, ROI distribution) (%)	Estimated 100Gy dose coverage based on *in vivo* MRI dosimetry (%)	Tumor volume in mm^3 measured on the *ex vivo* MRI	Volume holmium distribution mm^3 based on the *ex vivo* MRI	Microsphere coverage of the tumor (based on *ex vivo* MRI, ROI distribution) (%)
1	1	HoAcAc	1844	659	35.7	-	-	-	-
2	3	HoAcAc	565	120	21.2	-	-	-	-
3	6	HoAcAc	3436	646	18.8	-	-	-	-
4	1	HoPLLA	9616	1207	12.6	-	5439	1082	19.9
5	2	HoPLLA	1555	850	54.7	-	1395	351	25.2
6	3	HoPLLA	2151	93*	0.4*	-	2334	437	18.7
7	5	HoPLLA	4500	2478	55.1	43	3637	1318	36.2
8	1	HoPLLA	336	21	6.3	-	756	27	3.6
9	3	HoPLLA	9890	1177	11.9	30	8907	1191	13.4

No trend between the total number of injection sites and the HoMS distribution volume could be observed, R^2=0.05, for linear regression, with n=8 tumors, because tumor 6 was excluded for examination, due to the lack of comparable scans after the total number of

injections (**Figure 5**). A large spread between the varying tumors is clear in this figure, this spread is independent of the number of injection sites. Moreover, the tumor volume was compared to the microsphere distribution volume and the HoMS tumor coverage (**Figure 6**). Both show no significant relation, with low R^2 values.

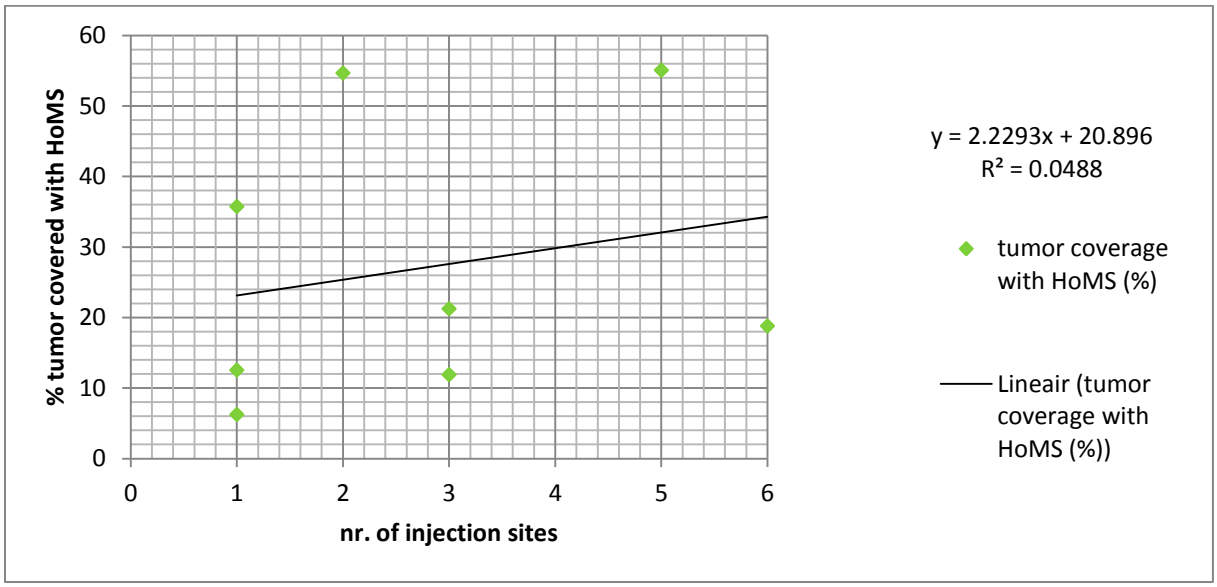

Figure 5: Regression line between the total number of injection sites and the % of the tumor covered with HoMS, as observed on MRI, calculated via the manual enclosure method

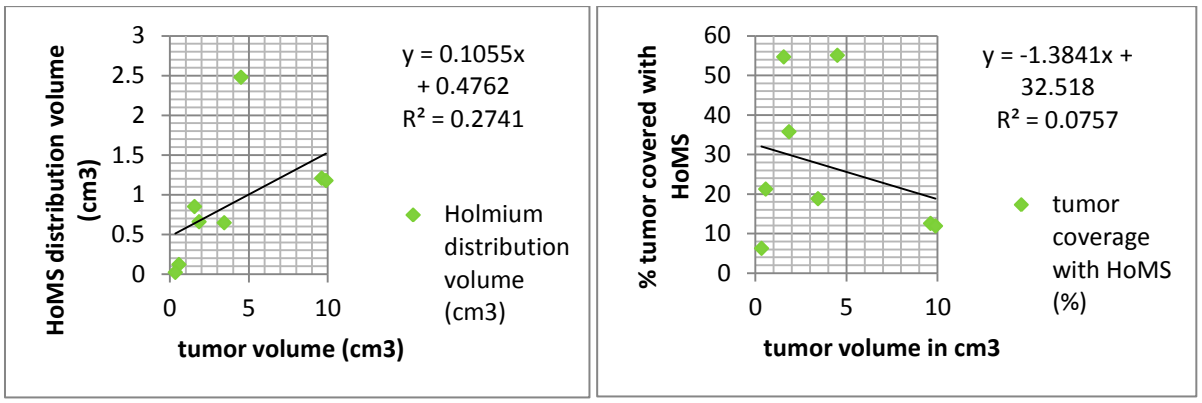

Figure 6: Regression lines between the tumor volume (cm^3), compared to the HoMS distribution volume and the tumor coverage in %, as observed on MRI, calculated via the manual enclosure method

Based on MRI dosimetry, isodose lines were modeled (**Figure 7**) and dose volume histograms were calculated (**Figure 8**). In tumor 7 (tumor in green on **Figure 7 and 8**), 26% of the tumor received a dose over 200Gy (**Figure** 7, orange line), 43% of the tumor was covered with a radiation dose exceeding 100Gy (**Figure 7**, blue line) and 57% was covered with a radiation dose over 50Gy. In tumor 9 (**Figure 7 and 8**, blue tumor), 18% of the tumor received a radiation dose exceeding 200Gy (**Figure** 7, orange line), 30% of the tumor received at least 100Gy (**Figure** 7, blue line) and 46% of the tumor received at least 50Gy.

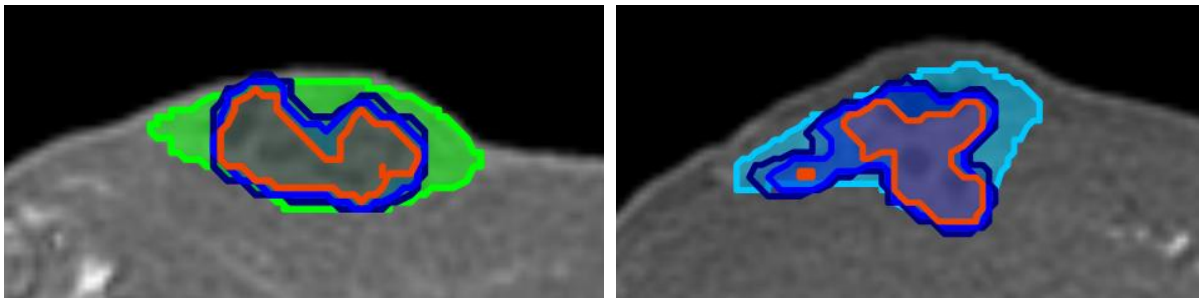

Figure 7: Isodose lines in the tumor. Tumor 7 is green, tumor 9 is light blue. The dark purple/blue line indicates a 60 Gy line, every area within this line receives at least 60 Gy, the blue line indicates the 100 Gy isodose line and the orange line indicates the outer borders of the 200 Gy area.

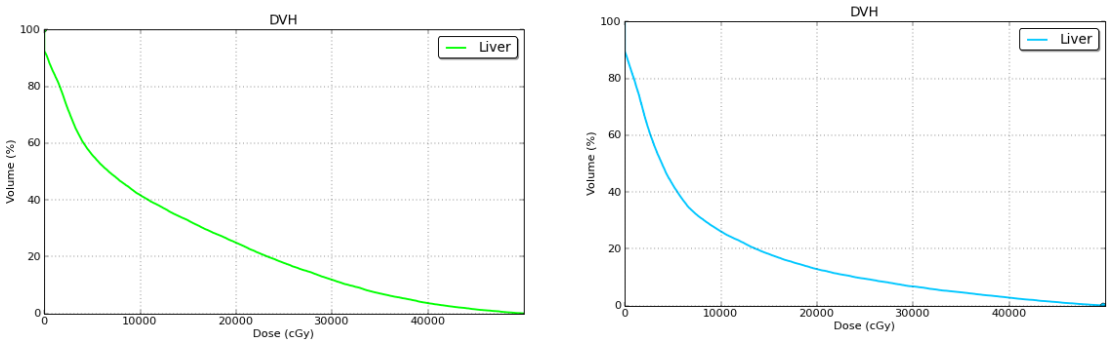

Figure 8: Dose volume histogram plot of tumor 7, green, and tumor 9, light blue.

Discussion

The variation between the measured volume in the *in vivo* MRI scans and the volumes calculated using a caliper may be explained by two factors. First, the used method is different, because the method using a caliper estimates the tumor volume, by assuming the shape of a tumor to be that of an ellipsoid.[74] Furthermore, estimations have to be made when measuring the tumor size with a caliper, although some research shows that the estimations of the tumor diameter with a caliper are comparable with the tumor diameters on echo images,[75] it can be difficult to give a proper indication of the tumor diameter, with the surrounding skin. Because of these estimations, tumor volumes can better be determined using the MR images, because these images are more precise and multiplication of slice thickness with tumor surface measurements per slice is therefore regarded as the golden standard in medical imaging.[74] Furthermore, the distribution volumes of microspheres and dose are determined on MRI or other 3D images and will be related to tumor size, advocating for volume estimation using comparable 3D imaging methods for uniformity of methods. The tumor volumes on the *ex vivo* MR images were in general smaller than on the *in vivo* images, with the same scan settings. Although this difference was not significant, a slight decrease can be expected expected, because it is generally known that formaldehyde fixation causes tissue shrinkage. This shrinkage is described for head and neck squamous cell carcinomas to be around 4-6% in every dimension[76] and the tumor margins are known to show an even higher shrinkage (47.3-22.7%).[77, 78] However, it should be taken into account that the tumor size is more difficult to determine on the *ex vivo* images and that in general some variation in tumor volume occurs when manually enclosing

the tumor area different times, due to intra- and inter-observer variability, as a consequence of the manual nature of the procedure.

Tumors 1 to 3 received HoAcAc microspheres, containing 2.5 times more holmium compared to the HoPLLA microspheres injected in tumors 4 to 9. The higher holmium content increases the visibility of single microspheres on MRI 2.9 times.[35] However the amount of HoAcAc microspheres injected in tumors 1 to 3 was about 3 times lower compared to the amount of HoPLLA microspheres injected in tumors 4 to 9. The combination of more holmium per microsphere and less microspheres per injection may explain the comparable distribution visibility between tumors 1 to 3 and 4 to 9. Furthermore, no difference regarding the microsphere distribution could be observed between the *in* and *ex vivo* MR images. Compared to *in vivo* MRI, *ex vivo* MRI has the disadvantage of displaying some air bubbles around the tumor surface sometimes, which can falsely be indicated as holmium, the *ex vivo* MR images are slightly less clear, due to the reduced tissue contrast. No difference between the distribution after varying numbers of injection sites could be found and are most probably due to the large variation observed in the tumor coverage, independent of the number of injection sites. It was hypothesized, that an increase in tumor volume will allow the microspheres to distribute over a larger distance towards the tumor borders, this relation was however not significant. Differences in intratumoral HoMS distribution are most probably due to difference in intratumoral structure varying for every tumor.

Different scan settings influence the MR signal.[27] Over time slightly different scan settings were used, therefore for the comparison between the different tumors, scans with the most comparable settings were chosen. For future experiments the same scan settings should be used, in order to make the data optimally comparable. Scan settings of the latest scans were most useful and should be used for future experiments: for anatomical scans: T2w_TSE_linear (FOV 160x48x160 mm, matrix 160x154, slice thickness 2.0 mm, repetition time 2177 ms and echo time 90.6 ms) and for the holmium qualification and quantification: 3D_UTE_koosh (FOV 128x128x128 mm, matrix 128x128, slice thickness 1.0 mm, repetition time 19.3 ms and 5 echo times 0.41 ms, 2.04 ms, 3.66 ms, 5.29 ms, and 6.91 ms), for both *in vivo* and *ex vivo* scans. The enclosing method has some disadvantages, compared to the validated R2* based MRI dosimetry. First, the other method is already validated.[53] Second, solely the HoMS distribution will not predict the treatment response, because the treatment response is dependent on the dose distribution, which is dependent on the microsphere distribution and the local HoMS concentration. For dosimetry purposes, the enclosure method is not suitable, because it disregards the holmium concentration, does not take a radiation range into account and it just considers the visible margins of the HoMS distribution for a specific contrast/brightness situation. This makes this method unfavorable for the comparison of the HoMS distribution for varying tumors, because it is not able to predict the treatment response. Moreover, the observed microsphere distribution is dependent of the scan settings, while the validated MRI dosimetry method uses the difference in R2* value of the tumor, a parameter independent of the exact scan settings,

but requiring multiple echo times. Furthermore, the enclosing method allows for intra- (and inter-) observer variability, making this method more prone to variation than the computerized R* based dosimetry. However, the intra-observer variability is tolerable with a standard deviation of 6%. Because of these disadvantages, the modeled dose distribution is the most appropriate parameter for the evaluation and comparison of the intratumoral HoMS distribution in different tumors. It may also be interesting to investigate the difference between the microsphere distribution volume and the tumor coverage in relation to the tumor size, because it is expected that the tumor influences both values. A large tumor may show a large HoMS distribution volume, because the HoMS are able to expand over a large distance, but may have a poor tumor coverage, because of the relatively larger volume that has to be covered with the same amount of microspheres. A relation between these factors could not yet be found.

In conclusion, no predicting variables for the microsphere distribution were found, this supports the idea that the HoMS distribution is highly unpredictable. This advocates for the microsphere distribution investigation after every injection, in order to be able to adapt subsequent injections to the observed HoMS distribution. For this purpose, MR imaging is a suitable option, because HoMS can be clearly visualized inside tissue using MRI. During HoMS treatment, tumor size estimations can best be made, using *in vivo* T2w_TSE scans MRI, because these scans provide most tissue contrast. For adequate microsphere distribution evaluation and comparison, pre- and post-treatment gradient echo scans are required, because these are suitable for the validated MRI based dosimetry. The resulting dose distribution maps, can be used to detect areas receiving too little dose and can be used for the selective retreatment of these areas. The possibility of MRI to guide needle placement to these areas is further evaluated in **Chapter 6**.

Chapter 4. The utility of combined computed tomography (CT) and single-photon emission computed tomography (SPECT) to elaborate the holmium microsphere distribution, dose distribution and organ shunting after intratumoral injection

Summary

Background ^{166}HoPLLA microspheres ($E_{\beta,max}$= 1.84 MeV, $t_{1/2}$= 26.8 hrs, maximum tissue penetration 8 mm) were previously used for local radiation treatment by arterial embolization of solid malignancies (i.e. radioembolization). A new use of these microspheres is the intratumoral injection into solid tumors. This study aims to investigate the suitability of combined SPECT/CT for the evaluation of the holmium microsphere distribution after intratumoral injections. Moreover, a CT-based dose distribution model is developed.

Methods In total, 9 Vx2 carcinomas in 8 New Zealand White rabbits, were injected with holmium microspheres. After holmium injection, these tumors were scanned by means of *in situ* SPECT/CT and/or *ex vivo* conventional CT. Post treatment SPECT images were made of 5 animals. The SPECT images were used to evaluate migration of ^{166}HoPLLA microspheres away from the target tissue and to visualize the distribution inside the tumor. Activity measurements on a twin scintillation counter were used as a gold standard for the shunting detection, in one tumor. In the CT images, the local holmium content was quantified using a CT calibration curve of ^{166}HoPLLA microsphere concentration gradient in agar. Finally, a three dimensional spatial radioactive holmium dose map was modeled by calculating the local dose per voxel using a ^{166}Ho tissue dose point kernel and a hypothetical specific activity of the ^{166}HoPLLA microspheres.

Results SPECT imaging displayed no microsphere migration to other sites of the body, but was not able to detect very small amounts of activity distant from the tumor. 5 kBq, 0.5% of the total amount injected in tumor 9, was found in the lungs using a twin scintillation counter. Moreover, SPECT imaging resolution was too low for the precise localization of microspheres inside the tumor. The used method for CT quantification rendered a concentration distribution image and allowed for the detection of voxels with a minimum holmium concentration of 8.6 mg/ml for the *in situ* scans and 31 mg/ml for the *ex vivo* scans. Total HoMS volumes detected using this method varied between 0 and 0.6 cm^3, with minimal variation between the *in situ* and *ex vivo* images of the same tumor. CT based dosimetry showed a 100 Gy tumor coverage between 0% and 116%, for a specific activity of 13.6 MBq/mg HoPLLAMS.

Conclusion This study describes a method for ^{166}HoPLLA microsphere dosimetry based on CT data. Conventional CT data are applicable for holmium microsphere distribution estimation and for dose distribution estimations. CT based tumor dose coverage varied per tumor. SPECT is useful for the rough qualitative localization of holmium and to rule out larger, clinically significant, amounts of shunting or aberrant holmium deposition but appeared not

suitable for high resolution imaging after intratumoral injection and the detection of small amounts of activity deposition elsewhere. The CT-based dosimetry model may provide a solution for intratumoral HoMS therapy monitoring and enhancement in the near future.

Keywords: Holmium microspheres, Computed Tomography, Single Photon Emission Computed Tomography, intratumoral injection, spatial distribution, dosimetry

Introduction

Microspheres containing the radioactive isotope ^{166}Ho ($E_{\beta,max}$=1.84 MeV, $t_{1/2}$=26.8 hrs, maximal tissue penetration 8 mm) are used to treat liver malignancies by radioembolization of hepatic artery branches.[40] ^{166}HoPLLA microspheres are also experimentally used for the treatment of non-excisable solid tumors in veterinary patients at the University Clinic for Companion Animals with varying results.[67] However, little is known about the interstitial distribution of holmium microspheres after direct intratumoral injection.

The distribution of holmium microspheres after radioembolization of liver malignancies has been investigated previously using SPECT and MRI.[46, 51, 53, 79] This has resulted in standard scan protocols for holmium radioembolization treatment, enabling HoMS distribution imaging and MRI-based dosimetry. Although CT imaging is rapid, relatively affordable and has been proven to be able to visualize holmium microspheres,[27] CT imaging possibilities for HoMS distribution and dosimetry have received little attention.

For these reasons, the use of conventional SPECT/CT was investigated for ^{166}HoPLLA microsphere distribution imaging possibilities in tissue. The biodistribution of ^{166}HoPLLA microspheres after intratumoral injection in Vx2 tumors (**chapter 2**) was investigated by means of *in situ* combined SPECT/CT and/or *ex vivo* CT imaging. The intended use of SPECT scans was to give an estimation of the biodistribution of the holmium microspheres inside/near the tumor and over the whole body. As a golden standard for the *in vivo* biodistribution over other organs, postmortem organ radioactivity was measured using a twin scintillation counter. CT imaging was investigated to obtain a more detailed description of the spatial distribution of the holmium microspheres and to model the accompanying dose distribution throughout the tumor. An estimation of the dose coverage per tumor will be determined.

Material and Methods

Tumor model

For this research, tumors 1 to 9 were used **(chapter 2**). *In vivo* MRI based, tumor volume varied from 0.3 cm^3 to 9.9 cm^3. The number of injection sites ranged from 1 to 6. The injected amount of holmium microspheres was aimed at 25 mg per tumor.

In situ scans

Tumors 1 to 3 were scanned one day after HoAcAc injection in the anesthetized rabbit, on a conventional SPECT/CT (Symbia T16 SPECT/CT Imaging Systems, Siemens Medical Solutions

USA, Hoffman Estates, USA), with SPECT settings, 1 sample per pixel, 240 frames, matrix 128x128, voxel size 4.80x4.80x1.0 mm and energy windows A: 74.9-87.1 keV and B: 110.9-125.1 keV; and CT settings 110 kVp, 15 mAs, slice thickness 1.5 mm, and voxel size 0.43x0.43x0.7 mm. A B31s convolution kernel was used for the CT data, a standard soft tissue convolution kernel.

After euthanasia, prior to tumor excision, the two rabbits with tumor 8 and 9 were scanned on the same Symbia T16 SPECT/CT system as described before. During the SPECT/CT imaging, rabbits were laid in a stretched prone position, in order to increase the lung field. First a static FLOOD image of the thorax was made in order to detect possible lung shunting. Areas containing activity on the FLOOD images, would be examined by means of SPECT/CT. SPECT scan settings were 1 sample per pixel, 240 frames, matrix 128x128, voxel size 4.8x4.8x1.0 mm and energy windows A:74.9-87.1 keV and B: 110.9-125.1 keV. CT scan settings were 110 kVp, 15 mAs, slice thickness 0.75 mm and voxel size 0.78x0.78x0.7 mm for the *in vivo* scans. A B31s reconstruction convolution kernel was used for the *in vivo* CT data. Images were exported as DiCom files.

Organ activity measurements

2 hours after microsphere injection in tumor 9, the rabbit was euthanized and 3.5 hours after euthanasia, the internal organs were removed and placed into 1L buckets. The bucket contained the liver, intestines, lungs and heart, and kidneys and spleen, respectively. After refrigerated storage overnight, the radioactivity levels in the organs and the tumor were measured using a twin crystal scintillation counter (TOBOR, Nuclear Chicago, United States of America). The obtained values in counts per second were corrected for the real decays per second. This was done using the factor expressing the difference between a calibrated dose calibrator (Veenstra Instruments, Joure, The Netherlands) and the TOBOR. (**Figure 9**)

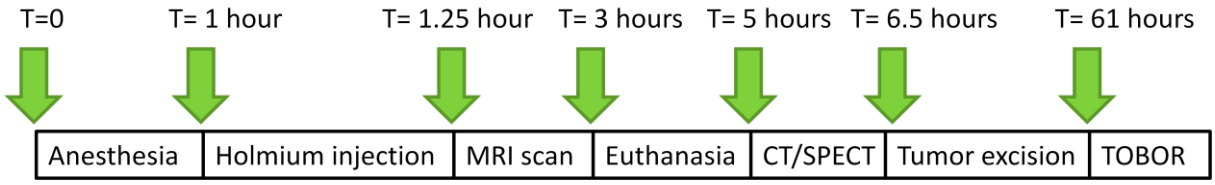

Figure 9: Flow schema of tumor 9, with relative treatment times and measurement times

Ex vivo scans

After euthanasia of the rabbit, the tumors were excised. After excision, radioactivity in tumor 9 was measured on a dose calibrator)and the tumors were stored in 4% buffered formaldehyde. Tumors 4 to 9 were stitched to plastic plates with orientation possibilities. After the placement of orientation markers, post-injection *ex vivo* scans were made of tumor 4 to 9. No *ex vivo* scans were made of tumors 1 to 3, due to initial survival of the animals and preparation for histopathology of these tumors after euthanasia. For the *ex vivo* CT scans, the tumors, attached to the plastic plates, were removed from the formalin, washed with water once and put into a large plastic box together. The box with the tumors was scanned on the same clinical Symbia T16 SPECT/CT scanner, on which the *in vivo*/*in situ* scans were

made. *Ex vivo* CT scan settings were 130 kVp, 25 mAs, slice thickness 3.0 mm and voxel size 0.74x0.74x1.5 mm for tumors 4 to 6 and 130 kVp, 25 mAs, slice thickness 1.5 mm, voxel size 0.74x0.74x0.7 mm for tumors 7 to 9. A B70s and a B31s convolution kernel were used for both datasets, for the final distribution evaluation the B70s kernel was used, because this kernel was sharper than the B31s kernel.

Local holmium microsphere concentration estimations for CT images

A CT holmium microsphere concentration calibration curve was set up using CT images of a 2% agarose gel containing increasing holmium microsphere concentrations. This calibration curve was used to determine the local holmium concentration in each voxel in the CT images of the tumors. For the calibration series, the same holmium HoPLLA microspheres were used as for the intratumoral injections (diameter 10-20 µm). The calibration setup contained five 25 ml falcon tubes with holmium microsphere concentrations of 0 mg/ml, 2.25 mg/ml, 4.64 mg/ml, 9.22 mg/ml and 18.59 mg/ml agarose gel. These tubes were scanned in the same clinical CT scanner as in which the in- and *ex vivo* tumor scans were made, with settings: 130 kVp, 25 mAs, slice thickness 1.5 mm and reconstruction convolution kernels B70s and B31 were used afterwards. All scan data were exported as DiCom files.

Average HU values per slice were taken thrice per tube and a calibration curve was made using Microsoft Excel®, resulting in the formula: $y = 5.9436x + 11.597$, $R^2 = 0{,}9766$, with 5.9 indicating the slope of the calibration curve in HU per mg HoPLLAMS per ml agarose gel; y HU (units); x mg/ml HoMS (units). The baseline *ex vivo* Vx2 tumor HU value was determined by scanning four Vx2 tumors without holmium, at the same scan settings used for the *ex vivo* tumors and the agar concentration line. The mean gray value of these tumors was 36.0±10.3 HU, which was considered to be the mean baseline HU tumor value without holmium and was used as the zero-intercept for the holmium concentration calibration curve. The final formula used to calculate the holmium concentration locally on the *ex vivo* images was: HU=5.9*[HoMS]+36.0, → [HoMS]=(HU-36.0)/5.9, with HU being the Houndsfield Unit value of a voxel and [HoMS] being the HoPLLA microsphere concentration of a voxel in mg/ml.

The baseline *in situ* tissue gray value was based on the measurements of normal muscle tissue of a rabbit, because no *in situ* or *in vivo* CT of Vx2 tumors without HoMS was available, and determined as 64.04±6.8 HU. For the *in situ* images, the following calibration function was used: [HoMS]=(HU-64.04)/5.9, with HU being the Houndsfield Unit value of a voxel and [HoMS] being the HoPLLA microsphere concentration of a voxel in mg/ml. For tumors 1 to 3, the same calibration function was used, but for these tumors it does not express the concentration microspheres, but it approaches the local holmium concentration, as if they would contain HoPLLAMS instead of HoAcAcMS.

Method of CT image analysis

The DiCom images of the tumors were analyzed, using the free software program ImageJ®. Image parts containing one tumor were excised from the image stack and saved as tiff-files. Radio-dense areas in the images that did not contain holmium, such as a near-by femoral

cortex, were erased from the images in the stack to reduce the chance of false positive areas. In the tiff-files, the lower threshold was set at 115 HU for the *in situ* CT scans, of tumors 1 to 3 and 8 and 9, a value on which visually almost all normal tissue had disappeared and only areas with a minimum holmium concentration remained visible, (115-64)/5.9=8.6 mg/ml. The resulting thresholded image contained values which were either 0, for original HU values lower than 115, or 255, for original HU values higher than 115 HU. The acquired stack was divided by 255 in order to acquire a stack containing only 0-1 values, a characteristic function. The characteristic function was multiplied with the original excised stack, using the Plug-in Calculator Plus of ImageJ®, in order to a obtain a stack containing the original grey values above threshold and no values below threshold. In order to express the varying concentrations per voxel in mg/ml, the gained images were corrected with the afore mentioned calibration function [HoMS]=(HU-64.04)/5.9, so first 64.04 was subtracted from the whole stack, secondly the whole stack was divided by 5.9 and finally the formed background was removed by again multiplying with the characteristic function. This resulted in a stack in which the gray values indicate the local holmium microsphere concentration in mg/ml. The concentrations in mg/ml were multiplied with the voxel volume, resulting in a gray value indicating the local holmium microsphere content in mg/voxel. The holmium content per voxel was multiplied with a hypothetical activity of $13.6*10^{6}$ Bq/mg holmium microspheres, the specific activity required to generate a standardized dose of 500 Gy by injection of 25 mg microspheres in a tumor treatment volume (1.5x the tumor volume) of 10.8 cm^3 (the average expected treatment volume of a VX2 tumor in the experiment, based on 2 tumors, 7 and 9, expected to have received ±25 mg HoPLLAMS), if the microsphere distribution is homogeneous. The result of this multiplication was a 3D distribution of the activity in Bq per voxel. Over these gray values a convolution with a holmium tissue dose kernel was calculated, using the Convolve 3D® plug-in of ImageJ®. This dose kernel was developed by using the holmium tissue dose kernel designed by van Elschot et al.[46] for SPECT dose calculation and transposing it for the used CT voxel-sizes. The result of this convolution was multiplied with the factor $1.60217733*10^{-19}/(7.176*10^{-6} * 1.06*$voxel volume in liter). The result of this multiplication is the dose per voxel in Gy/voxel. The acquired stack gives an estimation of the dose distribution throughout the tumor. In order to compare dose distribution volumes between tumors, a theoretical lethal dose threshold was set at 100 Gy. This results in areas covered by at least 100 Gy. The sum of all voxels above 100 Gy dose threshold (using the plug-in Voxel Counter of ImageJ®), results then in a dose-covered volume. (**Figure 10**)

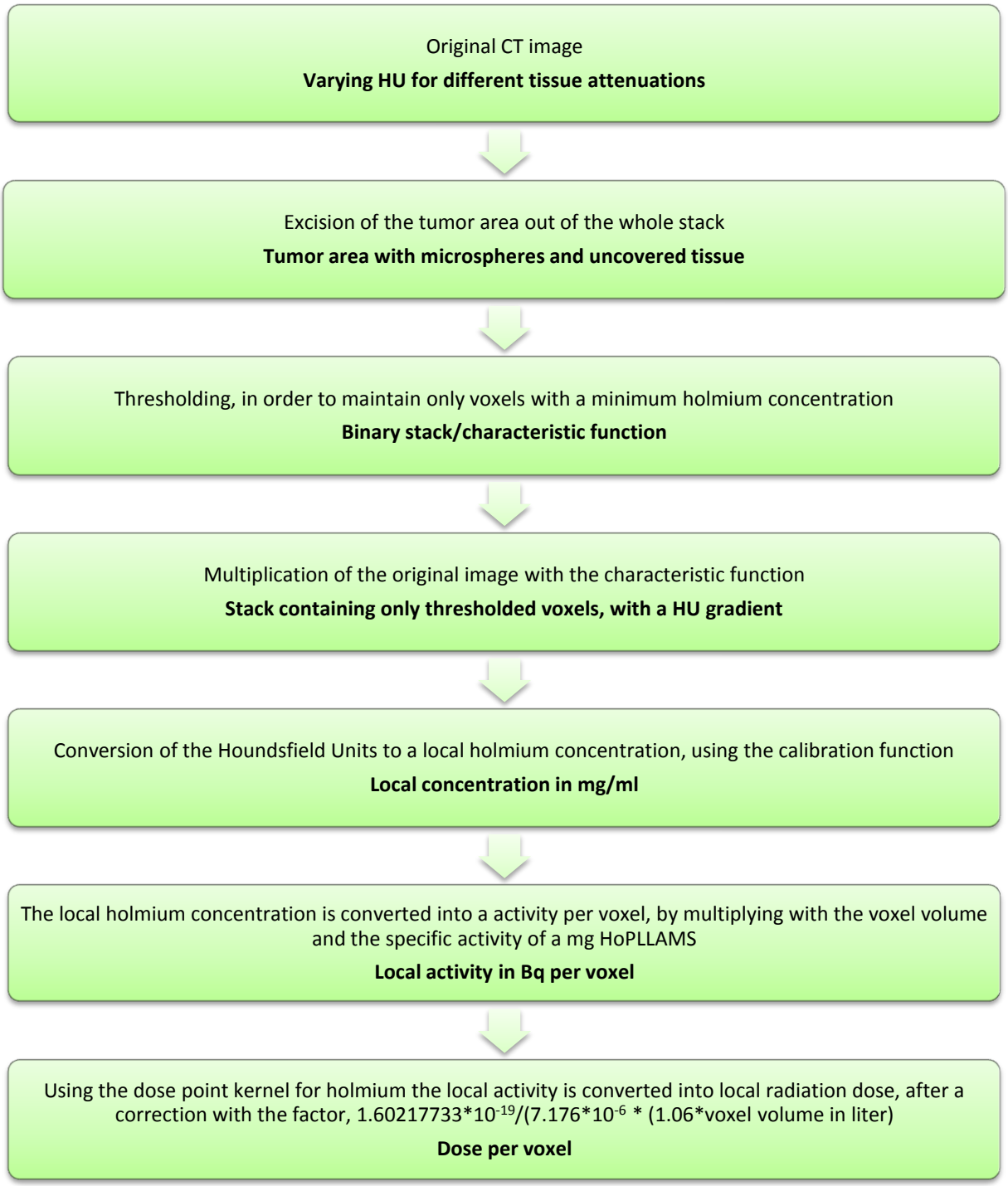

Figure 10: Flowchart indicating the sequence of steps taken to derive a CT based 3D holmium dose distribution

For the *in situ* scans a comparable method is used. The tumor area was excised from the whole stack. The threshold was set at 220 HU and background signal of the surrounding plastics were erased. This threshold allowed visualization of local HoMS concentrations above (220-36)/5.9=31 mg/ml. The thresholded image stack was converted into a binary stack and used as a characteristic function. On the remaining voxels, the calibration function [HoMS]=(HU-36.0)/5.9 was applied and the concentration was multiplied with the voxel volume and the specific activity of the microspheres to acquire the local activity per voxel in Bq. The dose point kernel was adapted for the voxel size of the *in situ* scans and a

convolution of the activity with the dose point kernel was calculated and after correction with the factor $1.60217733*10^{-19}/(7.176*10^{-6} * 1.06*$voxel volume in liter), the resulting values indicated the local dose per voxel. This resulted in a 3D dose distribution throughout the tumor area. The dose was thresholded at the same theoretical lethal dose of 100 Gy in order to compare the dose distribution inside the tumors. (**Figure 10**).

Results

2 hours after administration, no shunted activity could be detected on the static FLOOD images of the rabbits with tumor 8 and 9. However, some activity was found in the sample containing the lungs and heart of the rabbit with tumor 9, using the TOBOR. This was less than 0.5% of the activity found in the tumor. Activity measured in the other organs was negligible compared to the amount of activity in the tumor, less than 0.006%. (**Table 4**)

Table 4: activity measured in the internal organs 2 hours after injection.

Organ	Rabbit	Activity (Bq)	Variance	Activity compared to the tumor
Tumor	20140422-2763	1024000	0.16%	100%
Lungs and heart	"	4900	2.27%	0.5%
Intestines	"	0	*	0%
Spleen + kidneys	"	23	78.8%	0.002%
Liver	"	62	41%	0.006%

The SPECT data, combined with the CT data, resulted in a hot spot on the tumor location and no spots elsewhere. This hot spot was clearly located in the tumor centre in the area where most holmium was present. Small areas that were located more at the border of the tumor, and which contained holmium according to the CT images, received only a little to no activity, according to the SPECT data. (**Figure 11**) . Due to the low resolution of SPECT, only a rough estimation of the HoMS distribution in tissue can be given based on these images.

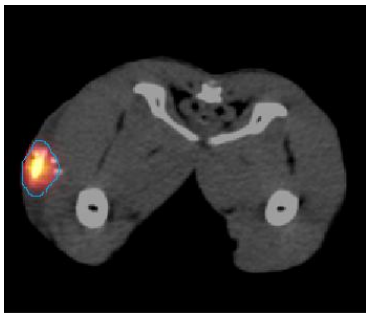

Figure 11: Transverse section through a combined SPECT/CT image of both hind limbs of a rabbit with a VX2 tumor on the left hind limb, tumor 9. Radioactive holmium is located in the tumor area. Some white spots can be detected next to the high activity spot, with no remarkable SPECT signal. (Blue line indicates the tumor area)

CT dose modeling, using the afore mentioned procedure of CT image processing, resulted in a dose distribution image, which can be placed over the tumor. The resulting images give a clear visual indication of the covered areas of the tumor. The image processing steps and an example of the resulting dose distribution images are illustrated in **Figure 11**.

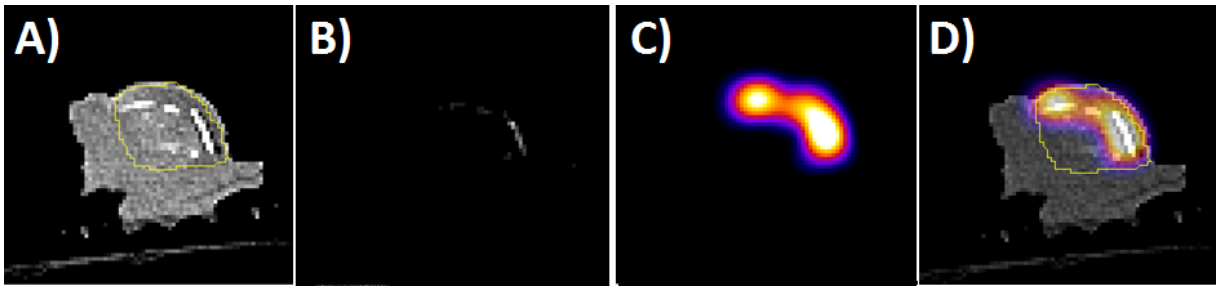

Figure 12: A) original *ex vivo* CT image of tumor 7 B) Gray values indicate the holmium content per voxel, C) Dose distribution, values are expressed in gray per voxel, D) Dose distribution inside the tumor. The transition black to blue-purple indicates the 100 Gy iso-dose line, the bright yellow indicates an iso-doseline of around 1000 Gy, in the white areas the dose can reach values up to 2000 Gy. (Tumor area is encircled in yellow)

On the *in situ* scans, holmium microsphere distribution volumes varied largely between the 5 available tumors, from 0 to 0.6 cm^3, and no association between the number of injection sites nor any difference between HoAcAc and HoPLLA microspheres could be observed (**Table 5**). The local holmium concentration was converted into a local radiation dose and tumor volume coverage with 100 Gy varied largely as well, between 0 and 100%, mean 57% ± 42%. (**Table 5**) In tumor 8, no microspheres were visible on the *in situ* CT scans, this resulted in no thresholdable voxels and therefore the microsphere volume and dose distribution of this tumor are 0.

Table 5: Microsphere distribution in the different tumors, based on the *in vivo* CT scans

Tumor nr	Nr of injection sites	HoPLLA / HoAcAc	Tumor volume Based on *in vivo* MRI (mm3)	Microsphere volume (mm^3)	Tumor coverage with microspheres(%)	100 Gy radiation range (mm^3)	100Gy tumor coverage (%)
1	1	HoAcAc	1844	286	15.5	1836	99.6
2	3	HoAcAc	565	42	7.4	569	100.7
3	6	HoAcAc	3436	220	6.4	1526	44.4
8	1	HoPLLA	336	0	0	0	0
9	3	HoPLLA	9890	564	5.7	4044	40.9

On the *ex vivo* CT images, the holmium distribution was clearer visible, compared to the *in situ* images, when using the scan settings described here (**Figure 13**). The most noticeable differences are the higher resolution of the *ex vivo* images and the higher contrast between holmium microspheres and tissue. Calculated microsphere distribution volumes on the *ex vivo* CT data varied between 4 mm^3 and 216 mm^3 (**Table 6**). Based on a 100 Gy threshold, dose distribution volumes varied between 0 cm^3 and 5.2 cm^3, resulting in a theoretical tumor coverage ranging between 0 and 116%, mean 56% ± 42% (**Table 6**).

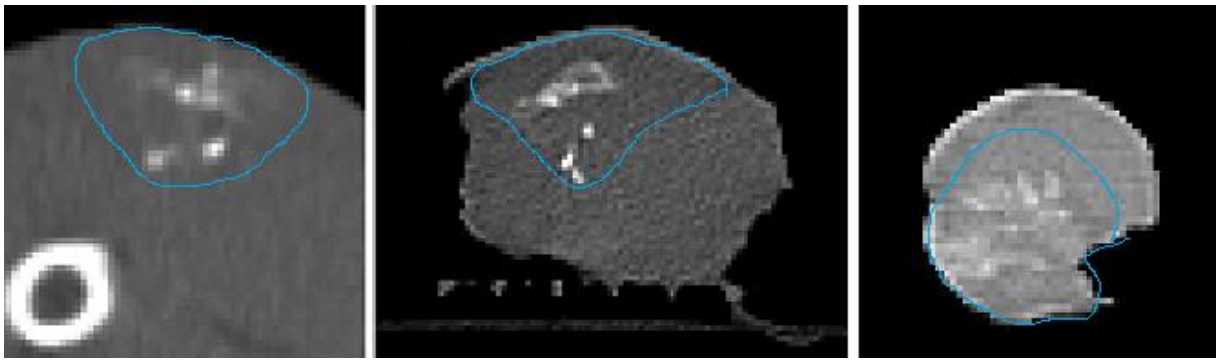

Figure 13: Left image *in situ* CT of tumor 9, middle image *ex vivo* CT image of tumor 9, right *ex vivo* CT image of tumor 4. Tumor areas indicated by blue line.

Table 6: Microsphere and dose distribution over the different tumors, based on the *ex vivo* CT scans, tumors ordered by number of injection sites

Tumor nr.	Nr of injection sites	Tumor volume (mm^3)	Microsphere volume (mm^3)	Tumor coverage with microspheres (mm^3)	100Gy Dose volume (mm^3)	100Gy Dose coverage (%)
4	1	9616	4.1	0.1	0	0
8	1	336	5.4	0.7	90	26.7
5	2	1555	51.2	3.7	1178	75.8
6	3	2151	65.3	2.8	1727	80.3
9	3	9890	216.3	2.4	3694	37.4
7	5	4500	194.9	5.4	5231	116.2

For the *ex vivo* CT images a trend towards a better tumor coverage for a higher number of injection sites is observed (**Figure 14**, right diagram), R^2= 0.7, n=6. However, when comparing the number of injection sites to the 100 Gy tumor coverage for the *in situ* data, no trend could be observed (**Figure 14**, left image), R~0, n=5. Combining these data favors for no relation between the different number of injection sites, and a wide spread between the observed values.

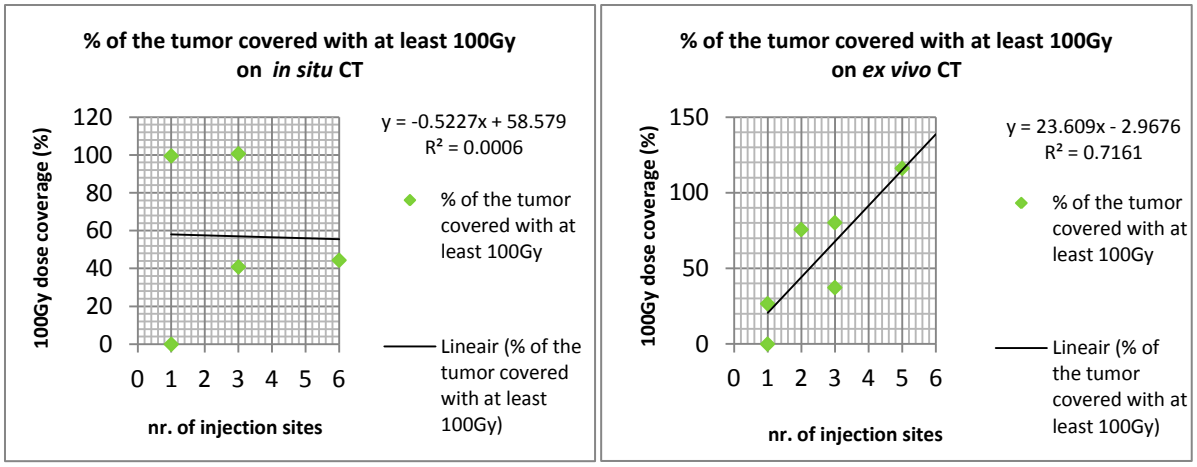

Figure 14: 100 Gy tumor coverage as a dependent of the number of the injection sites.

Discussion

Conventional CT, MRI and SPECT have been investigated previously for their sensitivity for holmium detection and their resolution.[27] This revealed, that SPECT was the imaging technique with the highest sensitivity for radioactive holmium microspheres, moreover SPECT is suitable and used for the determination of extra hepatic holmium depositions in human liver radioembolization patients.[79] Therefore it was hypothesized that SPECT would be the most suitable imaging technique to detect microsphere deposition on distant sites. The twin scintillation counter revealed that only a very small percentage, 5 kBq equaling 0.5%, of the activity administered to tumor 9 leaked to other organs, more specifically to the lungs. During injection, some small blood vessels might have been damaged, if microspheres enter the blood stream, they will get stuck in the next capillary bed they encounter, for intratumoral injection, this is the lung vasculature. This declares the often found deposition of low activity levels in the lungs.[18, 21, 22, 25] An even smaller fraction of less than 0.006% shunted to other organs like the spleen, kidneys and liver, under 0.006%. However, these very low activity levels for liver, kidney and spleen are not reliable and probably due to contamination during dissection. These low values could not be detected on conventional SPECT, suggesting that conventional SPECT is not sensitive enough for the detection of the very small amounts of activity shunting during the microsphere distribution study and that the other imaging techniques are unsuitable too. For these purposes a more sensitive method can better be used, like the used twin crystal scintillation counter. For the detection of clinical relevant distant activity depositions in patients, SPECT is however suitable and easily applicable, as shown in the HEPAR trial after liver radioembolisation.[80]

SPECT is used for dosimetry in human liver radioembolization patients.[79] However conventional SPECT has a minimum voxel size of around 4x4x1 mm, and for a tumor with a maximal diameter varying between 1.0 and 4.0 cm, this voxel size gives an imprecise indication of the distribution of the activity inside the tumor. Therefore the use of conventional SPECT is questionable in experiments on the precise holmium and dose distribution in a tumor model for intratumoral injections. µSPECT has been proven to be able to detect holmium depots and to give a better resolution, with reconstructed voxel sizes of

375 µm being possible in a study of intratumoral injection in renal carcinomas in mice.[41] These images display a detailed radiation distribution. (see also **Table 9** in **Chapter 8**) However µSPECT is not possible on living rabbits, due to the small gantry size. Nevertheless, excised tumors in normal tissue still containing activity have dimensions that fit in the apparatus, a characteristic that may be of use in future experiments. The low resolution of the conventional SPECT, possibly led to another remarkable feature: the observed activity on the SPECT scan of tumor 9 is accumulated at the center of the holmium distribution and small depositions of holmium microspheres in the border of the tumor area seem not to produce a detectable radiation dose at that location (**Figure 11**). This phenomenon may also be caused by the low activity levels of the used microspheres and the therefore low activity levels in the tumor borders.

Scan settings for the *in situ* and *ex vivo* CT scans varied to some extent. The *ex vivo* scans had a higher tube voltage (in kVp), a higher effective current (in mAs), and a B31s reconstruction convolution kernel was used for the in vivo scans, a smooth kernel, while for the *ex vivo* scans, a B70s reconstruction convolution kernel was used for the microsphere distribution evaluations. The B70s kernel is a sharp kernel and provides more tissue contrast. The consequence is that the *ex vivo* CT data are a bit clearer, than the *in situ* CT data, although the scan resolutions of both scan types did not vary much. Because the *in situ* CT scans have a higher importance for a clinical setting, due to the inability to excise a tumor from a patient in order to make an *ex vivo* CT scan, scan settings of the *in vivo* CT scans should be optimized in order to increase the sensitivity and the contrast between tissue and microspheres. In order to increase the contrast between holmium and surrounding tissue, the peak tube voltage (kVp) can be decreased, this also decreases the patient radiation dose, however it does also decrease the signal to noise ratio of the image.[27, 81] Another option to increase the detectability of the holmium microspheres is increasing the current (mAs). This does however also increase the patient X-ray radiation dose.[27, 82] Moreover the slice thickness and pixel size of the *in vivo* CT scans can be lowered to the smallest slice thickness available in order to increase the resolution. When setting the CT parameters, one should however always take the total patient radiation dose into account.

It should be noted that some annotations on the used method for CT dosimetry should be placed. Tumors 1 to 3 received HoAcAc microspheres, while the calibration curve was made for HoPLLA microspheres. However, the same calibration curve is used, because the holmium content is most defining for the slope of the calibration curve and the holmium is responsible for the tissue radiation, therefore the calibration curve is still suitable for dosimetry and treatment effect estimations, it should however not be used for quantification of the local microsphere content.[35] The thresholding method is a useful way to select voxels which most certainly contain a specific amount of holmium and to exclude other voxels, which do certainly not contain that amount of holmium, from further calculations. However, voxels containing a holmium concentration below 8.6 mg/ml, equaling 8.6 mg/ml*0.426*10^{-3} ml/voxel*13.6 MBq/mg=0.05 MBq/voxel, for the *in situ* CT

data and below 31 mg/ml, equaling 0.16 MBq/voxel, on the *ex vivo* CT data, are excluded in this method because they cannot be distinguished from normal tissue HU variation in the present CT images. Therefore, the volume of the thresholded voxels may be an underestimation of the total distribution volume of the microspheres. Depending on the amount of voxels falsely excluded in this way the effect of this underestimation varies, one missed voxel will not have a large effect on the total received dose of a tumor, while many voxels have. When many voxels are falsely excluded next to each other this missed dose may even exceed 100 Gy. A clear example of this problem is tumor 4 (**Figure 13 right tumor**). Based on the MR images (**Chapter 3**) and the µCT images (**chapter 5**), this tumor has a very homogeneous microsphere distribution pattern. However, due to the relatively low resolution and sensitivity of conventional CT images for HoMS the homogeneously distributed microspheres seem to dissolve in the CT image and become part of the background noise and only a small amount of voxels have a distinct higher HU-value and can be isolated using a threshold value. In this way it is possible that optical white voxels are not included in the thresholded voxels. However, this fenomenon was clearly present in only one tumor (tumor 4), and was less prominent for the other tumors. This, combined with the ease and speed of conventional CT, would make CT a valuable tool for holmium microsphere imaging and dosimetry in a clinical setting. Furthermore, for predicting the treatment effect, it is better to have a slight underestimation of the amount of holmium present, compared to an overestimation of the amount of holmium, because of its clinical consequences. Too little detectable holmium would result in retreatment of the tumor while an overestimation of the amount of holmium would leave untreated areas undetected and insufficiently treated. Moreover, the interpolation of the dose kernel gives rise to some inaccuracy for the CT based dose distribution, because the used dose kernel for the CT data originates from SPECT imaging techniques with a lower resolution, this inaccuracy is also present for the MRI based dosimetry, and increases with an increasing resolution. This effect is most evident in the centre of the dose point kernel, where the peak is flattened (figure 62). Therefore the used dose point kernel will give a slight underestimation of the dose near the centre of the kernel, thus near the location of the microspheres. In this area, the received dose will however be relatively high and this underestimation will not have a large influence on the volume radiated with at least 100 Gy and is probably not of clinical importance. Moreover, due to its clinical consequences, it is better to have a slight underestimation of the local dose than an over estimation. This problem can be tackled by improving the dose point kernel by performing a new Monte Carlo dose simulation and calculating a new tissue dose kernel for holmium. The lower sensitivity of conventional CT compared to MRI which can be clearly seen in tumor 4 (**Figure 13, right tumor and Figure 60**) has also been described in a distribution study of radioembolization in pig livers and in a phantom study on the use of holmium as a contrast agent for different imaging techniques.[27, 83] Therefore CT has always been considered as a minor imaging possibility, but this study does show its possible value.

In theory, more injection sites would improve the microsphere distribution volume, increase the associated dose distribution volumes and improve tumor coverage. An increase in tumor

coverage for multiple injection sites was however not found. The *ex vivo* CT dose coverage data suggest in this direction, but the *in vivo* CT dose coverage data show no relation at all. With the large variation observed between the different tumors, the few tumors used for this comparison may easily lead to falsely conclusions. Therefore, more holmium distributions in tissue should be investigated in order to be able to adjudicate about the relation between the number of injection sites and the tumor coverage. It should be taken in mind that the dose distribution volumes observed on the CT images may be partly located outside the tumor area, due to the radiation range. The relationship between tumor volume and a thresholded dose volume may therefore not perfectly overlap. This can be improved if it is possible to use the tumor volume as a characteristic function over the dose distribution volume, resulting in solely dose data for the tumor area.

In conclusion, it can be stated that SPECT imaging is not very useful for detailed investigation of the holmium microsphere distribution after intratumoral injection but probably useful for activity detection in a clinical setting. For organ biodistribution studies (shunting of holmium microspheres), a more sensitive technique, like a twin scintillation counter may be more useful. For the investigation of intratumoral microsphere distribution an imaging technique with a higher resolution than conventional SPECT should be used. Conventional CT images are useful for intratumoral holmium microsphere distribution investigations. Furthermore, this chapter demonstrates a method to model the HoMS dose distribution inside the tumor using CT data. Image-based dose modeling may turn out to be the only reliable way to monitor and improve intratumoral HoMS treatment.

Chapter 5. Micro computed tomography (µCT) for holmium distribution analysis after intratumoral injection in a Vx2 carcinoma model

Summary

Background Radioactive holmium microspheres are used for the experimentally treatment of solid tumors by intratumoral injection. However, little is known about the distribution of these microspheres after intratumoral injection. When the mechanism behind this distribution is known, it will be easier to predict the holmium distribution after a single injection and therefore it can improve the treatment procedure and therefore the treatment outcome.

Methods In order to investigate the microsphere distribution on a micrometer scale, micro computed tomography (µCT) was conducted on six subcutaneous Vx2 rabbit carcinomas injected with holmium microspheres intratumorally. Microsphere distribution was described qualitatively and a method for quantitative dose mapping based on µCT images was developed.

Results The µCT images provide a very detailed image of the microsphere distribution. µCT based dosimetry allows for the linkage of this precise microsphere distribution to the dose distribution inside the tumor. Volume covered with at least 100 Gy varied between 21% and 120% of the tumor volume, mean 57±55%, based on three tumors.

Discussion Based on the investigated six tumors, an anatomical theory of the mechanism behind the distribution pattern of the microspheres after intratumoral injection can be made. The microspheres seem to choose the path of least resistance through the tissues. In the used Vx2 tumor model, this path varies depending on the injection location in the tumor. In the centre of the tumor, a more explosive distribution is found, following a pattern of sheets and rows, resembling the interstitial space. More towards the tumor borders the microsphere distribution seems to be shaped by tissue layer transitions, resulting in thin sheets of microspheres. For the improvement of µCT based dosimetry, the tissue dose kernel of ^{166}holmium should be calculated again for the high resolution of µCT, using a new Monte Carlo based dose simulation.

Conclusion µCT enables a very detailed image if HoMS distribution in tissue, which seems to be influenced by (micro-) anatomical tissue structure. Based on these qualitative findings one would advocate for a few injections in the centre of the tumor in order to cover the whole tumor area, because injections placed here would distribute over a large area. If injections are placed in the outer layers, multiple injections will probably be needed, because here microspheres only distribute over a relatively short distance, between or against the flattened cell layers of the tumor. Based on the qualitative HoMS and dose distribution investigation, the used injection method of up to 6 injections seems to provide insufficient tumor coverage.

Keywords: spatial distribution pattern, holmium microspheres, intratumoral injection, local radiotherapy, Vx2 carcinoma, microcomputed tomography, dosimetry

Introduction

Microspheres containing the radioactive component ^{166}Ho ($E_{\beta,max}$=1.84 MeV, $t_{1/2}$=26.8 hrs, tissue penetration 8 mm) are used for the experimental treatment of non-resectable solid tumors in veterinary patients.[43] During this treatment the radioactive microspheres are injected directly into the tumor. This treatment shows promising results in some patients, but in others it does not. It is expected that the distribution of the microspheres inside the tumor plays an important role in the treatment efficiency.

The distribution of HoAcAc-MS after intratumoral injection in a Vx2 carcinoma model has already been elaborated on histopathology.[68] Based on the histology sections, the holmium distribution has been found to cover only parts of the tumor, but the 2D examinations of the histology slices are not suitable for a quantitative description of the HoMS and dose distribution and it is not able to use this technique for HoMS distribution investigation in patients. Furthermore, the HoMS distribution in 9 Vx2 tumors has been imaged using conventional scan techniques, like MRI and SPECT/CT (**chapters 3 and 4**). These methods were able to give a rough description of the microsphere distribution. In order to improve our understanding of the spatial microsphere distribution inside the tumor in a more accurate way, more precise scans, like µCT, are however required. µCT has already been used for the investigation of the distribution of HoPLLA-MS after intra-arterial radioembolization of a Vx2 liver tumor, and has shown itself useful for the qualitative and quantitative description of the HoMS distribution.[65] Moreover µSPECT and small animal MRI and CT have been used to study the distribution and clinical efficacy of ^{166}HoAcAc microspheres after a single intratumoral injection in a mice renal carcinoma model.[41] However, these renal tumors were very small and the microspheres and radiation dose covered the whole tumor area easily, while this would probably not occur in a larger tumor model, like the Vx2 carcinoma model. Studies describing intratumoral HoMS injection, have however not described the spatial distribution patterns of the microspheres in a detailed 3D fashion, so it remains unclear how the microspheres distribute exactly.

Therefore, in order to increase our understanding of the microsphere distribution after intratumoral injection, this study used µCT with voxel sizes down to 10µm in order to describe the microsphere distribution in more detail in a qualitative way and to use these qualitative data to describe a general distribution pattern. Furthermore, quantification of the HoMS distribution and a method for dose calculations based on the µCT images were evaluated.

Material and Methods

Tumor model

For the µCT distribution analysis, tumors 4 to 9 of the intratumoral HoMS distribution study were used (**chapter 2**). The used tumors had an *in vivo* MRI based mean volume of 4.7 ± 4.2 cm^3 on the day of fixation. The tumors were excised taking a 1-3 cm margin of surrounding normal tissue into account and sutures were placed at the dorsolateral and at the cranial side of the tumor, in order to keep the orientation. After formalin fixation, the tumors were sutured to a plastic grid in order to keep the orientation throughout the different imaging techniques. Tumor volume was determined based on the *ex vivo* MR images (**chapter 3**): mean 3.7±3.0 cm^3 and ranged from 0.8 cm^3 to 8.9 cm^3. Of the 6 tumors, tumors 4 and 8 were injected with one intratumoral holmium microsphere injection, tumor 5 received 2 injections, tumors 6 and 9 were injected with 3 injections and tumor 7 received 5 holmium injections. Per tumor, the total injected amount of holmium microspheres was aimed at 25 mg, but variation occurred. (**Chapter 2**)

µCT imaging acquisition

The µCT scans were made on a preclinical µCT (IVIS | Quantum FX, Caliper Life Sciences, Hopkinton, USA) at the Applied Molecular Imaging Erasmus MC (AMIE) facility in Rotterdam, the Netherlands. During transport to the scan facility, the tumors were stored in a watertight plastic box filled with water. At the scan facility the tumors were taken out of the water and placed on the scan table.

All tumors were scanned at a 60 mm field of view (FOV), except for the very small tumor 8, which fitted completely into a 40 mm FOV. X-ray current was 160 µA and the peak tube voltage was 90 kVp for all scans. Depending on the FOV the scan times changed a bit. For the FOV 60 mm scans the scan time was 2 minutes or 4.5 minutes. For the 30 mm FOV scans, scan time was 3 minutes. For the 24 mm FOV scans the scan time was 4.5 minutes. For the 20 mm FOV scans, scan time was 4.5 minutes. For the 10 mm FOV scans, scan time was 4.5 minutes. Finally the 5 mm FOV scans were made in 3 minutes. Depending on the tumor and the observed distribution, different FOV were chosen. Tumors 4 until 6 were scanned in November 2013, with ranging FOV settings. Tumor 4 was scanned at 60 mm, 30 mm, 10 mm and 5 mm FOV. Tumor 5 was scanned at 60 mm, 30 mm, 20 mm, 10 mm, and 5 mm FOV. Tumor 6 was scanned at 60 mm, 24 mm and 10 mm FOV. The other three tumors were scanned in May 2014, with more standardized FOV settings. Tumor 7 was scanned at 60 mm, and 30 mm FOV. Tumor 8 was scanned at 40 mm and 30 mm FOV. Tumor 9 was scanned at 60 mm and 40 mm FOV. During the scans of May a special method was used to keep the orientation while narrowing the FOV. The table centre position of the first scan, with the largest FOV was written down, while narrowing the FOV the centre position was kept stable and after this scan the table was moved, in such a way the next scan would continue at the location the previous one had stopped. All data were exported as DiCom files. After the scans of May 2014, for tumor 7 to 9, a correction of the gray values of the µCT was

conducted, in order to make them comparable to the standard HU values observed in clinical CT scanners.

Qualitative µCT image evaluation

The DiCom files were imported into ImageJ® and the tumor region was cut out and saved as tiff-file. The distribution of the holmium clusters was described in relation to the tumor structure, based on the 2D slices. Also, the images were thresholded, in order to visualize the holmium distribution, without the surrounding tissue. The thresholded images were converted into 0-1 images and multiplied with the original cutted image. These stacks, containing some information about the local HoMS concentration, were viewed with the plug-in 3D viewer of ImageJ®. This showed the 3D distribution of the microspheres with concentration differences. The original unthresholded stack was also observed in the 3D-viewer. By increasing the threshold of these images first the dark background disappeared, displaying the tumor borders. Hereafter the threshold was further increased, resulting in an image on which the holmium distribution could be observed. The combination of all these data, resulted in a qualitative description of the microsphere distribution.

Quantitative µCT image evaluation

As with the CT study (**chapter 4**), a method to model the dose distribution throughout the tumor was developed for the µCT images. The tiff-files of tumors 7 to 9 were thresholded at a gray value of 150 HU. From this value on all normal tissue had disappeared and only the holmium distribution remained visible. The thresholded images were converted into binary files, a characteristic function, and multiplied with the original image, using the plug-in Calculator Plus® in order to remove the background signal from the stack. The remaining gray values were converted into microsphere concentration values, using the following calibration function: HU=8.64*[HoMS] -64.08 → [HoMS]=(HU+64.08)/8.64. The slope of this calibration function was obtained by scanning a set falcon tubes with increasing HoMS concentration in agarose gel in the µCT scanner; the same set as was used for the determination of the conventional CT calibration function (**chapter 4**). The intercept of the previous function is the baseline tissue HU value on µCT, determined on a piece of muscle tissue, tumor tissue without holmium was not scanned on µCT. After adding 64.08, dividing through 8.64 and again multiplying with the characteristic function, the local concentration in mg/ml was obtained, without background. The concentration in mg/ml was converted into the activity per voxel by multiplying with the voxel size, $1.728*10^{-6}$ ml, and the specific activity of the holmium microspheres, set at 13.6 MBq/mg (**chapter 4**). Over this stack a convolution, using the plug-in Convolve 3D with the dose point kernel of holmium was made. This dose point kernel originated from the dose kernel designed by van Elschot et al.,[46] which was converted into a kernel suitable for the 60mm FOV µCT images. The obtained values were corrected with the factor: $1.60217733*10^{-19}/(7.176*10^{-6} * (1.06*\text{voxel volume in liter}))$. The result of this multiplication was a stack displaying the dose per voxel in Gray/voxel. This stack was thresholded at 100 Gy in order to give an estimation of the

effectively treated volume. The volumes of the areas receiving at least 100 Gy were compared for all three tumors.

Tumors 4 to 6, scanned in November 2013, were not corrected for the standard HU values and therefore these tumors were thresholded, at different HU values: tumor 4 (**Figures 15 and 16**) on -960; the tumor 5 (**Figures 17 and 18**) on -700; and tumor 6 (**Figures 19 and 20**) on -500). The agarose HoMS concentration line was also scanned by means of µCT, without the HU-correction. Based on this agarose line, a calibration function for these tumors was modeled: HU=5.875[HoMS]-767.07. The 0-intercept was the baseline tissue value, obtained by the determination of the mean HU value of muscle tissue, tumor tissue without holmium was not scanned on µCT. Because these steps contained more uncertainty and variation, only a rough estimation of the dose distribution could be given for these tumors, which are not very reliable.

Results

Qualitative description of the holmium distribution inside the tumors

Tumor 4

This tumor received only one injection with holmium microspheres. Remarkable is that in this tumor no very large clusters can be observed and that the HoMS concentrations remain relatively low throughout the tumor. However, a very explosive distribution can be observed and a large part of the tumor is covered with microspheres. The microspheres have distributed heterogeneously over the tumor, as if they are following each other in bands or sheets, close at each other with smaller and larger clusters along the way, forming a pattern which resembles the interstitial pattern, between the nodular, sheet-like and nest-like cell clusters, of a Vx2 tumor (**Figure 30 and 31**)[84]. Moreover at one edge of the tumor, a white layer containing microspheres can be observed, like the microspheres were stopped at this layer from distributing further to the borders of the sample. (**Figure 15 and 16**)

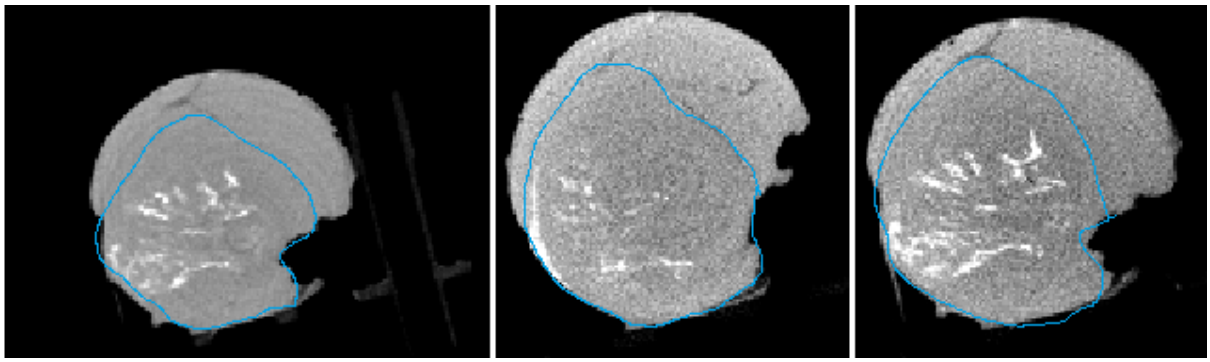

Figure 15: Tumor 4. Left image FOV 60mm, middle and right images FOV 30mm. All displaying a wide distribution of microspheres in the middle of the tumor. The middle image also shows a white band on the left, which is described as a sheet of microspheres at the edge of the tumor. Estimated tumor area in light blue.

Movie.avi

Figure 16: 3D animation of the holmium distribution in tumor 4. FOV 30mm

Tumor 5

This tumor sample consist of 2 parts, one large tumor and one smaller tumor, separated by some normal tissue and some air in the *ex vivo* situation. The sample received two injections in total, one for every tumor. In the sample, different distribution patterns can be observed. In the large tumor some small clusters can be detected in the centre of the tumor, seeming to follow the interstitial pattern of the tumor (**Figure 30 and 31**). To the borders of this tumor, more larger clusters can be observed and also the vague edges of a sheet of microspheres on the border of the tumor, outside this sheet no microspheres can be observed anymore. In the smaller tumor a few large clusters with a high holmium concentration are present. The interstitial pattern is missing in this area and holmium is only visible in these large clusters. (**Figure 17 and 18**)

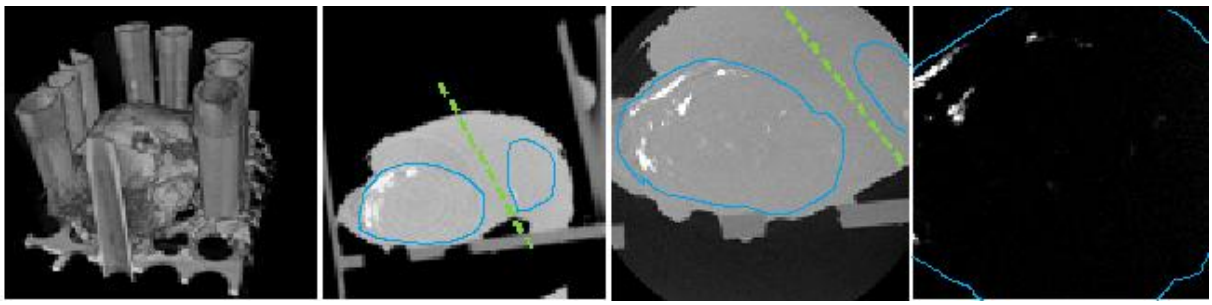

Figure 17: Tumor 5. Figure on the left: 3D reconstruction of the tumor and the used setting. Second figure is a slice from the 60 mm FOV, displaying flat clusters on the edge of the tumor. Stripped line indicates the global border between the large tumor on the left and the smaller tumor on the right, no clear tissue transition is visible in this figure. Third figure shows an image of the tumor with a 30 mm FOV, some small clusters are also present more in the centre of the tumor. Fourth figure shows a 10 mm FOV image, flat clusters on the left and some small clusters in the centre can be observed. (Tumor areas are indicated by blue lines)

Movie (tumor2).avi Movie (tumor 2, FOV 20mm).avi

Figure 18: 3D reconstructions of tumor 5, left movie originates from a 60 mm FOV scan, the right one a 20 mm FOV

Tumor 6

This tumor received 3 injections. Remarkable are one or probably even two injection canals filled with holmium (**middle figure of figure 19**). The centre of the tumor is filled with heterogeneously distributed microsphere clusters of varying sizes, again this distribution resembles the interstitial space. Moreover one large or two adjoining separate microsphere sheets are observed between the needle track and the centre of the tumor, again looking like the microspheres have spread between two tissue layers. (**Figure 19 and 20**)

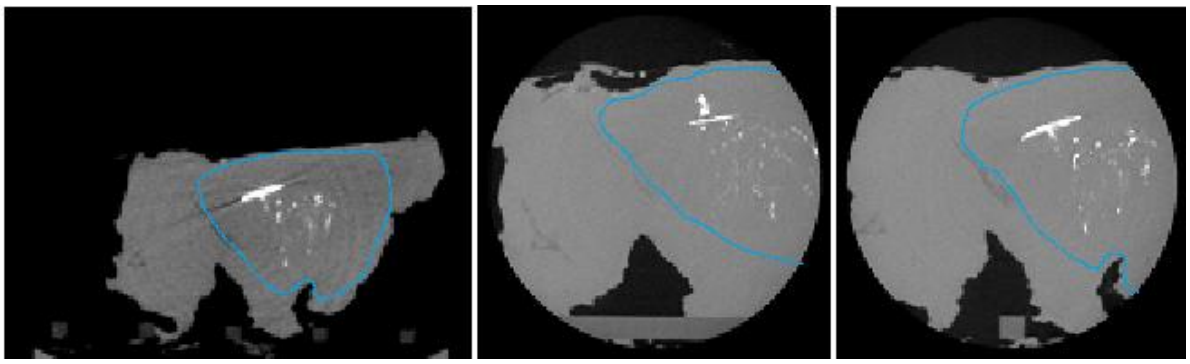

Figure 19: Tumor 6, left image 60 mm FOV, right two images 24 mm FOV, middle one displaying an injection canal. The flattened clusters are clearly visible, as well as some less dense distribution under the microsphere layers on the right of the image. (Tumor area indicated by blue lines)

Movie (FOV24mm).avi

Figure 20: 3D holmium distribution inside tumor 6, reconstruction originates from a scan with FOV 24 mm

Tumor 7

This tumor received 5 injections of holmium. Remarkable is that the first injection, the one placed in the centre of the tumor, spread out explosively, which can be seen in the centre of the tumor. The other four injections remained more locally, and spread in a sheet-like way, like the microspheres distributed between different tissue layers. Some holmium could also be observed on the surface, at the injection sites. (**Figure 21 and 22**)

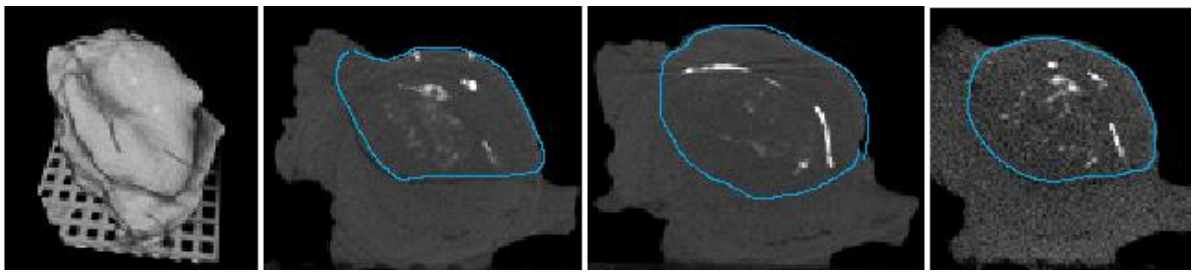

Figure 21: Tumor 7 The left image displays the tumor on a Ministeck® plate. The next 2 scans have a FOV of 60 mm, on the second image two injection sites are visible on the surface, on the third image, 2 flat microsphere stratums are visible, with a more diffuse distribution in the centre, the image on the right has a FOV of 30 mm, (Tumor area is indicated by the blue line)

Movie 20131219 FOV60mm.avi

Figure 22: 3D animation of the microsphere distribution in tumor 7

Tumor 8

This small tumor received only one holmium injection, but was ineffectively punctured with the injection needle without fluid injection multiple times before proper holmium injection was possible. A part of the injected HoMS suspension leaked out the tumor over the tumor surface, leaving much less than intended HoMS inside the tumor. On the µCT images holmium is only present inside the tumor, not inside the muscle, and seems to cover at least half of the tumor, although one side of the tumor seems to have a better coverage than the other side. Most of the microspheres seems to be divided over several larger clusters. No

interstitial pattern is seen. In this case, the borders of the tumor are clearly visible and contrast with the underlying muscle is sufficient to distinguish tumor from muscle. Some holmium spots are present on the surface of the tumor. These spots are most probably the injection site and the previous punctured sites (without holmium injection), where the holmium has leaked out, due to high intratumoral pressure. (**Figure 23 and 24**)

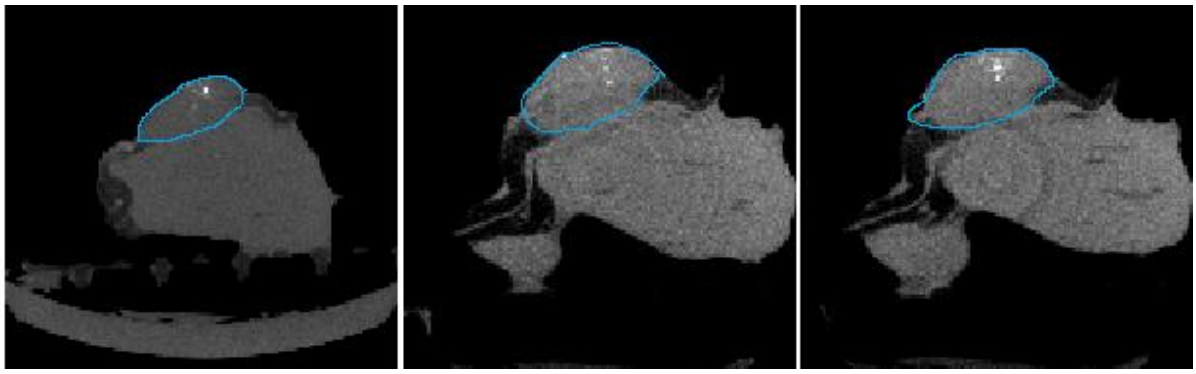

Figure 23: Tumor 8. First image FOV 40 mm, second and third image 30 mm FOV. On the second image some holmium is visible on the tumor surface. Tumor is the small ellipse shaped mass on the upper left site of the tumor. (Tumor is indicated by blue line)

Movie-20140311, FOV 30mm.avi

Figure 24: 3D animation of the holmium distribution in tumor 8

Tumor 9

This tumor received 3 holmium injections, with an exactly known total amount of microspheres, 21 mg microspheres. The tumor was placed upside down on the scan table, because it would not fit into the gantry when placed with the Ministeck® plate on the bottom side. In the tumor, the holmium microspheres fanned out over a big distance, but its distribution is heterogeneously, the distribution follows thin sheets and bands and it looks like the spheres enclose (sometimes spherical) tissue structures, with some branches into these structures, most probably the interstitial pattern of the tumor. The injection canal to the deeper tissue layers can be observed, containing some microspheres, with some microspheres spread out into deeper muscle tissue, fortunately these spheres remain quite locally at this location. (**Figure 25 and 26**)

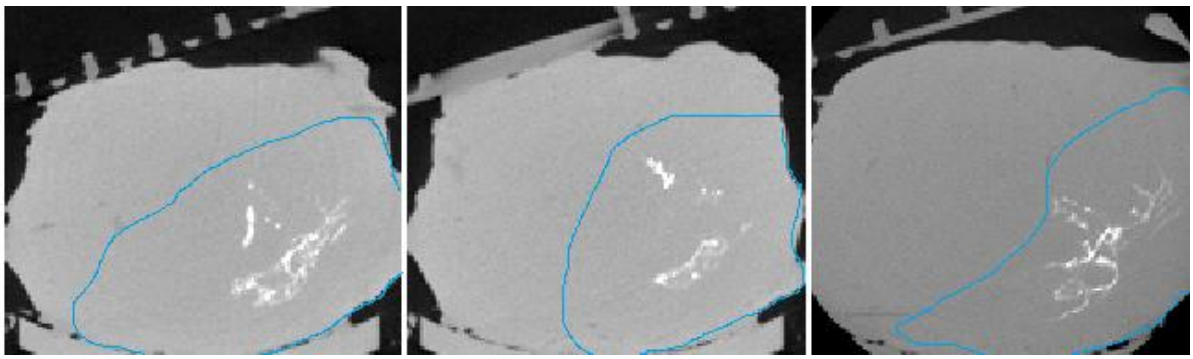

Figure 25: Tumor 9. First 2 images have a 60 mm FOV, with the middle one clearly displaying the injection deeper into the tissue. Third image shows the interstitial distribution pattern of the microspheres at a 30 mm FOV. (Tumor indicated with blue lines)

Movie-20140422-FOV60mm.avi

Figure 26: 3D reconstruction of the holmium distribution of the 60 mm FOV scans.

Quantitative dose distribution in the tumors

Examples of µCT dose maps and the process of dose map development are displayed in **figure 27 and 28**. When looking at these dose maps in relation to the tumor and the holmium distribution, it becomes clear that areas containing large clusters with a high holmium content are surrounded by most of the radiation dose injected in the tumor and that the fine distributed microspheres are only surrounded by a small part of the total dose. For example, in tumor 7 a fine distribution is seen in the middle of the tumor, but regarding the dose distribution, almost no dose is present in this area, maximal 30Gy, too low to show up on **figure 27D**. While the white areas near the borders of the tumor, containing those previously described sheets of microspheres receive over a 1000Gy (**Figure 27D**).

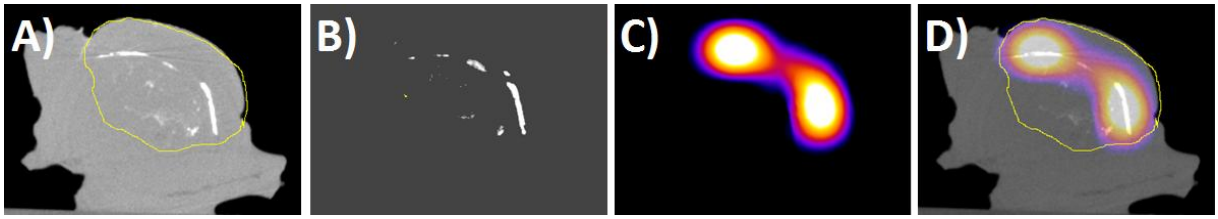

Figure 27: Procedure of dose calculations over tumor 7. A) displaying the original tumor. B) image displaying the local holmium concentration in mg/ml. C) Dose distribution, blue line indicates the 100 Gy iso-doseline, white area contains more than 1000 Gy. D) The dose distribution over the original tumor. Tumor borders indicated by yellow line

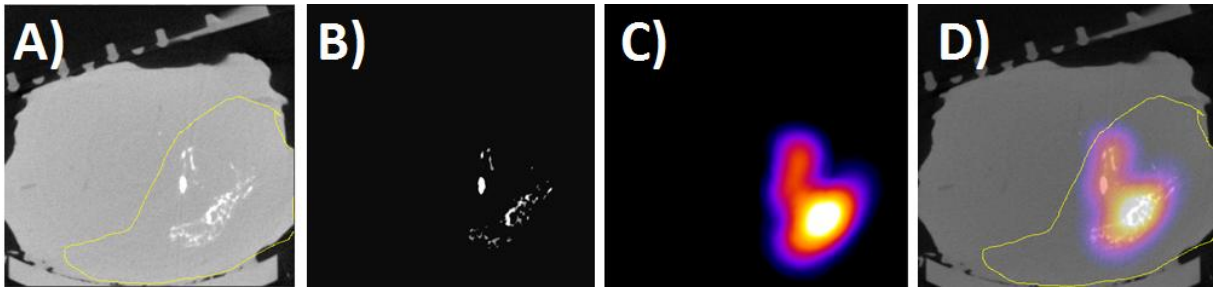

Figure 28: Procedure of dose calculations over tumor 9. A) displaying the original tumor. B) image displaying the local holmium concentration in mg/ml. C) Dose distribution, blue line indicates the 100 Gy iso-doseline, white area contains more than 1000 Gy. D) The dose distribution over the original tumor. Yellow line indicates the estimated tumor borders.

In tumor 9, something else becomes clear. Namely that the received local dose cannot be predicted based on a single 2D slice, but that the 3D configuration of the microsphere distribution is required for treatment effect estimations. This is illustrated by **figure 29**, based on the distribution pattern of the microspheres of a single slice, seen in the left image of **figure 29**, one would predict to find a larger area covered with sufficient dose of >100 Gy also reaching towards the borders of the holmium distribution, but instead a high dose area is mainly found in the centre of the distribution, and the left side of the holmium distribution receives only 50 Gy.

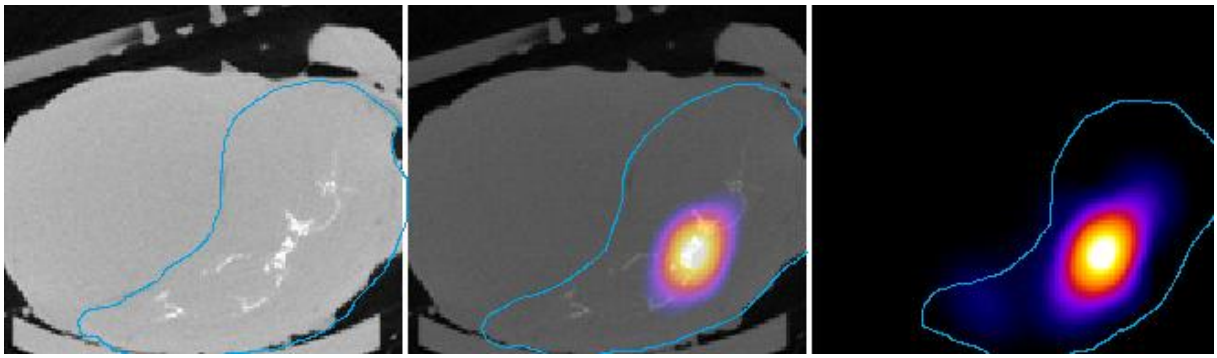

Figure 29: Tumor 9. Clear example of an area with visually a nice distribution of microspheres, centre lower part, left side of tumor area, but when looking at the received dose, the total local dose disappoints, because the present microspheres provides only a dose of 50Gy. The middle image shows the dose distribution in relation to the tumor with the blue area starting at 100Gy. Image on the right shows all the radiation received in this slice, with the visible radiation dose starting at 10Gy. (Tumor area lies within the blue lines)

The absolute volumes radiated by the holmium microspheres varied strongly between the three tumors (**Table 7**). Based on the dose calculations the following tumor coverages were achieved: at least 50 Gy was reached in 42-150% of the tumor volume and at least 100 Gy was reached in 21-120% of the tumor volume. Not all radiated areas are located inside the tumor area however.

Table 7: radiation range per tumor

Tumor	Nr injection sites	Tumor volume (based on *ex vivo* MRI) (mm^3)	V radiation range (100Gy) (mm^3)	Tumor coverage 100Gy (%)	V radiation range 50Gy (mm^3)	Tumor coverage 50Gy (%)
8	1	756	157	20.8	315	41.7
9	3	8907	2721	30.5	3741	42.0
7	5	3637	4362	119.9	5447	149.8

On tumors 4 to 6 a comparable dose estimation was made, however these values are not very reliable, because varying thresholds were chosen in order to be able to show some holmium distribution. For tumor 4, a minimal gray value of -960 was chosen in order to be able to still show some holmium. However when the calibration function HU=5.875[HoMS]-767 was used, this would result in almost only negative values for the local holmium concentration and therefore the resulting dose estimations would have no value. Tumor 5 was thresholded at -700, allowing for some dose, but all local dose values remained under 100 Gy. Tumor 6 was thresholded at -500, using the previously described method and calibration function, this led to a volume covered with 100 Gy of 1707 mm^3. This would cover 73% of the total tumor volume. The values are summarized in **table 8**.

Table 8: Estimated areas covered with sufficient dose in the tumors scanned on the 1st of November. No HU-correction was made on these scans. Values are very irreliable.

Tumor	Nr. Injection sites	Tumor volume (based on *ex vivo* MRI) (mm^3)	V radiation range (100Gy) (%)	Tumor coverage 100Gy (%)
4	1	5439	0	0
5	2	1395	0	0
6	3	2334	1707	73.1

Discussion

µCT has proven itself very useful for precise holmium distribution determination and for the investigation of the mechanism behind the distribution of the microspheres inside the tumor tissue. Although µCT has the disadvantage that is does not provide proper tissue contrast, a less radio-dense layer inside the tissue can sometimes be observed, which is most probably the transition of normal tissue to tumor tissue. Qualitative analysis of the distribution on µCT revealed some general distribution patterns. First, it becomes clear that when the holmium microsphere injection is placed in the centre of the tumor a distribution pattern consisting of thin sheets and fine bands is observed, sometimes seeming to distribute around spherical structures, which pattern brings the interstitial structure of the Vx2 carcinoma in mind, with the cells growing in the form of sheets, nodules and nests, surrounded by reticular fibers (**Figure 30 and 31**). [85-87] [84] The microspheres seem to follow the pattern of the reticular fibers. It should be noted that the centre of a Vx2 carcinoma often consists for a large part of necrosis and that the interstitial fluid pressure inside the tumor centre is high.[86, 88-90] Some of these necrotic areas are probably filled with microspheres and the high interstitial pressure may cause the microspheres to spread out explosively during injection, explaining the different cluster sizes in the centre. It is hypothesized that the microspheres distribute around the still existing cells and remaining connective tissue structures in the centre.

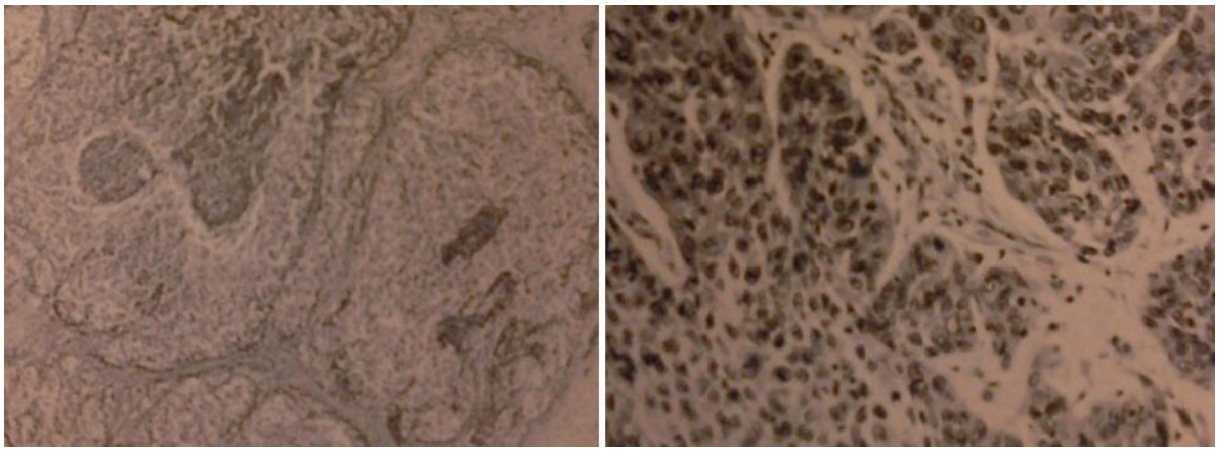

Figure 30: Left figure: Low power photomicrograph of transplant tumor showing a coarse nodular type of growth traversed by thin bands of stroma. Right figure: photomicrograph of transplant tumor. The tumors cells are growing in the form of sheets, nodules, and nests. Obtained from: Steward et al. [84]

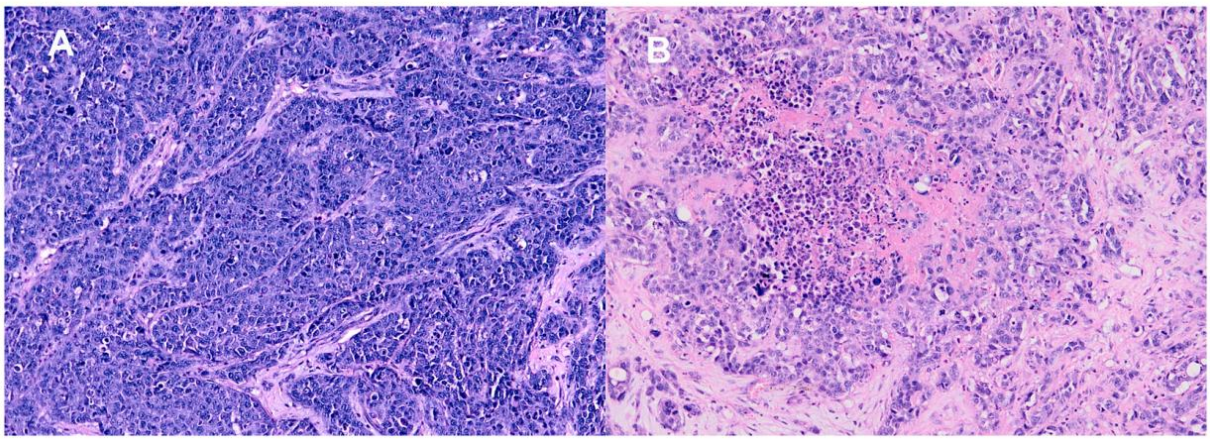

Figure 31: Histopathological appearance of a Vx2 tumor (H&E stain), of a Vx2 liver carcinoma model A) shows Viable VX2 cells with obvious nuclear atypia in the periphery of VX2 liver tumor. B) shows tumor necrosis in the center of VX2 liver tumor with large size. (Magnification ×100) obtained from: Wang et al.[91]

Secondly, near the well vascularized vital tumor border [89,90], the radial distribution of the microspheres through the necrotic centre seems to be blocked by this tumor border and start to move along the tumor borders, resulting in thin convex sheets of microspheres near the tumor edges. Sometimes more of these thin sheets are observed after multiple injections, like in tumor 7, indicating the existence of multiple vital structure layers near the tumor edges, between which microspheres can distribute. On histology images of Vx2 tumors, no tumor capsule nor clear shells of cells exist, but some connective tissue layers are observed between cell clusters(**Figure 30 and 31A**) and a basal membrane is present.[84] Moreover, some kind of pseudo-capsule/transition between Vx2 tumor tissue and muscle tissue can sometimes be observed. Around this transition it is very likely that microspheres gather or that they are blocked here (**Figure 32**), which is where the microsphere sheets are most probably located. [86, 91]

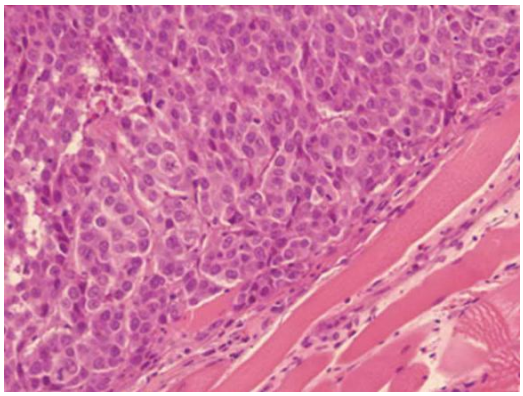

Figure 32: histopathological examination of Vx2 carcinoma in the gastrocnemius muscle of a NZW rabbit, 19 days post inoculation. (magnification, 20×10). Huang et al. [86]

Thirdly, as an artifact of the HoMS injections, the needle track is sometimes filled with microspheres. In this case, bands of microspheres can be observed inside the tissue, following the needle track and sometimes some microspheres are present on the tissue surface, even after formalin fixation and multiple washings with water.

In conclusion it becomes clear that the microspheres seem to distribute in such a way that the least resistance is met. This path depends on the anatomic location in the tumor. The following general patterns in the distribution were found for Vx2 tumors ranging in size between 0.7 and 8.9 cm^3. In the centre of the tumor, this path is radial expansive, between the necrotic cells and remaining tissue structures. At the edges it is between or along vital tissue layers, with or without connective tissue surroundings. The needle track also provides an empty area, which can easily be filled with microspheres. These needle tracks may also be an explanation for the leaking of a part of the interstitially injected microsphere suspension out of tumor 8, because this tumor received multiple ineffective injections, prior to a proper, centrally placed, holmium injection. This may have damaged the natural tumor structure and created empty cavity-like areas inside the tumor, which filled up with microspheres, leading to the large clustered HoMS distribution instead of the typical interstitial pattern inside tumor 8. To confirm our hypotheses, it would be very interesting to investigate the microsphere distribution in these six tumors by means of histopathology, in order to link the microsphere distribution to the cellular pattern of the tumor. However, 3 dimensional reconstruction ability of histology is very limited and can only be used for qualitative image analysis.

A method of µCT dosimetry was developed in this study, in which the 3 dimensional dose distribution can be investigated using µCT. This method was useful for the qualitative dose distribution evaluation and, moreover, it is a big step towards the quantitative evaluation the tumor dose coverage. Tumor coverage with at least 100 Gy was reached in 21-120% of the tumor volume for tumors 7 to 9. For tumors 4 to 6, the thresholdable values varied strongly between the tumors, so little reliance can be put out of these values for quantitative investigation. Moreover it is unclear if the calibration function was properly calibrated for these tumors. Some annotations should be taken into account considering the quantitative data analysis in general. First, the dose kernel used for the dose calculations, originates from the dose kernel for SPECT analysis. SPECT images have a relatively low resolution especially compared to the µCT images. The interpolation of the SPECT kernel to be applicable to the small voxel sizes of µCT causes an inaccuracy, especially in the high dose regions of the kernel. The difference between the original SPECT resolution, 4.7x4.7x4.7 mm, and the resolution of the 60 mm FOV µCT scans, 0.12x0.12x0.12 mm, is a factor of over sixty thousand. For the 40mm FOV scans with voxel sizes of 0.08x0.08x0.08 mm, this resolution is over a two hundred thousand times smaller, compared to the original SPECT resolution, and changes the dose point kernel into a sphere with value 1 and a radius of 3.8 mm in ImageJ®. This is not an accurate estimation for the dose decline from the microsphere to its surroundings. (**Figure 61**, in **chapter 8**) This problem can be solved by generating a new Monte Carlo simulation of the radiation particles distribution, and converting this simulation into a dose point kernel suitable for µCT resolutions. Also, a different software program should be used to convolve the dose point kernel over the activity per voxel images, because ImageJ® can only work with integers in its 3D matrix, which results in the afore mentioned sphere with a limited variation in the value of the kernel for high resolutions. A different, but

smaller, inaccuracy of the used method for HoMS dose volume distribution values for tumor coverage is that the values of the dose distribution volume that are related to the tumor volume are not necessarily restricted to the radiated volumes located inside the tumor area. If a dose volume extends beyond the tumor margin, it is still considered in the tumor coverage relation and hence may overestimate tumor coverage to some extent. The best estimation of the tumor coverage would be acquired when the dose volume can be linked solely to the tumor volume, and the tumor coverage estimations only apply to the radiated tumor volumes. Finally, the agarose HoMS concentration line used for the holmium concentration calibration curve contained concentrations up to ±20 mg microspheres/ml. For further research, a concentration curve of for example up to 50 mg/ml would necessitate less extrapolation for the high holmium concentrations found locally, and would therefore be more accurate. Furthermore, the agarose samples can be made in duplicate or in triplicate, for a higher reliability of the calibration curve.

A remarkable finding of the qualitative evaluation of the dose distribution was that some tumors showed a well extended distribution, but these areas sometimes contained a too low local holmium concentration, to provide this area with a sufficient dose, above 100 Gy in this study (as displayed for tumor 9 in **Figure 24**). Most important for the total dose were the large clusters containing a large part of the injected microspheres. In these areas local doses exceeding 1000 Gy were encountered. This gives an unequal distribution of the total dose over the whole tumor and can affect the treatment outcome negatively. When considering the 50 Gy dose distribution, the tumor coverage data are more promising, because in this case the areas covered with many small clusters with lower local holmium concentrations, would be included in the tumor coverage estimations as well. A total tumor dose of 50 Gy is too low for microbrachytherapy, where the intended tissue dose ranges from 200-1000 Gy over the whole tumor.[70] On the other hand, 50-70 Gy is the maximum total tumor dose, which can be achieved with external beam radiation, often related with severe damage of the surrounding tissues[92] and therefore a whole tumor coverage with at least 50 Gy is not low by itself. However, the added advantage of (micro-)brachytherapie is the use of much higher radiation doses with less side effects. The improved dose coverage when considering a 50 Gy versus 100 Gy threshold, is most probably due to the inclusion of low HoMS concentration areas. Increasing the injected HoMS amount or raising specific activities will allow these areas to also receive an adequate dose coverage, without changes in the distribution pattern. Another possibility for the low dose values in the areas with an extended holmium distribution and therefore sometimes lower holmium concentrations is the thresholding induced underestimation of the number of voxels containing holmium, as already described in chapter 4 for conventional CT. How much the modeled dose area is affected by underestimation versus inadequate HoMS distribution versus inadequate injected HoMS quantity remains to be investigated.

Based on the qualitative and quantitative data one would advocate for multiple injections in the centre of the tumor in order to cover the whole tumor area, these injections will spread

more equally over the tumor centre and will form a sheet of microspheres near the vital tumor borders. However some tendency seems to exist for microspheres to accumulate at the tumor edge where the needle penetrated the tumor, and has created a tract of low resistance. Therefore multiple injections should probably be placed in the tumor center, penetrating the tumor surface at different sites to enhance HoMS and dose coverage of the whole tumor. If injections are placed in the outer layers, more injections will be needed to cover the whole vital tumor border because the microspheres will remain locally around the injection site. Using this injection method, one should also take extra care to avoid leakage of microspheres next to the tumor, with higher risk of leaking radioactivity to other organs.

Chapter 6. Image guided administration of holmium microspheres

Summary

Background: Intratumoral injections with radioactive holmium microspheres is a potential new treatment for non-resectable solid tumors. However, after intratumoral holmium injection, not every part of the tumor is covered sometimes. Uncovered areas receive a too low radiation dose for effective treatment of these areas and are therefore believed to be a cause for tumor recurrence. Therefore this study aims to develop a method to monitor and visually guide intratumoral holmium injection towards these uncovered areas.

Methods: The possibilities of MRI and CT guided holmium administration were investigated. Different phantom models were developed to elaborate needle visibility and traceability, for MRI guided needle placement. Four Vx2 rabbit carcinomas were injected with non-radioactive holmium microspheres under MRI guidance, evaluating several scan settings to develop a MRI guided treatment protocol. For this purpose a MRI and CT compatible needle aiming and fixation device was developed. CT guided holmium administration was investigated as an alternative for MR guided injection.

Results: Because of the large field disturbances of stainless steel on MRI, titanium needles should be used for MR guided injections. Needle placement and intratumoral HoMS injection were detectable using near-realtime MRI imaging. The needle fixation device improved aiming and image-guided HoMS injections. CT guided injections using the needle fixation device is possible, but had weak tissue contrast as a disadvantage.

Discussion MR guided needle administration was possible, but the treatment procedure is still time consuming and further improvements of the injection protocols are required to make this injection method clinically operable. CT guidance is possible, but MRI guidance is more favorable, due to its better tissue contrast.

Conclusion: An MR guided intratumoral HoMS injection technique enables proper 3 dimensional visualization of the tumor, a controlled intratumoral needle placement, and visual monitoring of the resulting HoMS distribution and is therefore promising for the improvement of intratumoral holmium treatment. Further investigation and fine-tuning of the technique is required to make this method suitable for clinical use. CT guidance is a possible alternative for MRI guided HoMS injection.

Keywords: Holmium; internal radiation therapy; microbrachytherapy; magnetic resonance imaging; magnetic resonance guidance; distribution; dosimetry

Introduction

Cancer is a very common disease nowadays, with multiple treatment options. At the moment a focus to more local therapy strategies can be observed[4] in order to reduce the adverse side effects of for example systemic chemotherapy, external beam radiation

therapy, or wide surgical excision. Examples of these local therapies are HIFU, chemoembolization, brachytherapy, microbrachytherapy and radioembolization. For the last two local therapies, small radioactive ^{166}holmium microspheres ($E_{\beta,max}$=1.84 MeV, $t_{1/2}$=26.8 hrs, maximum tissue penetration 8 mm) are available.

These particles are used for radioembolization of liver malignancies in humans,[40] and are experimentally used for intratumoral injections in veterinary patients with non-resectable solid tumors[67]. Intratumoral HoMS injections in veterinary patients are at this moment placed 'free hand' and the intratumoral holmium distribution is not evaluated directly after injection. In this way certain tumor areas may remain undertreated because of an inadequate HoMS distribution over the tissue which can be a possible reason for tumor recurrence. In order to detect tumor areas with inadequate holmium content it would be desirable to visualize the microsphere distribution after injection. Furthermore, after detection of uncovered areas, the treatment method would also greatly benefits from the possibility to guide needle placement towards the uncovered areas and to retreat these areas. Moreover, image guided needle placement will allow for the injection of deeper tissue structures.

Therefore, the possibilities for image guided needle placement and holmium injection were elaborated in a Vx2 carcinoma model. An experiment was set up in order to relate intratumoral needle placement to the resulting observed HoMS distribution pattern and to elaborate the possibilities for precise targeting of HoMS injections inside the tumor. MRI and CT were investigated as possible image guiding techniques. MRI guided needle placement was investigated *in vitro* and in an *in vivo* Vx2 model and the possibilities of CT guided injections were investigated in a literature search and on an euthanized rabbit.

Materials and Methods

Agarose and chicken breast model

Prior to the animal experiments, phantom experiments with 2% agarose gel with 0.002% manganese chloride and chicken breast as tumor models were conducted in order to investigate the feasibility of MRI to guide needle placement. In the agarose phantoms, different needle types, stainless steel, 27G, 23G, 22G, 20G, 19G and 18G (BD™ Regular Bevel Needles, New Jersey, Canada), and titanium, 22G (MRI Chiba biopsy needle, Somatex, Teltow, Germany), were investigated for their needle artefact and tip accuracy.[93] Moreover different needle angles, towards the magnetic field, 89°, 80°, 65°, 36° and 2°, were investigated for their effect on the needle visibility and needle artifact on different MRI settings.[70, 93] Moreover the image guided approach was tested on chicken breast embedded in agarose gel.[93]

MR guided intratumoral injections in a Vx2 rabbit carcinoma model

For these experiments subcutaneous Vx2 carcinomas on the hind limbs of New Zealand White rabbits were injected under MR guidance with HoPLLA microspheres. For a

description of the tumor model and the preparation of the microspheres one is referred to **chapter 2**. The general treatment procedure was as follows:

1. The rabbits were anesthetized and put in a lateral position, with the tumor facing upward on the scan table of a 1.5T whole body MR scanner (Achieva, Philips Healthcare, Best, The Netherlands). The anesthetized rabbit was fixated to the table, to immobilize the rabbit. F**igure 33**, displays the MR scanner during treatment.

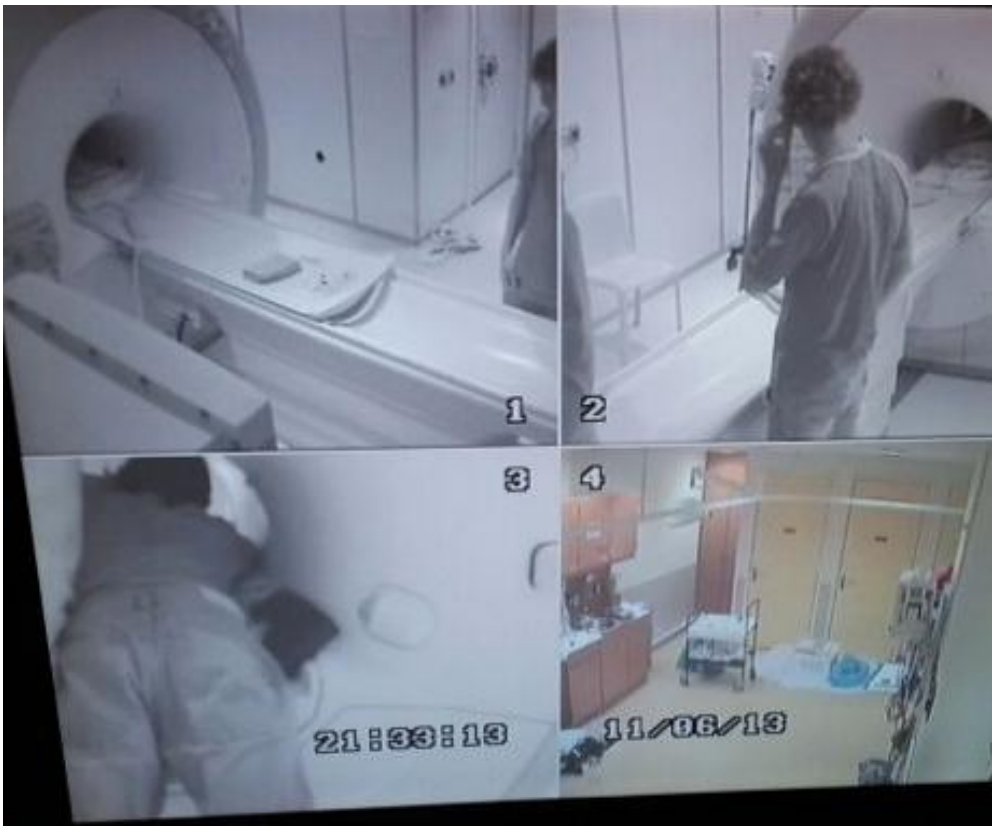

Figure 33 overview of the experimental set up during the MRI guided experiments

2. From tumor 6, the needles were filled up with suspension fluid before tissue penetration, to avoid air artifacts in the tissue. For these two tumors, 6 and 7, the hanging drop method was used prior to syringe connection, if the needles were localized at the right position.
3. Needle stabilization was evaluated for the manual injection without other stabilization devices, an agar mold placed over the tumor (**Figure 34**), and for a custom developed MRI/CT compatible needle fixation device (**Figure 35**)
4. Needle trajectory was determined based on 3D_UTE scans.
5. Needles were placed under MRI guidance into the tumor, using 2D_UTE scans.
6. After proper needle placement, the syringes were connected and the HoMS were injected under 2D_UTE scan guidance.
7. After the experiments the rabbits were euthanized with an overdose of pentobarbital. (**Table 1)**

The first rabbit obtained two tumors, tumor 4 and 5. Tumor 5 was first covered with a 2% agarose, with 0.002% manganese chloride, mold for needle track determination. (**Figure 34**) The desired injection site and needle track were determined on 3D_UTE scans. The tumor was approached through the agarose, with a 22G titanium needle (MRI Chiba biopsy needle, Somatex, Teltow, Germany) surrounded with a 20G catheter, under the guidance of real-time dynamic 2D dual-plane free induction decay (FID) scans, settings (FOV 192x192 mm, scan matrix 128x128, slice thickness 6 or 8 mm, repetition time 3.5 ms, echo time 0.8 ms). For tumor penetration another 22G titanium needle was used. Holmium injection was visualized using the same 2D scan settings. The spatial distribution of the microspheres was investigated using 3D gradient echo scans (FOV 128x128x128 mm, matrix 128x128, slice thickness 1.0 mm, repetition time 4.4 ms and echo time 0.34 ms.). A second injection was placed in this tumor, using the same protocol, however, this injection went next to the tumor, due to hand instability of the researcher.

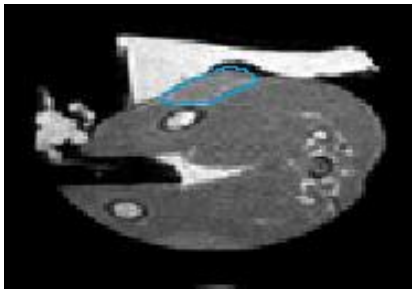

Figure 34: Tumor 5 with the agar mold on top of it. Tumor area indicated by the blue line.

The second tumor, tumor 4, was injected free hand. Using the researchers finger, the injection site and needle angle were determined on real time 2D scan, settings as described before. Microspheres were injected after needle localization. The distribution of the microspheres was investigated on a 3D_UTE_koosh_mFFE scan (FOV 128x128x128 mm, matrix 128x128, slice thickness 1.0 mm, repetition time 4.4 ms and echo time 0.34 ms.)

For the third tumor, tumor 6, a 5% agarose mold with 0.002% manganese chloride, was used for better needle stabilization. Preferred injection site and trajectory were determined on a 3D_UTE_mFFE scan. A catheter was placed in the agarose towards the tumor under real-time 2D_UTE scan guidance (settings as previously described). A titanium needle filled with suspension fluid, was placed through the catheter in the tumor. Using the hanging drop technique, the syringe was connected and microsphere injection was recorded with 2D_UTE scans. Microsphere distribution was investigated using 3D_UTE_koosh scans. Hereafter, the agarose mold was removed and a free hand injection was placed in the tumor under MR-guidance. A third injection was also placed free hand and in a tumor location with little microspheres present, for this injection microcoils were placed, allowing for a more precise microsphere distribution estimation.

For the fourth tumor, tumor 7, a MRI-compatible needle fixation device was designed.[70] (**Figure 35**) The rabbit was put in a lateral position and the device was placed over the rabbit, with the needle fixation tube around the tumor. First anatomical reference scans were

made, for example a T2W_TSE_proflinear (FOV 160x48x160 mm, matrix 160x154, slice thickness 2.0 mm, repetition time 2177 ms and echo time 90.6 ms), for tumor size determination, and a 3D_UTE scan was made for base R2* value determination (FOV 128x128x128 mm, matrix128x128, slice thickness 1.0 mm, repetition time 19.3 ms and 5 echo times 0.41 ms, 2.04 ms, 3.66 ms, 5.29 ms, and 6.91 ms). The first needle, filled with suspension fluid was placed on the skin and a 3D_UTE scan was made in order to determine the right injection position. When the needle was at the right location the height adjuster was lowered until the determined depth of 0.5-1.0 cm was reached. However, in this way it was not possible to penetrate the skin, so therefore the height adjuster was initially lowered further in order to allow for needle penetration of the skin with a higher force. In this way, the needle could pass the skin and could be placed in the tumor. Needle location was checked on a 3D_UTE scan. Using the hanging drop method, the syringe containing the microspheres was connected to the needle and the microspheres were injected.[70] A 3D_UTE scan was made in order to visualize the microsphere distribution after one injection. Hereafter 2 more needles were placed, following the afore mentioned procedure, with the extra lowering of the height adjuster in order to be able to penetrate the skin. Needles were placed at a half centimeter depth. Syringes were attached using the hanging drop method and microspheres were injected. A 3D_UTE scan was made after injection. Finally 2 more microsphere injections were placed as described before. Afterwards the device was removed and again TSE and UTE scans were made, with the settings described before. After the scan procedures, MR based holmium quantifications were made of this tumor, as described in chapter 3. The local holmium concentrations were converted into local radiation doses and these were displayed in a dose map of the tumor. (**Figure 36**)

Figure 35: Left two figures, needle injection with the needle fixation device in an experimental set up. Right figure, schematic drawing of needle fixation device.

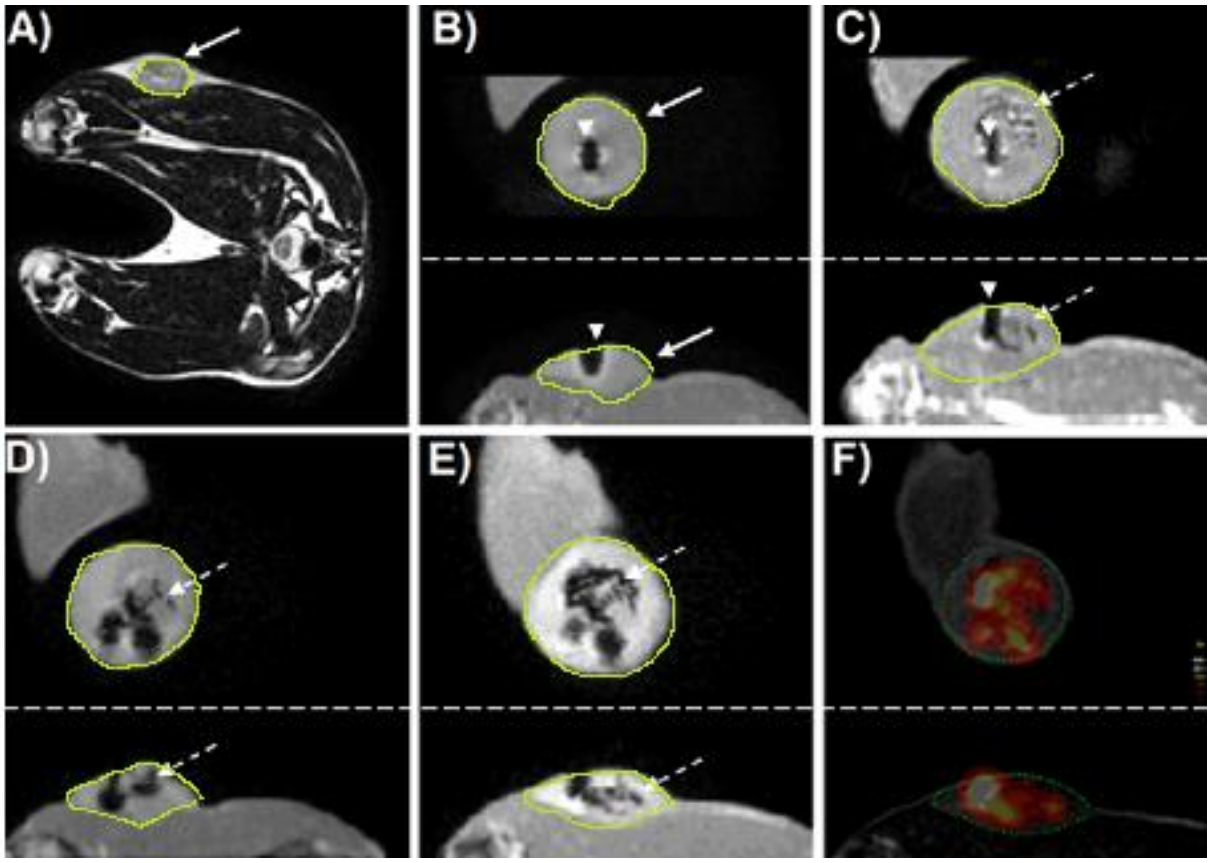

Figure 36: Treatment protocol of tumor 7. A) Anatomical overview of the rabbit's hind legs and tumor (white arrow) before treatment, transverse plane B) Placement of first needle. Upper image: coronal plane through tumor, lower image: transverse plane through tumor The needle (arrowhead) is placed inside the tumor (arrow) C) Ho-MS distribution after first injection (striped arrow) with the needle still in the tumor (arrowhead) D) Ho-MS distribution after injection at 3 sites (striped arrow) E) Ho-MS distribution after injection at 5 locations (striped arrow) F) Estimated dose distribution image after injection at 5 locations. Gray areas remain insufficiently irradiated. (Tumor indicated by green lines)

CT as an alternative for the MRI guided administration

In order to find an alternative for the MRI guided administration, CT guided administration was considered. The characteristics of CT were compared to those of MRI, based on a test using the needle fixation device on an already euthanized rabbit to test the injection protocol and a literature search on contrast agents for CT.

Results

The phantom experiments, with the chicken breast and agarose gel, showed that stainless steel needles, even the thinnest ones, are not appropriate for MRI guided holmium administration, because the resulting needle artifact is too large. This, and the needle tip cannot be localized accurately, because the variance is at least 6mm. Titanium needles are appropriate for MR guided purposes, because the needle tip accuracy is better, around 1mm and the caused artifact is smaller.[93] The needle artifact changes with the needle angle towards the magnetic field. The artifact increases with increasing angle and is at its maximum when perpendicular to the magnetic field (**Figure 37**).[70] On the contrary, when the needle is placed parallel to the magnetic field the image of the needle shaft sometimes completely disappears, the needle tip accuracy is highest for this position however.[93] Real time needle guidance was shown to be possible in a chicken breast embedded in agar.

(**Figure 38**) In the same model the HoMS distribution was visualized during injection. (**Figure 39**)

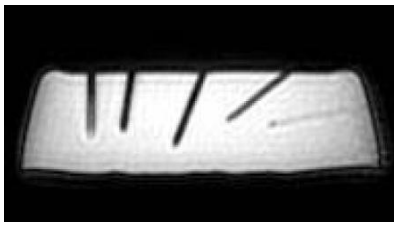

Figure 37: Insertion of titanium needles in an agarose mold under varying angles. 3D_UTE_koosh scan. Magnetic field is directed from the left side of the image to the right side of the image.

mri guided naald injectie in kipfilet.avi

Figure 38: MRI guided needle injection into a piece of chickenbreast embedded in agar (2D_Dual_UTE_8mm scans)

microsphere injection in chicken breast.avi

Figure 39: microsphere injection in chicken breast under MRI guidance (2D_Dual_UTE_8mm scans)

Manual needle placement has the advantage that it does not require specific equipment and that the injection method is straightforward. It was however difficult to keep the needle stable at the same position using this method. This caused one injection placed manually to be injected next to the tumor.

The agarose mold provided a clear surrounding for the determination of the needle trajectory (**Figure 37**). However, an agarose mold also has disadvantages. The agarose has to be kept at 60°C in order to keep it liquid. However, it cannot be applied on a live animal at this temperature. Therefore, it has to be cooled down to 43°C before it can be applied at the bare skin. However, when the agarose reaches temperatures below 40°C it starts to solidify. For needle stabilization, an agarose concentration of at least 5% is required, because lower concentration will not provide enough strength to hold the needle. However, higher concentrations of agarose make the gel less manageable and makes straight needle insertion difficult. For a good skin attachment of the agarose, a large area needs to be shaved thoroughly, which can make it time consuming, and can be undesirable if the animal has to survive the experiments. Moreover, the agar mold makes it impossible to fixate the tumor that lies subcutaneously, which sometimes leads to pushing the tumor away during needle placement. This may cause air to slip under the agar mold which interferes with needle visibility. All in all the agarose mold is not practical for use for needle fixation purposes.

The needle fixation device turned out to be useful for the fixation of different amount of needles. It can position needles and can keep these needles fixed in the same position for a longer period of time. Furthermore, the design of the device also partly holds the tumor in a fixed position so it will not move away during needle insertion. An extra advantage of the device is that Perspex acts as a shield for β-radiation from the holmium microspheres. Needle insertion into the tumor was possible, but was difficult through the intact skin.

CT guided holmium administration has a few advantages and a few disadvantages, compared to MRI. Advantages of CT are that CT does not require agarose gel or comparable substances for needle track visualization, because the needles provide contrast to surrounding air and tissue. Moreover, the needles do cause smaller artifacts as observed in MRI (**Figure 40**), CT acquisitions are in general a lot faster compared to MRI acquisitions, CT is cheaper and does not require special MRI compatible equipment, and CT imaging is easier to perform and interpret and therefore easier to learn for the researcher. Disadvantages of CT are the X-ray exposure of the patient. Real time imaging of free hand needle placement, as done using MRI, would lead to an undesirably high X-ray exposure of the researcher.[94] Moreover CT has a lower sensitivity for HoMS[27] and CT provides little tissue contrast and it is therefore more difficult to link the needle placement to the exact tumor location. Possibilities for contrast enhanced CT in order to image the needle placement and the microsphere distribution in relationship to the tumor are limited because CT contrast agents only cause a temporarily enhanced tumor contrast, during the vascular phase. After the vascular phase, tissue contrast declines for a prolonged period, the interstitial phase, because contrast agent concentrations inside the interstitial space increases to equal the plasma levels. During the final phase, the excretion phase, the contrast agent is cleared from the blood and tissues by renal excretion. Because these last two phases take a considerable time, over a hour in rabbits for most commercial available contrast agents, the tissue contrast is reduced over a long time period.[95-105] Moreover, due to the presence of the contrast agent in the interstitial space the holmium microspheres will be harder to visualize, because both cause higher tissue attenuation.

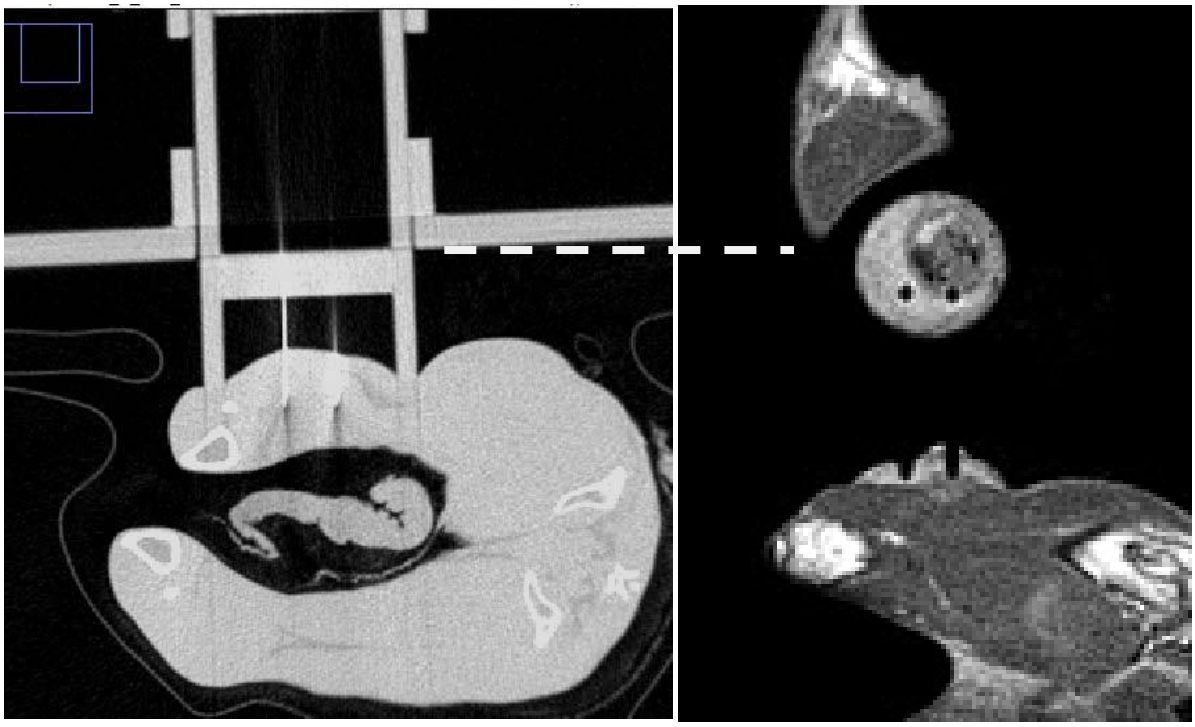

Figure 40: The insertion of 2 needles, using the needle fixation device. Left image shows the insertion on CT, the right image shows the injection on MRI, upper image coronal plane, lower image transverse plane through the tumor

Discussion

For MRI guided experiments titanium needles should be used, because stainless steel needles provide too much artifact on the MR images. Needle artifacts may be a problem if the needle has to be guided to a precise location, because it makes the needle placement more inaccurate. The effect of the artifact on the accuracy depends on the symmetry of needle artifact. If multiple needles have to be placed next to each other, the needles are best injected more parallel to the magnetic field otherwise the different needles cannot be distinguished from each other. If only one needle has to be injected at the time, the needles are best injected more perpendicular to the magnetic field, because the tip accuracy is then better.

During the MR guided *in vivo* experiments, an agarose mold for needle trajectory visualization and needle stabilization, provided many difficulties, of which some could not be overcome easily. Therefore an agarose mold is not very practical for MR guided needle injection. The needle fixation device was more useful (**Figure 35**). It is possible to fixate multiple needles with the device at a preset distance from each other and reduces the radiation exposure of the investigator. However, it is not perfect yet and during some other experiments (**Chapter 8**) the device also showed some disadvantages. As already encountered during injection of tumor 7 it is difficult to penetrate the skin using this device and image guidance is needed in order to visualize the location of the needle after injection, because needle location after injection is unclear after blind injection, using this device. Moreover, it is difficult to fixate the tumor, while using this device. The Perspex tube itself is not always able to fixate the tumor sufficient, especially if the tumor is small, the skin lies loosely above it and the tumor is pushed away with the needle, needle insertion in the tumor is difficult. Manual fixation while using the device is not possible, due to the surrounding Perspex. The use of a needle fixation device will however be necessary for MRI and CT guided experiments and treatments, because it is not possible to keep a needle stable at the same position for several minutes. Furthermore, manual fixation of the needle and tumor will cause a high radiation exposure for the practitioner. Therefore, improvements to the needle fixation device should be made. These should include a more adjustable needle position, because at the moment the tumor has to be located directly under the device, parallel to the height adjuster in the middle of the device, and the injection angle and location of the needle tube cannot be adjusted. Secondly, the device should provide a possibility to fixate the tumor during the injections, to ease needle injection and to keep the orientation stable throughout the protocol, during different injections. For this purpose, a vacuum system is considered as a possible option. At this time the MRI guided experiments were time consuming and the experiment protocols should be further optimized. This should however not discourage one from investigating MRI guided holmium administration, because we showed that MRI provides the possibility to combine guided needle placement and dosimetry of a tumor, allowing for the guidance of new injections to areas specifically lacking microspheres and thus radiation.

If required, CT guidance can be used as an alternative for MRI guidance, but it will not be the favorable option, due to the tissue contrast disadvantages and the extra radiation exposure. With some adaptations to the scan protocol CT contrast agents may be used to increase the tissue contrast temporarily. This phase of the contrast enhancement should be scanned and used as an overlay for the next scans. However, the contrast agents will still influence the visibility of the microspheres after injection, which is the largest disadvantage because the CT dosimetry method described in **chapter 4** will be influenced by the higher tissue attenuation. Another alternative is not using contrast agents, but this will not show the tumor borders and therefore the dose maps will be more difficult to interpret.

Image guided administration was possible and gives an added value to the treatment procedure, because it allows for the detection of uncovered tumor areas and directed needle placement. For use in a clinical situation, special radiation-safety precautions should be taken in order to reduce the risk of HoMS contamination of the area and to reduce the radiation exposure of the patient and clinician. More research after this injection method should be conducted.

Chapter 7. Distribution of radioactive holmium microspheres in two cats with lingual squamous cell carcinoma after intratumoral injection

Summary

Background: At the University Clinic for Companion Animals, cats with oral squamous cell carcinoma have previously been treated with radioactive holmium microspheres. Treatment outcomes are varying, and are believed to depend on the dose distribution inside the tumor, and therefore HoMS distribution. The goal of this case study was to investigate the HoMS distribution and dosimetry in two SCC of the tongue that became available after treatment due to death of one cat directly after treatment and another cat 2 months after treatment.

Methods: Two feline lingual squamous cell carcinomas were treated with radioactive holmium microspheres and were excised after euthanasia of the cat. One tongue was excised directly after injection, the other two months after HoMS treatment. After formalin fixation the tumors were scanned by means of conventional MRI and CT and µCT. On the CT and µCT images, dosimetry calculations were conducted.

Results: Conventional CT and MRI provided an estimation of the intratumoral microsphere distribution. µCT allowed for a more detailed HoMS distribution evaluation. The (µ)CT based dose distributions show coverage of almost 100% of the tumor areas, due to the radiation range of holmium.

Conclusion: This case study applies previously described techniques to evaluate the microsphere distribution and dose distribution after intratumoral HoMS injections in two feline patients. µCT allows for precise HoMS spatial distribution imaging and was performed together with conventional CT and MRI, which are applicable in the live animal and may be used after (or during) holmium treatment in a clinical setting. The resulting dose distribution data can be used to detect untreated areas. Using these advanced imaging-based HoMS dosimetry methods may enable subsequent targeted administration of additional HoMS at those undertreated areas in clinical patients in the near future.

Keywords: veterinary solid tumors, oral squamous cell carcinoma, cat, holmium treatment, microbrachytherapy, microsphere distribution, dosimetry, dose distribution

Introduction

Cancer is a common cause of human death with 8 million deaths worldwide a year[1], but its impact on domestic animals cannot be understated either, with an estimated one in four cats and dogs dying from cancer or cancer related disease[106]. Tumors in the oral cavity account for almost 10% of all feline neoplasia, and over 60% of these neoplasia are oral squamous cell carcinoma. These tumors often have a poor prognosis, due to their local aggressiveness and infiltrative behavior[107]. Treatment options for these tumors are limited, due to the location of the tumor, often on the ventral side of the tongue near the

frenulum,[107] and consist of surgery and fractionated radiotherapy, with treatment outcomes, expressed in median survival times, ranging from 5.5 months, to 14 months[107-109].

Because the previous combination is not always possible, a new treatment option for these tumors has been developed at the Utrecht University Clinic for Companion Animal Medicine, the intratumoral injection with radioactive holmium microspheres ($E_{\beta,max}$=1.84 MeV, $t_{1/2}$= 26.8 hrs, tissue penetration 8 mm). Complete response rate, a decrease of tumor volume of over 70% or sufficient shrinkage for subsequent surgical removal, has been 43%. Median survival time has been 78 days overall, and 382 days for the group with complete response.[43] Varying treatment outcomes have possibly been caused due to differences in holmium distribution. Therefore, a study after the HoMS distribution has been conducted in an animal tumor model (C**hapter 2**). However, it is not clear to what extent the distribution in this tumor model mimics the distribution in spontaneous occurring tumors in veterinary patients.

Therefore, two feline lingual squamous cell carcinomas, treated with radioactive HoMS, were scanned *ex vivo* by means of conventional MRI and CT and preclinical µCT, in order to visualize the HoMS distribution inside these tumors. Besides the microsphere distribution, dose calculations were made in order to evaluate the treated area.

Case introduction

The first cat, used in this thesis, had a sublingual oral squamous cell carcinoma, with abundant tissue necrosis and ulceration on the base of the tongue (**Figure 41**). Tumor volume was 4.8 cm^3 on pre-treatment contrast enhanced CT. This tumor received 116 MBq, divided over approximately 102 mg HoAcAc-MS, injected in 17 injections. This patient suffered from respiratory complications during anesthesia and was euthanized after an unsuccessful reanimation attempt, directly after the HoMS injection procedure. After euthanasia, the whole tongue, including the supporting structures and the os hyoideum, were removed and stored in 4% buffered formaldehyde.

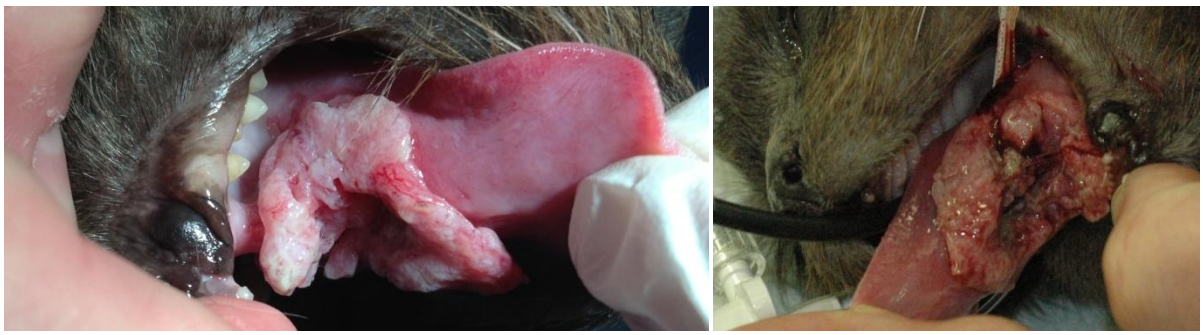

Figure 41: The first cat of this thesis at the time of first presentation at the university clinic (left) and prior to HoMS treatment (right), showing a large mass at the ventral side of the tongue, diagnosed as a oral squamous cell carcinoma.

The second cat had a squamous cell carcinoma on the right side of the tongue, with a large ulceration site at the tumor location, growing into the bottom of the jaw (**Figure 42**). Tumor volume was 4.4 cm^3 on contrast enhanced CT. This tumor received 227 MBq, divided over 155 mg HoAcAc-MS, divided over 5 syringes. After treatment, this cat initially showed some

tumor regression, especially in the massive part of the tumor. However after a while, the ulceration continued and tumor recurrence was present on the tumor edges, near the jaw side of the tumor. Because the clinical condition of the cat deteriorated, the cat was euthanized 2 months after holmium injection. After euthanasia the tongue was removed and stored in 4% buffered formaldehyde.

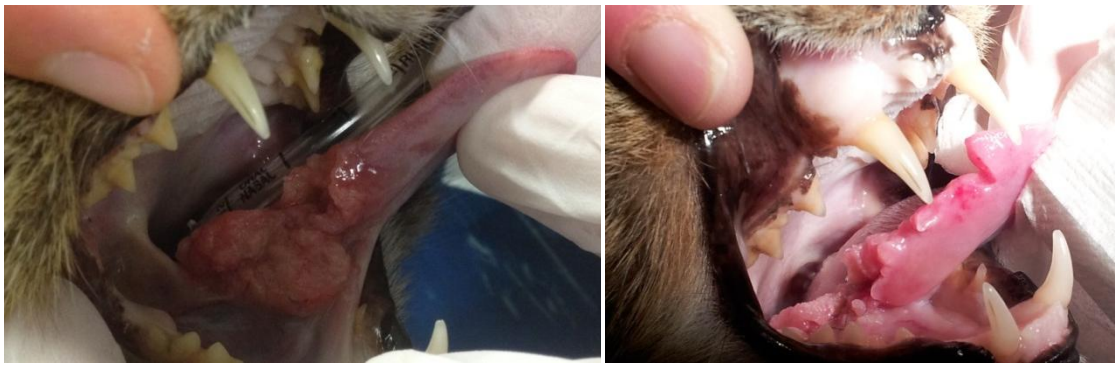

Figure 42: The second cat of this thesis, prior to holmium treatment (left) and a month after treatment (right), showing a infiltrative mass at the right side of the tongue, diagnosed as a oral squamous cell carcinoma

Ex vivo imaging of the tongues after formaldehyde fixation

Both tumors were scanned *ex vivo* on a conventional CT scanner (Symbia T16 SPECT/CT Imaging Systems, Siemens Medical Solutions USA, Hoffman Estates, USA), a conventional 1.5T whole body MR scanner (Achieva; Philips Healthcare, Best, The Netherlands) and a preclinical µCT scanner (IVIS | Quantum FX, Caliper Life Sciences, Hopkinton, USA). For all scan sessions, the tumors were taken out of the formalin and washed with water. For the (µ)CT scans, the tumors were surrounded by air and for the MRI scans, the tumors were surrounded by a MnCl solution of 30 mg/L. Settings for the *ex vivo* CT scans were 130 kVp, 25 mAs, slice thickness 1.5 mm, voxel size 0.74x0.74x0.7 mm. Settings of the 3D_UTE_mFFE MRI scans were FOV 128x128x128 mm, matrix128x128, slice thickness 1.0 mm, repetition time 19.3 ms and echo times 0.41 ms, 2.04 ms, 3.66 ms, 5.29 ms, and 6.91 ms. Settings of the µCT were 90 kVp, 160 µA, scan time 2 minutes, slice thickness 0.118 mm and voxel size 0.12x0.12x0.12 mm, FOV 60 mm.

The first cat

The tongue of the first cat was sutured to an arrow shaped Ministeck® plate, with the right side attached to the plate (**Figure 43**). In the sample, the supporting structures of the tongue are also included and can be used as reference points, like the os hyoideum. The tumor is located at the ventral side of the tongue.

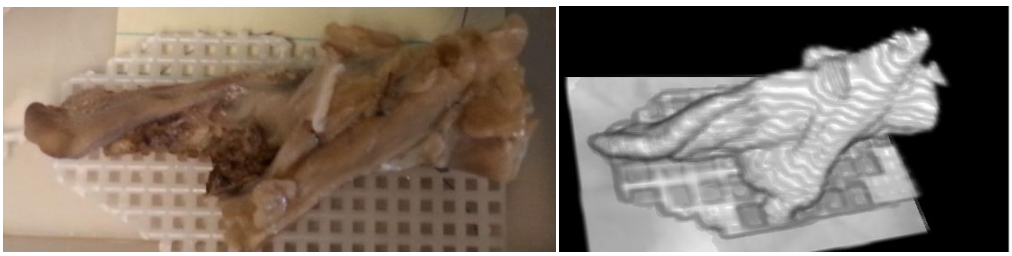

Figure 43 Photograph of the setting, left, and 3D CT image of the setting right.

Conventional CT and MRI

On conventional CT and MRI, a large part of the tumor seems to be covered with microspheres (**Figure 44)**. On both the CT and MR images, the tumor borders cannot be distinguished. The geniohyoideus muscle on the ventral side of the tongue is not covered with HoMS, but the presence of some HoMS near the tumor area cannot be excluded, due to the little tissue contrast. Based on the 2D CT and MR images, some small areas inside the tumor seem to lack holmium, especially near the tumor surface, but overall the HoMS cover most of the tumor area.

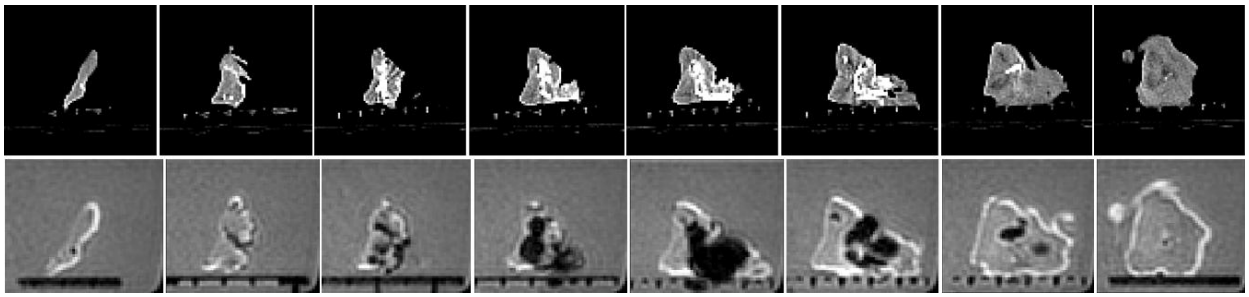

Figure 44: Upper images, CT slices of the tongue of the first cat. White areas contain holmium microspheres. Lower images, 3D_UTE MRI of the some tongue. Black areas inside the tissue contain holmium microspheres. Left side of the images is the dorsal side of the tongue, while the right side of the images contains the ventral side of the tongue. Slices are taken from rostral to caudal.

CT based dosimetry was conducted as described in **chapter 4**. Specific activity of the holmium in the microspheres was first set at the same value used for the Vx2 tumors, 13.6 MBq/mg for HoPLLA-MS and was then set at the value agreeing with the activity injected during microsphere treatment, 0.47 MBq/mg, 27 times lower than the fictive activity used during the rabbit experiments. (**Figures 45 and 46**) If the high specific activity is used, a large part of the tumor area is covered with a radiation dose exceeding 2000 Gy and on some locations the whole tongue section seems to receive a radiation dose above 100 Gy (**Figure 46**). The real activity level, provides more accurate distribution images, with some parts of the normal tongue tissue surrounding the tumor receiving a lethal radiation dose. Based on these images it is estimated that the complete tumor area receives a sufficient radiation dose, although it remains difficult to indicate the exact borders of the tumor on CT (**Figure 46**).

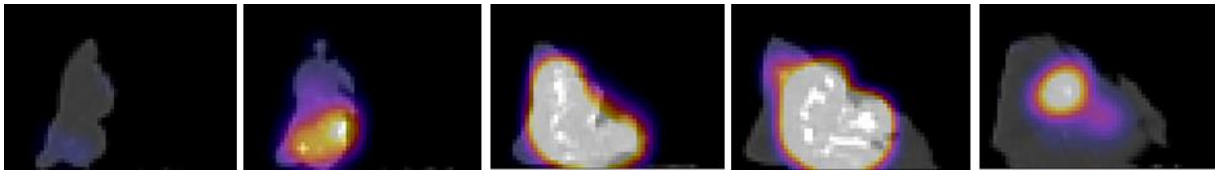

Figure 45: CT based dosimetry of the tumor of the first cat, slices are taken from rostral to caudal. Specific activity 13.6 MBq/mg (based on HoPLLA-MS) Clearly visible blue areas receive at least 100 Gy, white regions receive over 2000 Gy.

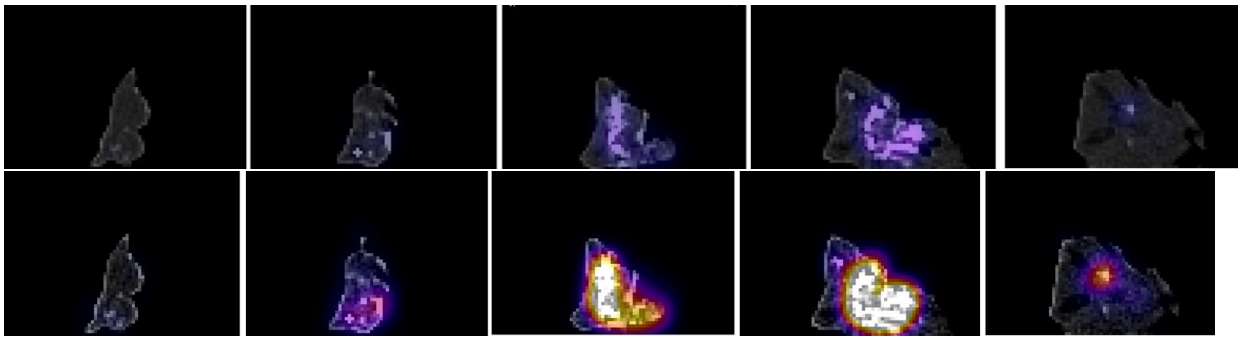

Figure 46: CT based dosimetry of the tumor of the first cat, slices from rostral to caudal. Specific activity is 0.47 MBq/mg (based on HoPLLA)= 1.14 MBq/mg HoAcAc, this is in comparison with the original injected dose. Upper series, have the same contrast values as image 31, blue areas over 100 Gy, white values, not available, would contain over 2000 Gy. Lower series have a range between 0 Gy to 200 Gy, blue starts just above 0 Gy, everything white receives over 200 Gy.

µCT

Qualitative analysis of the µCT images shows an extended HoMS distribution, with clusters of different sizes. Many smaller clusters are present throughout the whole tongue. In the tumor area in the centre of the sample, larger clusters are found. Some of these clusters seems to extend over a large distance and to surround some tissue structures (**Figure 47**, orange circle). In the same figure (**47**) the centre of the tumor area is lacking microspheres. **Figure 48** displays the 3D distribution of the microspheres in relation to the tongue tissue.

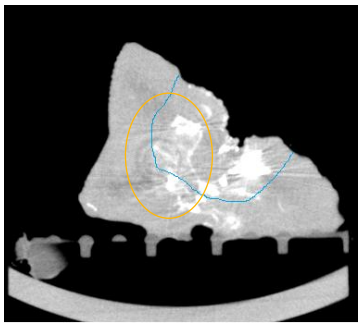

Figure 47: microsphere distribution in the tumor area. Left side of the image shows the dorsal side of the tongue, the right part is the geniohyoideus muscle on the ventral side of the tongue. In the centre part the tumor is located, with clearly microspheres present. On the left side of the tumor area, the microspheres seems to distribute around some tissue structures (orange circle). Estimated tumor area indicated by blue line.

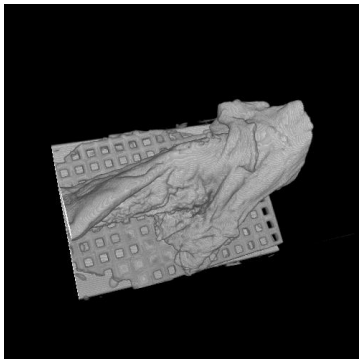

Movie_Charly tongue.avi

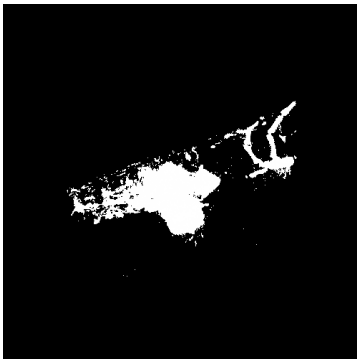

Movie_Charly holmium.avi

Figure 48: 3D distribution of the holmium microspheres in relation to the tongue tissue. on the right side the os hyoideum is visible

µCT based dose calculations were also performed. The image processing was the same as for the Vx2 tumors (**chapter 5**). The procedure is shortly displayed in **Figure 49**, with first the original µCT image, secondly only the voxels containing a minimum concentration holmium

microspheres are displayed with the HU value of the voxels transformed into a local holmium concentration. This holmium concentration is transferred into a local activity, using the specific activity of the microspheres, 1.14 MBq/mg HoAcAc-MS, 0.47 MBq/mg if this value is transferred to a value for HoPLLA, which calibration curve was used. Over the local activity, a convolution with the dose kernel of holmium was calculated, resulting in a radiation dose per voxel. This resulted in a dose map over the tongue (**Figure 49**, right image). This dose map shows a radiation dose for most of the tumor area, but some parts of the tumor area, especially towards the ventral surface of the tongue sometimes seem to lack radiation dose. (**Figure 50**)

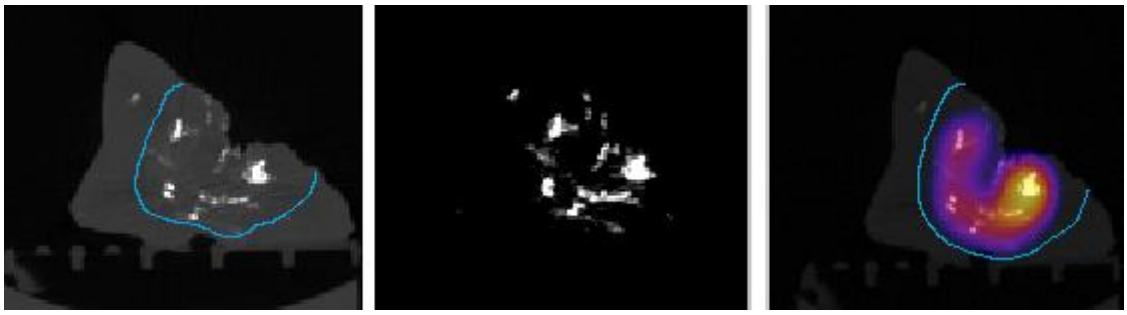

Figure 49: Dose distribution in the tongue of the first cat. Left image is the original µCT image, the middle one the holmium distribution in mg/ml and the right image displays the dose distribution in relation to the tongue (Blue areas receive at least 50 Gy, white areas over 400 Gy. (Blue lines indicate the estimated tumor areas)

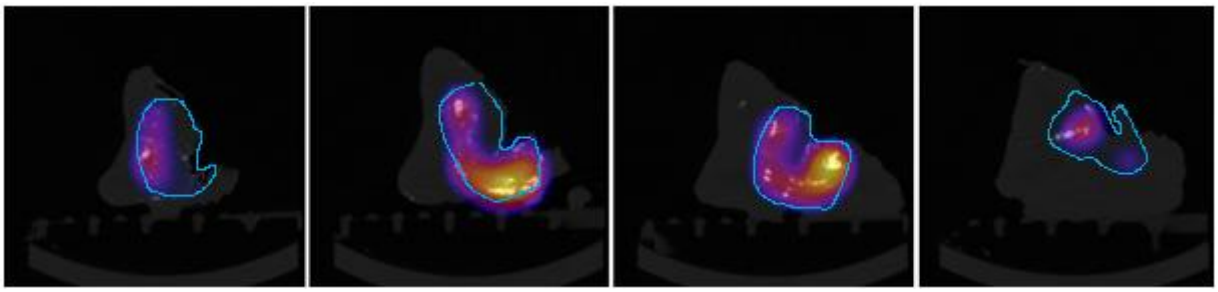

Figure 50: µCT based dose distribution in the first cat, with the real injected specific activity. blue areas contain at least 50 Gy, white areas over 400 Gy. Light blue lines indicate the estimated tumor borders.

The second cat

The tongue of the second cat was also sutured to an arrow shaped Ministeck® plate. The tumor is located at the right side of the tongue. At the tumor location, the tissue shows prominent ulceration **(Figure 51**).

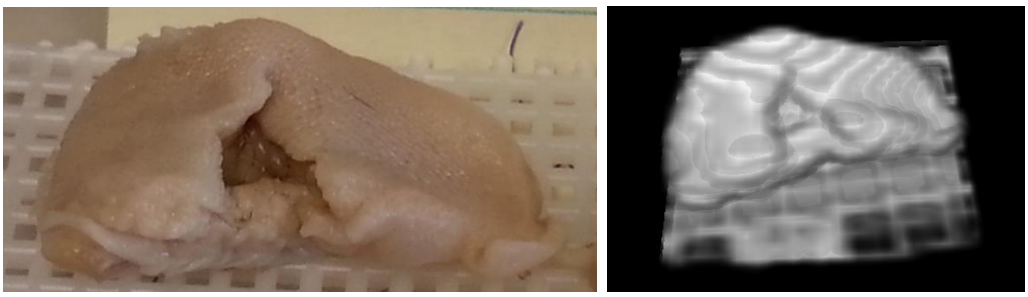

Figure 51: The tongue of the second cat. Left image a picture of the fixated tongue. Right image, a 3D reconstruction of the CT images

Conventional CT and MRI

Both CT and MRI show HoMS presence in a large part of the sample. It is however not possible to link the microsphere distribution to the exact tumor architecture, because the tumor borders are not visible on both scan types. On MRI it is even difficult to distinguish the general tissue borders. Furthermore, MRI shows large artifacts due to the present holmium, making a precise HoMS distribution description impossible. On the CT scans the artifact is smaller, but the resolution is low, so a precise description of the microsphere distribution cannot be given either. (**Figure 51**)

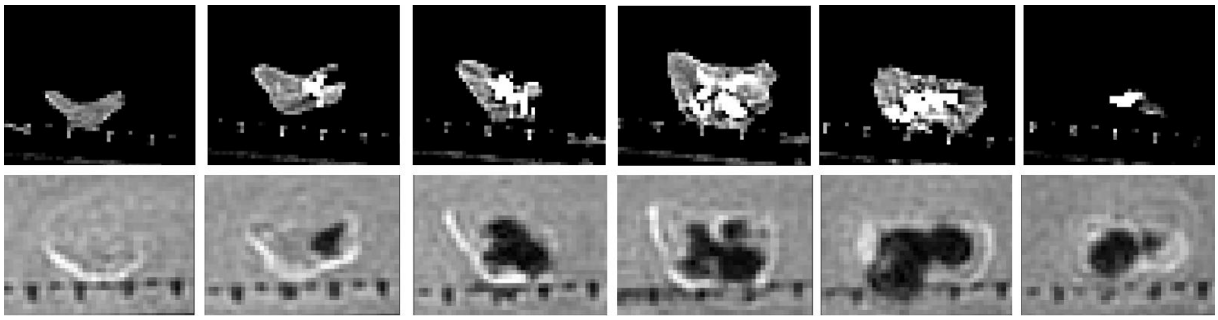

Figure 52: Conventional CT and MRI of the tongue of the second cat. Slices are taken from rostral to caudal, the tumor is located at the right side of the tissue.

CT based dosimetry was conducted on the tongue, as described before (**chapter 4**). Specific activity was first considered at the same value used for the Vx2 tumors, and then the dose distribution for the used activity was determined. The specific activity used for the Vx2 tumors, provides a dose distribution, with many areas receiving a dose of 2000Gy or even higher, almost the whole tongue seems to receive a high radiation dose, using this activity, indicating that this specific activity is probably too high for clinical use. When considering the dose distribution of the used specific activity 1.49 MBq/mg HoAcAc, the whole tumor area seems to receive radiation, most of the time exceeding 200Gy. At the most caudal part of the sample, some holmium is still present. This may indicate that the transition between supporting structures and the tongue/tumor was not taken out and the distribution of this area cannot be investigated for its radiation dose distribution. (**Figure 53 and 54**)

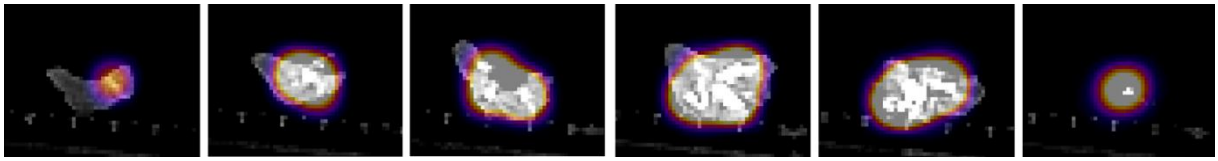

Figure 53: CT-Dosimetry of tongue of the second cat. Specific activity of microspheres at 13.6MBq per mg (based on HoPLLA-MS). slices taken from rostral to caudal. Blue areas contain at least 100 Gy, white areas receive over 2000 Gy.

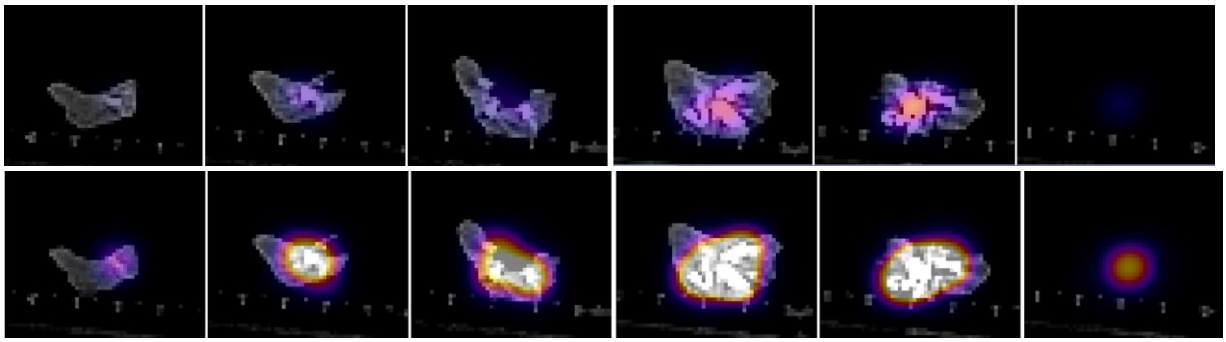

Figure 54: CT based dosimetry of the tongue of the second cat. With a specific activity of 0.53 MBq (based on HoPLLA-MS) = 1.49 MBq/mg HoAcAc-MS. Upper series display the same color values for varying doses as in image 39, range 0-2000 Gy, blue starts around 100 Gy, white areas contain over 2000 Gy. The lower series display a range between 0 and 200 Gy. Blue area starts a bit above 0 Gy, the white areas receive over 200 Gy.

µCT

Qualitative analysis of the µCT images shows that a large part of the tongue seems to be covered with microspheres. An area with very little holmium is observed near the ulceration site of the tumor (**Figure 55**). Smaller holmium clusters are present throughout the whole tongue. Larger clusters are present towards the middle of the tongue, at the tumor site and are most probably the injection locations. At these injection locations, smaller and larger areas are covered with varying microsphere concentrations. Sometimes, some less radio-dense areas are present inside these large clusters, advocating for the presence of some denser tissue structures impermeable for HoMS (**Figure 55**).

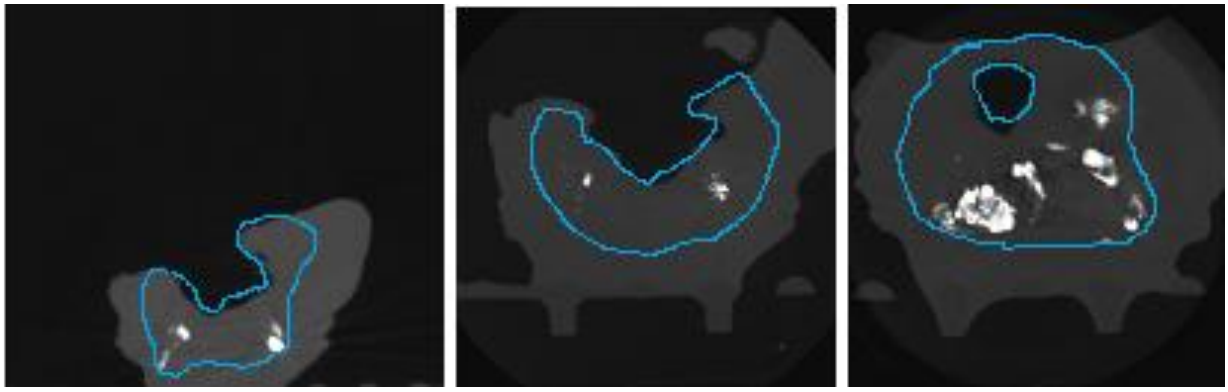

Figure 55: Ulceration at the location of the tumor, this area seems to lack microspheres. The right image displays varying cluster sizes. Left image 60 mm FOV, middle and right image 20 mm FOV. (Estimated tumor area encircled in light blue)

µCT based dosimetry was also conducted, using the specific activity injected in the tumor, 1.49 MBq/mg HoAcAc. It is difficult the relate the observed microsphere distribution to tumor coverage, because the tumors borders are unclear and some areas near the dorsal surface of the tongue seems to lack radiation dose, but it is not clear if tumor tissue is located here. At the ulceration site, where on HoMS distribution images, some slices with only little holmium are present, a dose over 100 Gy seems to cover the whole area (**Figure 55**). The radiation range of holmium is apparently sufficient to cover this area. (**Figure 56**)

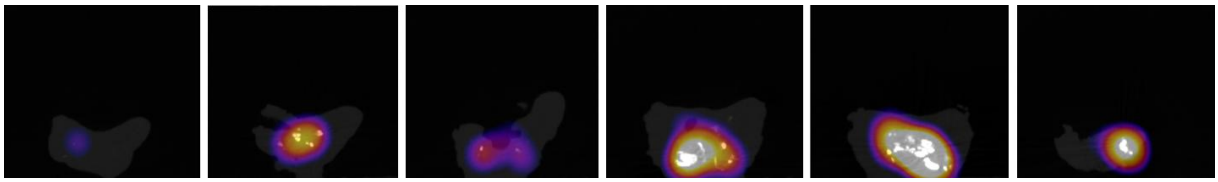

Figure 56: µCT based dosimetry using the real injected specific activity, blue areas contain over 50 Gy, white area contain over 400 Gy.

Discussion

The two feline tumors investigated here are useful for the comparison of the different imaging and dosimetry methods for clinical applicability, because during this study, the same HoMS amounts and activities were used, as would be used for future (experimental) treatment in (veterinary) patients. Based on MR and CT distribution and CT based dosimetry, the tongue tumors seem to be covered sufficiently with holmium microspheres for complete tumor irradiation. The µCT based dosimetry shows a more localized dose distribution, with some areas in both samples with a doubtful coverage, although some tumor tissue is expected at these sites.

Because the feline squamous cell carcinomas are treated with an 8 times higher amount of microspheres compared to the Vx2 tumors, and with microspheres which have the possibility to contain a 2.6 times higher holmium content, compared to HoPLLAMS,[35] the total amount of holmium contained by the feline tongues is much higher than for the Vx2 tumors. The feline lingual tumors are therefore very suitable for the investigation of the effect of higher local holmium concentrations on the varying imaging techniques. On MRI the caused artifact becomes very large and only a rough description of the distribution can be given. On the CT images the distribution of the microspheres is clearer compared to the MRI images, because the CT signal remains more localized at the voxel containing the microspheres, although some dispersion, white stripes around the high holmium concentrations, may be visible on the CT images. Compared to the Vx2 tumors, the high holmium concentrations in the feline tumors, favors CT for MRI, because this imaging method is better able to deal with high holmium concentrations. µCT has proven itself very useful for the precise holmium visualization, because this imaging technique allowed for high resolution scanning. If the dose point kernel is optimized for the µCT images and a more advanced software program is used, the µCT data can also be of use for detailed dosimetry. (µ)CT has the advantage that the signal increases with an increase of the holmium concentration and that it is less sensitive for signal disturbances. A disadvantage of µCT is the inability to use this method in the live patient, therefore conventional scan techniques are suggested as the best post-treatment imaging methods in the live patient. Precise µCT-based dosimetry can however be used to validate conventional imaging techniques for dosimetry. Of these conventional images, CT provides the best estimation of the microsphere distribution in veterinary patients, because it is better able to deal with high local holmium concentrations at the moment. The *ex vivo* imaging in general has the disadvantage that it is not possible to distinguish the tumor borders. This problem is often present for *ex vivo* CT imaging, and in a lesser extent for *ex vivo* MRI. However, the large

artifact caused by the high amount of holmium in these tissue samples also interferes with a proper tissue distinction on MRI, which will most probably also be true for *in vivo* MR imaging.

In the near future, an optimized CT-dosimetry model may enable veterinary patients to be scanned directly after intratumoral HoMS injection on a conventional CT scanner and to image the microsphere distribution and determine dose coverage. This information could then be used during the same treatment session to inject more HoMS at specified tumor locations to improve dose distribution. It will be interesting to also investigate the treatment response in these cases and to investigate if the improved dose coverage does indeed provide a better treatment response. At the moment no linkage between tumor response and HoMS distribution can be made, because neither follow up data nor initial distribution data are available for the two investigated samples. A general disadvantage of the *ex vivo* imaging is that it is only possible to investigate the microsphere distribution after the microspheres have emitted most of their radiation. However, it is not clear at the moment how the microspheres distribute over time and therefore how the HoMS distribution was at the time of treatment and thus was the initial dose distribution. Moreover, most of the time, the tumors available for *ex vivo* imaging will be of patients with disease progression, showing only one side of the story. For these reasons *in vivo* imaging is preferred over *ex vivo* imaging, because it can be used on the live animal, and it allows for initial biodistribution and dose investigation.

Chapter 8. Comparison of different imaging techniques and general discussion

8.1 Introduction

During the study on the biodistribution and dosimetry of holmium microspheres after intratumoral injection, different imaging techniques have been used (**chapters 3 to 5**). In this chapter the different imaging techniques are qualitatively and quantitatively compared with each other in order to point out the most appropriate imaging technique for different purposes. For this comparison the results of the previous chapters are used. Moreover, this chapter will give an overall picture of the found results, encountered difficulties and will sketch the future perspectives.

8.2 Qualitative comparison of the distribution on the different imaging techniques

In order to visualize the differences between the different imaging techniques in sensitivity and resolution, slices of the various scans of tumor 9 are displayed next to each other and compared for their utility in the description of the microsphere distribution. (**Image 57-60**)

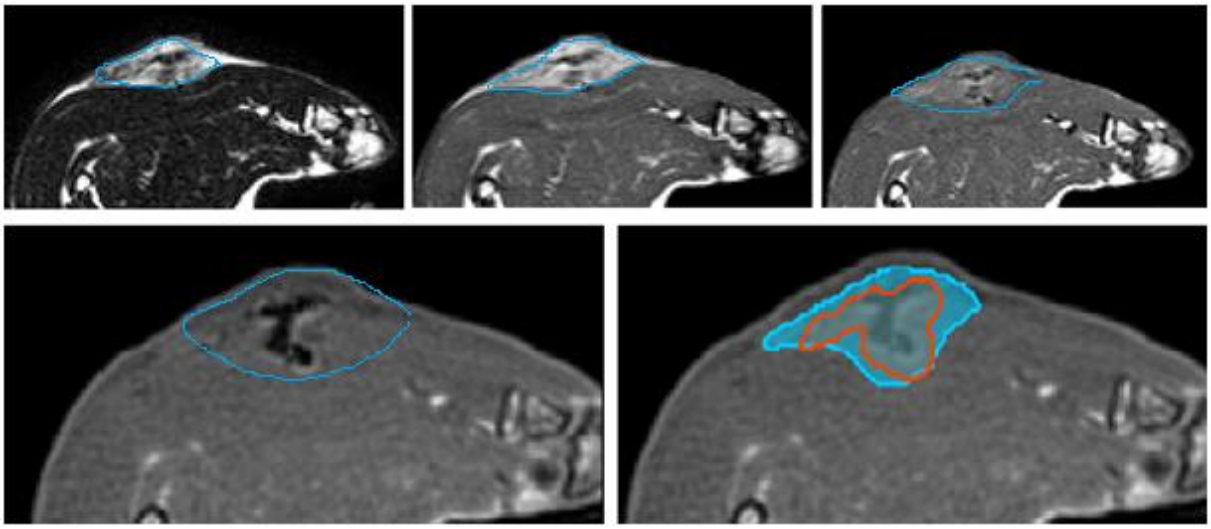

Figure 57: MR scans of tumor 9, T2_TSE_proflinear, T2_TSE_proflowhigh, T1_TSE_proflowhigh, 3D_UTE_koosh without and with 100 Gy dose line. Tumor area indicated with light blue

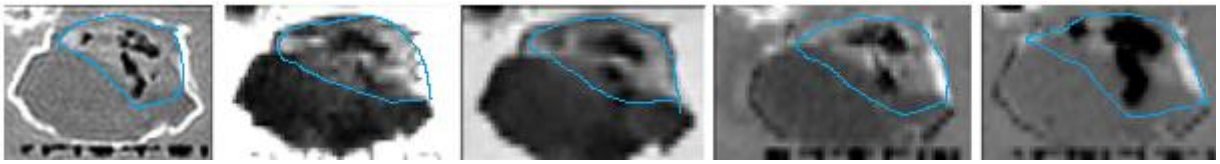

Figure 58: *Ex vivo* MRI of tumor 9, 3D_UTE_koosh. T2W_TSE_proflinear. T2W_TSE_proflowhigh. T1W_TSE_proflowhigh. T1W_GE. Tumor area indicated in light blue.

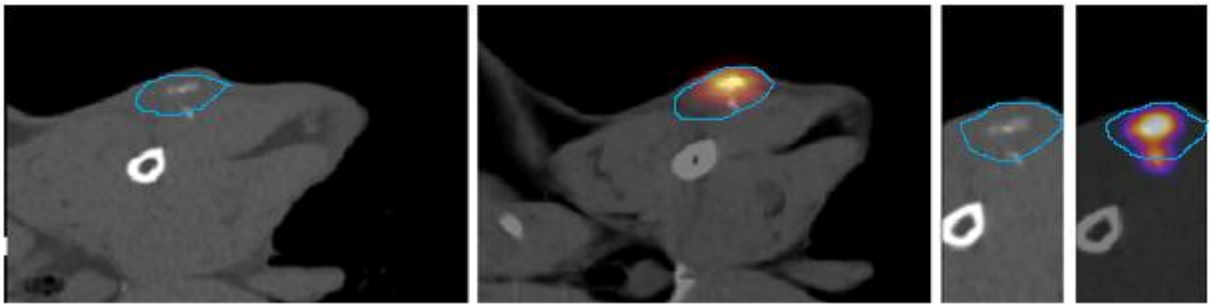

Figure 59: *In situ* CT and combined SPECT/CT, coronal section of the hindlimb of the rabbit, with tumor 9, last two images show *in situ* CT based dosimetry of the same section. Tumor area in light blue.

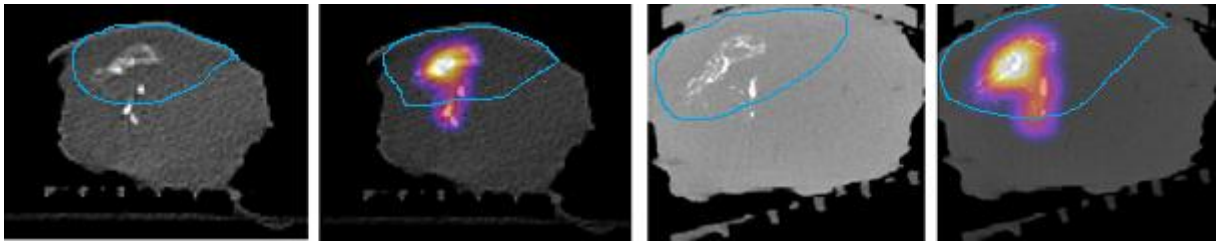

Figure 60: *Ex vivo* CT, left; and µCT, right. First the original CT image and secondly the dose distribution image of intratumoral HoMS distribution are displayed. (Tumor area in light blue)

In general, all imaging methods show resemblance in the microsphere distribution. µCT provides the most detailed image of the spatial HoMS distribution and is therefore very suitable for studies of the fine microsphere distribution after intratumoral injection and the mechanism behind this distribution (**Image 60**). When the research question deals more with the dose coverage throughout the tumor, a less fine imaging technique, conventional MRI or CT is also suitable, because the high dose area distribution does not change much for the varying imaging techniques, MRI and (µ)CT. This indicates that the small clusters may not affect the dose distribution images much, making very fine resolution scanning not necessary for efficiency predictions. Moreover, the conventional imaging techniques are more appropriate for protocol development for the clinical situation, because the conventional scanners are suitable for clinical use. Therefore, one should pick CT or MRI, depending on the research question, taking the following differences into account. *In vivo* MRI has a higher natural tissue contrast, compared to CT imaging, but this difference might partly be overcome by contrast enhanced CT. The sensitivity for holmium is lower for CT than MRI. This is especially visible in tumors with a widespread distribution, and therefore low local holmium concentrations, like tumor 4 (**image 61**). The lower sensitivity of CT for holmium microspheres has been described in *in vitro* and *in vivo* studies. [27, 83] During an *in vivo* study on radioembolization in pigs, it was even stated the sensitivity of CT would be too low for treatment dose distribution predictions.[83] However, we have developed a method, allowing for CT based dose distribution estimations, which shows resemblance to the MRI based dose distribution (**Chapter 4**, and **Image 57 till 60**). The high sensitivity of MRI might also be a disadvantage for MRI, because it makes MRI unfavorable for the imaging of high local holmium concentrations, because in this situation the microspheres form a large black spot, as seen in the two feline tongue tumors (**Chapter 7**). Another advantage of CT compared to MRI is that CT is able to distinguish microspheres from air, because they have

contrasting colors, while on MR images both are black. This makes 3D reconstructions of the microsphere distribution for CT easier than for MRI, because the areas containing microspheres can be extracted from the original stack by increasing the threshold value.

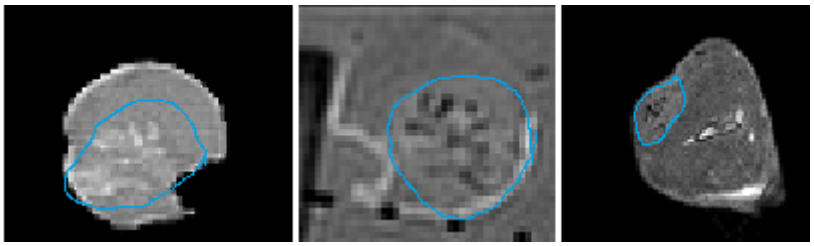

Figure 61: *Ex vivo* CT, *Ex vivo* MRI and *In vivo* MRI of tumor 4, displaying an area with low local holmium concentrations

During treatment or directly after treatment of a (veterinary) patient, it is desirable to already investigate the spatial microsphere distribution for the *in vivo* situation. For a clear tissue contrast, one can consider MRI, or contrast enhanced CT, because in a life patient it is possible to make pre-and post contrast scans. In the treatment of (veterinary) patients, very high HoMS amounts are found locally. In this occasion, one would prefer CT imaging, because this imaging method shows less HoMS induced artifacts and is therefore able to give a more detailed image of the HoMS distribution inside the tissue and contrast enhanced CT will allow for more tissue contrast. Subsequent, CT or MRI based dosimetry would allow for the detection of untreated areas, allowing for the selective treatment of these areas.

For *ex vivo* imaging, (µ)CT is preferred for MRI, because subjectively the *ex vivo* CT images are clearer, due to the tissue changes on MRI after formalin fixation, causing white artifacts making orientation more difficult. Moreover, the *ex vivo* MR imaging has the risk of false inclusion of air bubbles around the tumor in the microsphere distribution, the inability to conduct *ex vivo* MRI based dosimetry and the large artifacts for high holmium concentrations. µCT provides the most detailed microsphere description and with some adaptations to the dose kernel reliable dosimetry will be possible in the future, allowing for a very detailed description of the dose distribution.

Conventional SPECT imaging is considered as a suboptimal imaging technique for the estimation of the precise microsphere distribution, because of the low resolution in relation to the time consuming nature of SPECT. Moreover SPECT is unable to detect very low amounts of shunted activity towards other organs in an experimental setting (**Chapter 4**). For this purpose, the more sensitive TOBOR, twin crystal scintillation counter, can be used post-mortem in experimental studies, allowing for the determination of the exact amount of activity per organ. However, for detection of clinically relevant leakage of HoMS to distant sites in patients, SPECT is probably sufficient as has been demonstrated in liver radioembolisation patients.[80]

8.3 Quantitative comparison of the radiation dose on the different imaging techniques

The HoMS distribution volumes based on MRI and (µ)CT images are not comparable with each other, because of the different methods for distribution volume estimations. The dose distribution volumes should however ideally be the same for all methods and are therefore compared.(**Table 10**)

Unfortunately, only two tumors were available for MRI based dosimetry, making a quantitative comparison between different dose volume values of this technique and (µ)CT based dosimetry difficult. The qualitative dose distributions can however be compared. The general dose distribution pattern is comparable for all dosimetry methods. Remarkable are the higher local doses reached with (µ)CT based dosimetry, although theoretically an underestimation of the dose distribution was expected, because low holmium concentrations are disregarded on (µ)CT and therefore not included in the calculations.

The theoretical 100Gy dose distribution is comparable for the CT and µCT data (mean difference -12% for 3 tumors). This may have several explanations. First, very small microsphere clusters may contribute only little to the total received dose, because they contain a relative low activity.[65] Second, the dose kernel is not optimized for µCT imaging, with its fine resolution, causing an underestimation of the radiation dose near the centre of the kernel, due to the interpolations that had to be made (**Figure 62**). Moreover, the used software program was not able to use decimals in its convolution kernel. For this reason, the dose kernel for the 60mmFOV µCT scans consisted of only 6 values, 0-5. This leaves room for the improvement of the µCT dose distribution kernel, not taking off the value of the already described µCT based dosimetry.

Table 9: Comparison of the different dosimetry methods. (-) means that this data is not available for this specific tumor. The (0) for the CT dosimetry indicates that no thresholdable voxels were present or that the 100Gy is not exceeded

Tumor nr	Nr. Of injection sites	*In vivo* tumor volume (based on *in vivo* MRI) (mm^3)	Visual HoMS coverage as a % of tumor volume on *in vivo* MRI	100Gy dose coverage on *in vivo* MRI, based on MR dosimetry	100Gy volume compared to tumor volume (%) on *in situ* CT	*Ex vivo* tumor volume (based on *ex vivo* MRI) (mm^3)	Visual HoMS coverage as a % of tumor volume on *ex vivo* MRI	100Gy volume compared to tumor volume (%) on *ex vivo* CT	100Gy volume compared to tumor volume (%) on *ex vivo* µCT
1	1	1844	35.7	-	99.6	-	-	-	-
2	3	565	21.2	-	100.7	-	-	-	-
3	6	3436	18.8	-	44.4	-	-	-	-
4	1	9616	12.6	-	-	5439	19.9	0	-
5	2	1555	54.7	-	-	1395	25.2	75.8	-
6	3	2151	0	-	-	2334	18.7	80.3	-
7	5	4500	55.1	43	-	3637	36.2	116.2	119.9
8	1	336	6.3	-	0	756	3.6	26.7	20.8
9	3	9890	11.9	30	40.9	8907	13.4	37.4	30.5
Mean	-	$3.8^e3 \pm 3.6^e3$	24.0± 20.1	36.6±9.4	57±43	$3.7^e3 \pm 3.0^e3$	19.5±11.0	56±42	41±47

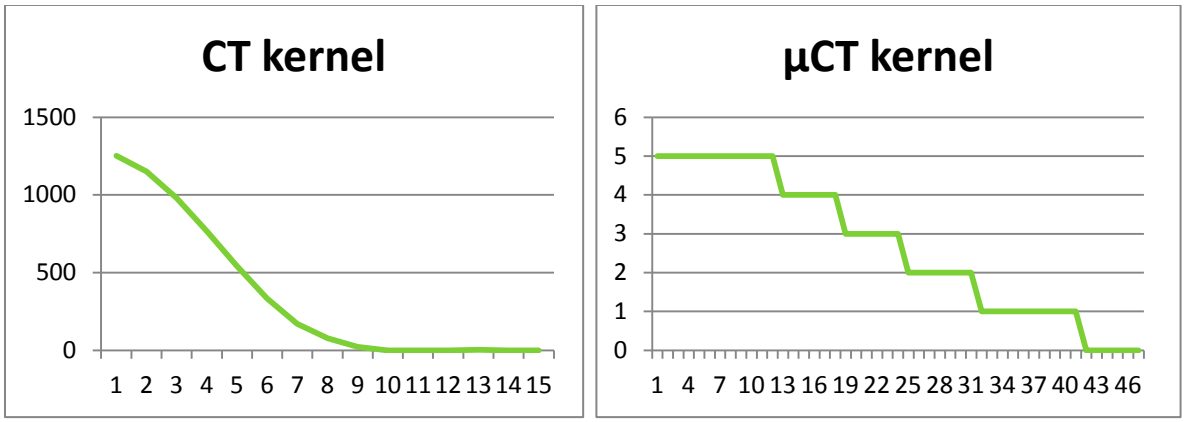

Figure 62: Effect of interpolation on the dose point kernel. The diagrams display the dose gradient for different kernels in one direction, this gradient is convolved in a 3D fashion over the local activity. Left diagram displays the dose kernel for the CT resolution, right diagram for 60 mm FOV µCT.

Differences in sensitivity for holmium of the varying scan techniques and the principles underlying the holmium quantifications for each technique, may explain the differences in observed absolute values for the HoMS dose distribution. During MRI based dosimetry, the size of the signal loss due to the field disturbing holmium, observed on T2*weighted images is expressed as the change in R2* values, by the formula $R2^*=R2^*_0+ (92.6\pm3.2)C[s^{-1}.ml.mg^{-1}]$, with sensitivity $92.6\pm3.2s^{-1}.ml.mg^{-1}$.[27] During our CT based dosimetry calculations the local HoMS concentration is calculated by the difference in HU value, by the formula $CT=CT_0+(5.9)C[HU]$, with a sensitivity around 5.9 HU $ml.mg^{-1}$. For µCT the formula was $CT=CT_0+(8.6)C[HU]$, with a sensitivity around 8.6 HU $ml.mg^{-1}$ (**chapter 4**, and Seevinck et al.[27]). This shows that MRI is 15.5 times more sensitive for HoMS than CT, and 11 times more than µCT. CT has been shown to be more sensitive for an increase in HoMS concentration for ascending HoMS concentrations, compared to MRI.[27] Because of the signal induction and high sensitivity of MRI, this imaging method has the tendency to show large black areas for high holmium concentrations, while on CT the holmium signal remains more localized. For both imaging techniques, the quantification of holmium concentrations exceeding ±20mg/ml are based on extrapolation based on calibration curves of agarose gels with rising HoMS concentration. Both imaging techniques, MRI and (µ)CT are prone to dose underestimation, but due to several reasons. First (µ)CT is not able to detect HoMS concentrations under a specific value. This leads to the exclusion of a certain amount of HoMS from the calculations. For example, for the latest tumor (9), *in situ* CT displays in this method 66% of the total injected holmium amount, comparing the total injected amount to the integral of the CT stack displaying the mg per voxel. *Ex vivo* CT displays in this method 57% of the total injected holmium amount and on µCT 32% of the injected holmium amount is visible. The displayed amount of HoMS depends on the present local microsphere concentrations and will vary per tumor. Therefore CT will give an underestimation in the low concentration areas. Second, the MRI based dosimetry method will give an under estimation of the high concentration areas, due to the inability to quantify very high local HoMS concentrations. During intratumoral injection and especially during treatment situations (**Chapter 7**), locally very

high microsphere concentrations are present, containing much of the total activity, this would advocate for CT based dosimetry in intratumorally injected tumors, because this method is more able to deal with these high concentration. For radioembolization, the local concentrations are lower, making MRI based dosimetry more suitable for this treatment. (**Table 10**)

Table 10: Different performance features for the different image acquisition possibilities. Presence of formalin fixation tissue changes on MRI are unfavorable.

Performance feature	SPECT	µSPECT	MRI	CT	µCT
Sensitivity	++	++	+-	-	-
Detectability	++	++	+-	-	-
Resolution	--	+-	-	+-	++
Anatomical reference	--	--	++	++	++
Changes on tissue visibility due to formalin fixation	--	--	++	--	--

8.4 Conclusions on microsphere distribution

This thesis has shown and compared different imaging techniques able to detect HoMS distribution. Moreover it has shown a new method for holmium dosimetry, based on (µ)CT images. The varying imaging techniques showed the same distribution patterns, making them all valid for the microsphere distribution investigation, with µCT being the gold standard, due to its high resolution and ability to measure high concentrations. To improve µCT based dosimetry, the dose point kernel should be calculated again for the high resolution of µCT. When this is done, µCT based dosimetry may be considered as the gold standard for the dose distribution, because it considers even very small microsphere clusters and shows the dose distribution in great detail. This recalculated dose point kernel may also be used to improve the kernels used for MRI and CT based dosimetry, because both originate from the same rough SPECT holmium dose point kernel.

Although the tumor coverage increased with every injection during the MR guided experiments, no difference between the number of injection sites can yet be made, if the total injected HoMS amount is equal, because the (dose) distribution volumes vary strongly between different tumors, independent of the number of injection sites, making the dose distribution unpredictable solely based on the number of injection sites. It did however become clear, that it is difficult to reach complete tumor coverage with a sufficient dose using blind injections, because the radiation dose is distributed unequally over the tumor, with large parts receiving less than the fictive 100Gy, while other areas receive over a 1000 Gy. This may be an explanation for the varying treatment responses in veterinary patients. In the two cats in **Chapter 7**, however a good dose distribution was observed, probably due to the higher number of injection sites in the cats, >15 sites.

The basic principle behind the microsphere distribution is probably the path of the least resistance in the tissue. This path depends on the injection site and the location inside the tumor. Towards the tumor centre, the interstitial fluid pressure increases,[90] injection in the tumor centre therefore may give a very wide distribution, while injection in the tumor

borders will remain more locally and distribute against/between the vital structure layers and basal membrane of the tumor. To confirm this hypothesis more tumors should be injected intratumorally and investigated by means of µCT. Furthermore, histopathology of the tumors already available would allow for linkage between the detailed 3D microsphere distribution, observed on µCT, and the tumor structure, visualized by means of histopathology.

Although an idea of the general HoMS distribution after injection inside the tumor tissue exists, it is still not possible to predict the microsphere distribution after intratumoral injection based on number of injections. Considering the individual variation of intratumoral HoMS distributions between tumors, one may conclude that a good estimation of HoMS distribution is not possible without post/peri treatment imaging of the microsphere distribution. Peri- or post treatment imaging would allow for the detection of untreated tumor areas, and chapter 6 has shown that it is possible to guide needle placement towards these areas and to selectively retreat these areas. Depending on the specific aims of the image guided administration, CT or MRI is preferred. MRI is preferred for its better tissue contrast, its higher sensitivity for holmium and the lack of X-ray radiation exposure for practitioner and patient. CT has however the advantage that it can better model the dose distribution after intratumoral injection in patients, because it can better measure high local HoMS concentrations, and the caused needle shaft artifact is smaller for CT, compared to MRI (Figure 39). For veterinary patients complete image guided treatment is maybe unaffordable for patient-owners for clinical application. However, a single CT/MRI scan after injection may be sufficient to determine the areas insufficiently covered with holmium microspheres, and to link this to its anatomical location and to use this anatomical location for retreatment of this area.

8.5 Consequences of the used methods and general problems encountered

During the conducted experiments, the research questions dealt with the HoMS microsphere distribution. However at the same time, some general aspects of the used method were encountered and will shortly be described here.

Tumor take rate

Not all inoculated tumors arose and some variation between the take rate of the three different original frozen Vx2 cell suspensions existed. (**Table 11**) Remarkable is that the 3rd cell line did well after inoculation from frozen cell suspension, but after the first transfer, tumor take rate decreased dramatically.

Table 101: Take rate different cell lines, during the whole experimental period 2012-2014

Cell line nr.	Rabbits	Intended tumor sites (nr.)	Take rate
1st cell line, frozen suspension	3	6	4 out of 6 → 67%
2nd cell line, tumor pieces from donor rabbits	3	6	4 out of 6 → 67%
3rd cell line, frozen suspension for donor rabbits	2	3	3 out of 3 → 100%
3rd cell line, tumor pieces from donor rabbits	8	16	2 out of 16 → 13%

The decreased tumor take rate during the latest experiments was very unfortunate because it took over 2-3 weeks before it could be clear if an inoculated tumor would arise or would not and the period between tumor inoculation in a donor rabbit and the treatment of an experimental tumor took over 6-8 weeks. Therefore the tumor take rate strongly influenced experiment progression. For our experiments it is unclear why the tumor take rate was so low, because normally tumor take rate using vital tumor pieces is reported to be around 60%[59] and previous experiences with this tumor model within the research group, using very small tumor pieces, were take rates over 90%,[61, 62] the same held for another research group using the same vital tumor pieces we did (data not published). It has however been stated that vital Vx2 tumor pieces and thawed, cryo-preserved cell suspension have a lower take rate compared to fresh Vx2 cell suspension and that vital tumor pieces show more spontaneous remission after inoculation, till a late stage of tumor development. Possible reasons for the lower take rate are higher numbers of dead cells in the tumor pieces, causing an immunization effect, stimulating an effective immune response and preventing outgrowth of tumor.[59, 60] However during our experiments the take rate of cryo-preserved cell suspension was 78%. Most probably differences with the literature and previous findings are caused by differing quality of the used tumor material. Furthermore, 4 inoculations with vital tumor pieces were placed in two rabbits who showed no tumor growth after the first injection, increasing the risk of a secondary immune reaction against the tumor cells.[56] In this case only one tumor arose. Furthermore, it was stated that the tumor does badly in subcutaneous connective tissue during the early development of the Vx2 tumor model,[56] possibly explaining part of the difference between the reported take rates up to 100% for intramuscular injection of cell suspension.[110] However, this statement is in contrast with other research showing take rates over 97% for s.c. inoculations.[61]

The use of different microsphere types

Different holmium microspheres, HoAcAc and HoPLLA, were used during the experiments. Because they both have the same particle size, a smooth surface, and are injected in the same way, it is expected that the distribution of both microsphere types will not vary considerable. A difference between these microspheres that should be taken into account is the difference in holmium content. HoAcAc microspheres contain 2.5 times more holmium compared to HoPLLA microspheres. This makes individual microspheres easier visible for the used imaging techniques, MRI and CT.[35] For dosimetry purposes this difference is unimportant however, because the mass attenuation coefficient for the microspheres on CT

and the r2* relaxivity on MRI, depend largely on the holmium concentration, the element responsible for the radiation.[35] The holmium amount injected per injection varied per injection, but this variation is comparable for the HoAcAc and HoPLLA microspheres, allowing for comparison between the two subgroups. No difference in distribution volume between the two types of microspheres was found during our research (**chapter 3**).

Injection methods

Some difficulties were encountered during the microsphere injections. Injections placed with the needle fixation device caused bleedings sometimes and due to the lack of fixation possibilities of the tumor and the flexibility of the needles, it was very difficult to place the needles properly inside the tumor, because, depending on the tumor, skin and tumor penetration were difficult till impossible. The difficulties during injection make the needle fixation device inappropriate for holmium injection without image guidance, because the needle location inside the tissue is unclear after needle insertion. Free hand injection using simple 23G hypodermic needles was easier and faster, compared to the injections with the device and the long, flexible 10cm 22G titanium needles. Another disadvantage of the titanium needles is the large death space of 0.15ml, requiring much suspension fluid, without microspheres, to fill this death space, if the injection of air has to be prevented.

Increase of the time between re-suspending of the microspheres and real microsphere injection, increases the risk of needle blockage due to early microsphere precipitation. Therefore, the syringes should be agitated vigorously prior to injection in order to achieve a homogeneous microsphere suspension and time till injection should be kept minimal, moreover a higher viscosity of the suspension fluid and smaller microspheres may increase microsphere suspensibility.[42] Injection of too much suspension fluid made tumor 8 leak holmium suspension after injection. An optimum for the amount of suspension fluid injected should be found, because too much suspension fluid will strongly increase tumor interstitial fluid pressure, increasing the chance of microsphere leakage out of the injection sites. Too little suspension fluid will hamper microsphere injection however, due to the high density of microspheres inside the fluid and the increased change of early precipitation, moreover it has already been shown that more suspension fluid will increase microsphere distribution.[111]

Radiation safety of the injection procedure

Because the microspheres are radioactive during tumor treatment in (veterinary) patients, the injection method should be safe and no activity should be spilled during the administration. For this purpose, all the used materials were measured for activity with a Na(Tl)-crystal γ-detector after the treatment procedure of tumor 8 and 9. For tumor 9, no detectable activity was found on the used instruments, only the used syringes and needles contained activity, displaying the safety of the injection procedure. Due to the many perforations, tumor 8 leaked activity. As a consequence, the sutures were placed in a contaminated area and the instruments used for the skin closure contained some activity therefore. These instruments were temporarily stored and could be used again after a few

days. No contamination could be detected around the working area and after removal of the disposable coverings. It was concluded that the administration of holmium microspheres is relatively safe, if injection hygiene is kept in mind and the necessary precautions are taken, like disposable coats and gloves for the researchers, working glasses and shielding of the syringes and tumor with Perspex during and after injection. Radiation exposure to the surrounding can be kept minimal with Perspex shielding and contamination of the treatment area and scan areas can be prevented or kept minimal by placing the rabbit in a large plastic box and covering the areas with sufficient absorbing materials.

Treatment safety for the patient

During a first test after the microsphere migration in one rabbit, this migration was minimal. 2 hours after intratumoral injection, only 0.5% of the total administered activity leaked to other organs, only detectable using a sensitive twin scintillation counter, and not on the γ-camera of a conventional SPECT. The other 4 rabbits investigated with SPECT 2-24 hours after injection, also revealed no visible organ shunting, indicating that if organ shunting is present, the quantity is low. The shunting values for holmium microspheres are lower or comparable to the tumor leakage of other radioisotopes used for intratumoral injection. Some shunting to the lungs is often observed in *in vivo* distribution studies.[18, 21, 22, 25] High amounts of lung shunting may be declared be the fact that the lung capillaries are the first small vessels the microspheres will encounter when they have shunted into the blood. After the intratumoral injection in internal organ tumors, like colon carcinomas and pancreatic carcinomas, some shunting to nearby vital organs, like the stomach, liver and intestines is also encountered sometimes. The spleen is sometimes also seen as a reservoir for some activity. Moreover, a part of shunted ^{188}Re will be excreted by the urine.[18, 20-22, 25, 112] Although our data are comparable to literature, a precise prediction of the quantity of leaked activity is difficult, because data of only one rabbit are available. During following experiments the activity in bone, should also be measured, because it is known that, like yttrium, holmium is a bone seeking element and accumulation is expected in this tissue.[16, 32] During the previous conducted experiments, no adverse side effects could be detected. These lack may be due the almost immediate euthanasia after intratumoral injection. Possible side effects of internal radiation therapy can be bone marrow suppression, weight loss, lethargy, ataxia, rhinorrhea, loose stool, abnormal urination, low body temperature, distention of abdomen, dehydration and ulceration of the injection site,[22] but none of these were encountered in the test animals till now.

8.6 Future perspectives

In this thesis a proof of principle for the further evaluation of holmium microsphere distribution after intratumoral injection is shown. In future experiments, the developed methods should be conducted on more Vx2 tumors, in order to be able to draw conclusions about the most optimal number of injection sites, to confirm spatial HoMS distribution hypotheses and to be able to estimate the mean amount of distant microsphere deposition after HoMS injection. In short the rabbits should be scanned by means of pre- and post-

treatment *in vivo* MRI in order to be able to conduct R2* based dosimetry, euthanized after post treatment MRI and scanned by *in situ* CT the same day. After *in situ* CT, the tumors should be excised and radioactivity levels should be measured. Moreover the intern organs, lungs, heart, liver, spleen, kidneys and intestines, and the femora/humeri should be removed, weighed and radioactivity levels should be measured using a twin scintillation counter and expressed as a percentage of the injected dose per gram tissue (%ID/g). More *ex vivo* MRI and CT scans should be made to compare the relationship between *in* and *ex vivo* scans and biodistribution observed on both types of scans. To improve the µCT based dosimetry, and CT/MRI based dosimetry in general, the dose point kernel should be calculated again, with new Monte Carlo dose calculations. Moreover, another software program should be used for the dose calculations on µCT, because ImageJ was only able to work with integer numbers in the dose point kernel, leaving room for further optimization. A new agarose calibration curve for (µ)CT quantification should be made in duplicate/triplicate and higher HoMS concentrations should be aimed for, to reduce the interpolation for high concentrations, and scanned at the settings used for the *in situ* scans and the *ex vivo* scans. In order to prevent microsphere clumps in the agarose, the microspheres should first be suspended in 2% Pluronic F-68 and put in an ultrasound bath for a few minutes. µCT data are especially useful for the investigation of the precise holmium distribution. If the µCT based dosimetry method is optimized and validated it may even be used to improve the MRI based dosimetry. Moreover, it is interesting to further investigate the possibilities for real time image guided administration, because it may even be more important to be able to do peri-treatment treatment adaptations based on the observed microsphere distribution, than to try to give an optimal number of injection sites, because the microsphere distribution, especially in spontaneous tumors, may be very dependent on the tumor architecture. Using image guided needle placement the injection location can be neatly determined and the distribution can be linked precisely to this position, moreover the needle placement can be guided to an area containing too little microspheres allowing for full tumor coverage with a sufficient radiation dose. For this purpose, several items could be developed: first the developed dosimetry methods should be incorporated in a computer program, automatically calculating the radiation dose over an indicated area. Second, this program might be linked to a computer-controlled administration device, guarding the needle exactly towards the location entered in the system. An automated mechanical administration device will reduce the radiation exposure of the practitioner and if it is linked to the dose maps, it can acquire full tumor coverage. During the development of such equipment, the dose calculations can be made manually and the needles can be placed using a manually adaptable needle fixation device. For the development of this device the following aspects should be considered: in order to make the device suitable for MRI, it should not contain any metals; it should be able to inject the needles via different angles at different sites into the tumor; it should provide the ability to fixate the tumor; and the device should provide sufficient support to make the attachment of syringes to the needles possible, without needle displacement. In veterinary patients, an intermediate of the real time image guidance may be used as described before,

consisting of the intratumoral injection of HoMS as usual. Hereafter, the patient is transported to the CT (or MRI). The tumor is scanned and the HoMS and dose distribution are modeled. Based on the modeled dosimetry retreatment of low dose areas is conducted, based on anatomical reference points.

Finally, it is interesting to investigate the most optimal tumor coverage dose and the treatment effect of intratumoral holmium treatment, during a survival study in an experimental tumor model, if a method to achieve complete tumor coverage is developed. Moreover, the possible side effects can be investigated during the survival study, using a check list with possible side effects and the microsphere shunting to other organs can be investigated over time, if the intern organs are excised directly after euthanasia. During this survival and dose escalation study, normal histopathology combined with immunohistochemistry is suggested, besides tumor size measurements, as a method to determine the treatment effect. *Ex vivo* scans with orientation markers can be used to link the tumor reaction: necrosis, apoptosis, with anti-caspase-3[113, 114] or TUNEL[115, 116], and proliferation, with Ki-67[113, 114, 117, 118]; to the dose maps throughout the tumor. For this reason *in vivo* dose maps should be made of the tumor and these should be linked to the *ex vivo* situation, with the Ministeck® plates as orientation marker. In order to be able to conduct immunohistochemistry, the formalin fixation of the tumors, should not take more than a week.[118]

Chapter 9. Nederlandse samenvatting

In dit HP report wordt eerst een algemene introductie in het gebruik van radioactieve deeltjes voor de interne radiotherapie van tumoren gegeven. Voor deze doeleinden zijn verschillende radio-isotopen gebruikt, zoals ^{90}Yttrium, ^{32}Fosfor, ^{186}Rhenium en ^{188}Rhenium, en ^{166}Holmium. Al deze radio-isotopen hebben met elkaar gemeen dat ze β-straling uitzenden en daardoor lokaal een heel hoge stralingsdosis kunnen bereiken, terwijl ze het omringende weefsel sparen, dit is een groot voordeel in vergelijking met externe bestraling. ^{166}Holmium beladen microsferen zijn ontwikkeld voor de radioembolisatie van lever tumoren. Naast deze behandeling worden deze microsferen sinds enige jaren ook experimenteel bij honden en katten met niet resecteerbare tumoren gebruikt voor intratumorale injectie, als microbrachytherapie. De resultaten van deze behandeling in honden en katten varieert sterk. Als oorzaak hiervoor komt de variërende ruimtelijke verdeling van de microsferen in het weefsel naar voren. Deze verdeling bepaalt namelijk ook de verdeling van de stralingsdosis binnen de tumor, en daarmee die van het therapeutische effect. Over de ruimtelijke verdeling van de microsferen in het tumor weefsel, was tot nu toe echter weinig bekend en daarom werd er een verdelings- en dosimetry studie opgezet. **Hoofdstuk 2**, beschrijft de opzet van deze verdelings- en dosimetry studie in Vx2 tumoren bij konijnen, waarbij de holmium verdeling binnen de tumoren op verschillende manieren in beeld gebracht wordt.

Hoofdstuk 3 beschrijft de holmium biodistributie binnen de Vx2 tumoren met behulp van MRI. Aan de hand van anatomische MRI scans kan het tumor volume ingetekend worden met behulp van het software programma ImageJ. Op gradiënt echo scans kan de holmium verdeling in beeld worden gebracht. Op deze scans is de holmium verdeling ingetekend met behulp van ImageJ en het verdelingsvolume van de microsferen is vergeleken met het tumorvolume. Daarnaast kan met behulp van de gradiënt echo scans de lokale holmium concentratie bepaald worden aan de hand van de verandering in R2* waarde van een voxel. Deze lokale holmium concentratie kan vervolgens met behulp van een dosis kernel omgezet worden in de lokale dosis. Op deze manier kan een dosis map van de tumor verkregen worden. Aan de hand van deze dosis map kan bepaald worden welke gebieden wel en niet voldoende bestraald worden en kan een algemene tumor dekking worden gegeven.

In **hoofdstuk 4** wordt de toepasbaarheid van gewone CT voor de holmium visualisatie onderzocht. Op *in situ* and *ex vivo* CT scans wordt de lokale holmium concentratie benaderd met behulp van een agarose holmium concentratie ijklijn. De lokale holmium concentratie wordt ook hier omgezet in een fictieve lokale activiteit, waarna met behulp van de dosis kernel van holmium de stralingsdosis verdeling over het weefsel onderzocht wordt. De dosis coverage van de verschillende tumoren wordt met elkaar vergeleken aan de hand van een hypothetische dosis threshold.

De ruimtelijke verdeling van de holmium microsferen is behalve met conventionele scanners ook onderzocht op micrometer niveau, met behulp van een µCT scanner, **hoofdstuk 5**. Uit de

hier verkregen data blijkt dat de microsferen de weg van de minste weerstand in het weefsel kiezen en dat het verloop van deze weg per tumor locatie verschilt. In het midden van de tumor wordt een heel uitgewaaierd patroon gezien, waarbij de microsferen over een grote afstand verspreiden, totdat de microsferen bij de rand van de tumor aankomen, waar ze lijken te worden tegen gehouden in hun expansie naar buiten en zich langs de tumorrand beginnen te verspreiden. Als microsfeer injecties meer aan de rand van de tumor worden gezet, lijken ze zich eveneens in platte lagen langs de rand van de tumor te verdelen. Indien er steekkanalen aanwezig zijn in het weefsel, dan worden deze ook vaak opgevuld met microsferen. Daarnaast is er op 3 tumoren holmium kwantificatie en dosimetry toegepast met behulp van de agar concentratie reeks en de dosis kernel voor holmium. Aangezien µCT in staat is om heel nauwkeurig de verdeling te scannen en zelfs in gebieden met een algemeen lage holmium concentratie voxels met holmium weer te geven, kan dosimetry met behulp van µCT in de toekomst heel belangrijk worden om de werkelijke dosimetry over de gehele tumor weer te geven op zeer gedetailleerd niveau.

Aangezien het verspreidingspatroon na intratumorale injectie sterk lijkt te verschillen tussen injecties, is er tevens onderzoek gedaan naar een meer gecontroleerde en gerichte toedieningstechniek, namelijk het visueel geleid toedienen van de microsferen met behulp van MRI en/of CT, **hoofdstuk 6**. Deze manier van toedienen maakt de opsporing van onbehandelde gebieden mogelijk en zorgt ervoor dat deze gebieden opnieuw behandeld kunnen worden met holmium. Dit hoofdstuk laat zien dat MRI geleid injecteren mogelijk is, maar dat het nog steeds ingewikkeld is en dat er daarom nog meer onderzoek nodig is, voordat deze imaging techniek in de praktijk toegepast kan worden. CT geleid injecteren kan worden gebruikt als een alternatief voor MRI geleid injecteren, maar heeft als grote nadeel dat het weinig weefselcontrast geeft. Als de procedure voor het beeld geleid injecteren verder is uitgewerkt, gaat dit een heel belangrijke stap in de verbetering van de holmium behandeling zijn, waarbij meer onderbouwd en gestuurd kan worden toegediend.

Naast de intratumorale verdeling in het Vx2 tumor model is ook de microsfeer verdeling in veterinair patiënten materiaal onderzocht. Twee feline linguale plaveiselcel carcinomen, behandeld met radioactief holmium intratumoraal, werden na euthanasie van de katten ook onderzocht op hun microsfeer verdeling, **hoofdstuk 7**. De microsferen lijken zich over een groot deel van de tumor verspreid te hebben. Daarnaast is op deze twee tumoren de ontwikkelde (µ)CT dosimetry toegepast, welke een aardige verdeling van de stralingsdosis door een groot gedeelte van het tumor gebied laat zien. Het voordeel van de 2 katten tumoren ten opzichte van de experimentele Vx2 tumoren is dat ze behandeld zijn, zoals veterinaire patiënten op het moment behandeld worden en humane patiënten wellicht in de toekomst behandeld zullen worden. Hierbij worden vaak grotere hoeveelheden microsferen geïnjecteerd, om een betere dosisverdeling te verkrijgen. De katten tumoren laten zien dat voor intratumorale injecties op CT gebaseerde dosimetry wellicht bruikbaarder gaat zijn dan op MRI gebaseerde dosimetry, aangezien MRI zeer veel veldverstoring laat zien voor de hoge holmium concentraties, wat kwantificatie lokaal lastig maakt.

Tot slot worden alle beeldvormingtechnieken met elkaar vergeleken en worden de mogelijkheden voor vervolg onderzoek aangewezen, **hoofdstuk 8**. µCT is met name waardevol gebleken bij het onderzoek naar de precieze verdeling van de microsferen in het weefsel. Verder is het mogelijk gebleken om de lokale stralingsdosis te berekenen aan de hand van kwantitatieve µCT. Enkele optimalisaties van op µCT gebaseerde dosisberekeningen zijn nog mogelijk, maar dit zijn enkel kleine stappen in de verbetering van het dosimetry proces. Dosimetry gebaseerd op CT en MRI kan klinisch grote relevantie hebben, aangezien beide in principe zelfs nog tijdens het behandelingsproces kunnen worden uitgevoerd. MRI dosimetry is al gevalideerd als methode, de hier ontwikkelde CT dosimetry kan daar in de toekomst aan toe worden gevoegd, waarbij op CT gebaseerde dosimetry het voordeel heeft dat het lokaal hogere concentraties kan waarnemen. Voor vervolgonderzoek wordt vooral gedacht aan het voortzetten van de opgezette distributie studie, het verder uitwerken van de beeldgeleide intratumorale holmium injecties en histologie van de tijdens deze studie onderzochte tumoren. Daarnaast kan er als er meer bekend is over de verdeling van de microsferen een dosisescalatie studie opgezet worden, waarin het effect van intratumorale injecties met radioactieve holmium microsferen onderzocht wordt.

Chapter 10. Dankwoord

Dit onderzoek is tot stand gekomen met de nodige tegenslagen, maar heeft er uiteindelijk toe geleid dat er een behandelprotocol voor de komende verdelings- en dosimetry experimenten aanwezig is. Zonder de bijdrage van velen was dit onderzoek niet mogelijk geweest en daarom wil ik graag aan iedereen die betrokken is geweest mijn blijk van waardering geven. Het is onmogelijk om iedereen bij naam te noemen, zonder mensen te vergeten, maar de volgende personen verdienen toch wat extra aandacht.

Dr. van Nimwegen, Bas, als dagelijks begeleider en ook hoofd begeleider nadat Jolle naar Amerika vertrok, had je de taak om het onderzoek in goede banen te leiden. Dit was af en toe een uitdaging, omdat het onderzoek niet altijd verliep zoals van te voren gepland. Daarnaast heb je me geholpen met mijn wetenschappelijke vorming en bekeek je mijn gemaakte werk steeds kritisch en had je goede suggesties voor verbetering.

Prof. Dr. Nijsen, Frank, als 'vader van de holmium microsferen', heb je de voortgang van dit onderzoek altijd in de gaten gehouden en af en toe belangrijke knopen doorgehakt. Daarnaast konden we op je ervaring en kennis met dierproeven vertrouwen.

Drs. Van Leeuwen, beste Bo, als er zich iemand het eerste halfjaar van dit onderzoek heeft ingezet voor een zo volledig mogelijk onderzoek, dan ben jij het en je was eigenlijk bij alle facetten van het onderzoek betrokken. We hebben samen de nodige tegenslagen te verwerken gehad, maar je inzet was eindeloos.

Prof. Dr. Kirpensteijn, ondanks dat je al vrij snel naar Amerika vertrok tijdens mijn onderzoeksperiode, ben je wel degene geweest die nauw betrokken is geweest bij het opzetten van de samenwerking met het UMC en de start van de holmium behandeling bij veterinaire patiënten, zonder deze samenwerking was mijn onderzoek niet mogelijk geweest.

Alle onderzoeksstage studenten tijdens mijn honours periode: Bert, Wouter, Sabine, Claire en Menette van het holmiumteam, bedankt voor de gezelligheid op kantoor en jullie hulp tijdens mijn onderzoek.

Onze biotechnicus Angelique Barten-Rijtbroek, je hebt ons erg geholpen tijdens de dierexperimenten en hebt daarnaast ons als studenten een beetje in de gaten gehouden.

Dr. Chris Oerlemans en Menno de Vries, we waren niet altijd even stil op kantoor, door regelmatig onderling overleg binnen het holmiumstudententeam, hopelijk hebben jullie niet te veel last van ons gehad. Daarnaast wil ik Chris bedanken voor de samenwerking binnen de tumorlijn en zijn vrijgevigheid met betrekking tot de Vx2 tumor stukjes.

Binnen dit onderzoek zijn verschillende beeldvormingtechnieken aan bod gekomen en zonder de hulp van de specialisten, was dit onderzoek niet mogelijk geweest. Dr. Peter Seevinck heeft mij en mijn voorgangers steeds geholpen met de MRI geleide experimenten

en de scanavonden tot na 12en werden langzaam berucht. Tijdens de laatste experimenten heeft Gerrit van de Maat ons steeds geholpen bij het MRI scannen van onze konijnen en tumoren en heeft ons daarnaast met zijn kennis over de verschillende beeldvormingtechnieken geholpen bij het gebruik en het ontwikkelen van dosimetry methoden voor de verschillende technieken. SPECT/CT was niet mogelijk geweest zonder de hulp van de laboranten van de nucleaire geneeskunde, waarbij we met name Nikki de Wit, Susan Tempert en John Bemelmans even in het zonnetje willen zetten, Nikki heeft vanaf het begin af aan ons geholpen met de SPECT/CT's en heeft bij haar vertrek alle kennis en protocollen fantastisch doorgegeven aan haar opvolgers. Susan bedankt bij je hulp bij het laatste konijn en de scans tussendoor. John bedankt voor het regelen en inplannen van mensen die ons wilden helpen tijdens onze experimenten.

µCT beeldvorming was niet mogelijk geweest zonder samenwerking met de Applied Molecular Imaging Erasmus MC (AMIE) Institute Rotterdam. Deze samenwerking heeft geresulteerd in een basis idee van de verdeling van de holmium microsferen na intratumorale injectie en biedt zeker mogelijkheden voor goed vervolg onderzoek en een verdere samenwerking. Speciale dank aan Joost Heack, die ons geholpen heeft met de µCT scans.

Daarnaast verdienen de mensen van de klinische fysica, en dan met name Rob van Rooij nog een extra biertje. Rob, bedankt voor al je geduld en goede uitleg, iedere keer als Jut en Jul weer langskwamen met vragen over de verschillende scans, scan instellingen en mogelijke opties voor de beeldverwerking

Wat kan het holmium team zonder alleskunner Remmert de Roos? Hij heeft ons steeds geholpen bij de bollen productie en het suspenderen van de microsferen voor behandeling en heeft altijd nog goede ideeën als je experiment in eerste instantie niet helemaal lukt. Gerard Krijger kon je altijd om advies vragen met betrekking tot het gebruik van radioactieve deeltjes en wist ervoor te zorgen dat bestelde gereedschappen steeds vlot in huis waren.

De afdeling stralingsbescherming van het UMC heeft onze SIT aanvraag met extra vaart behandeld, zodat onze eerste dierexperimenten met radioactiviteit volgens schema van start konden gaan.

In dit verslag minder aanwezig, maar wel betrokken bij het holmium onderzoek was het departement pathologie van diergeneeskunde. Speciale dank aan Rebekah Fleis-Keesler and Ronald Kisjes, voor hun hulp bij de ontwikkeling van een protocol voor toekomstige immunohistochemie op de Vx2 tumoren en de hulp tijdens de paraffine inbedding experimenten, die in dit report niet vermeld worden, maar uitgebreid beschreven staan in her verslag van Sabine.

Zonder HP commissie, geen honours programma diergeneeskunde en ik ben de leden van de commissie dankbaar dat ze mij deze kans hebben willen geven en voor het beoordelen van dit HP report

Chapter 11. References

1. Ferlay, J. *et al*. GLOBOCAN: Incidence/mortality data
. GLOBOCAN 2012 v1.0, Cancer Incidence and Mortality Worldwide: IARC CancerBase No. 11 [Internet]. Lyon, France: International Agency for Research on Cancer; 2013. Available from: http://globocan.iarc.fr, accessed on 26/05/2014.

2. Merlo, D F Rossi, L Pellegrino, C Ceppi, M Cardellino, U Capurro, C Ratto, A Sambucco, P L Sestito, V Tanara,G Bocchini, V. Cancer incidence in pet dogs: findings of the Animal Tumor Registry of Genoa, Italy. *Journal of veterinary internal medicine* 22, 976-984 (2008).

3. http://www.cancerresearchuk.org/our-research.

4. Wolinsky, Jesse Colson,Yolonda Grinstaff, Mark. Local drug delivery strategies for cancer treatment: gels, nanoparticles, polymeric films, rods, and wafers. *J. Controlled Release* 159, 14-26 (2012).

5. Brouwer, G. & Van den Eijnde, J. in *Practical radiation protection* 143 (Syntax Media, Arnhem, 2010).

6. http://www.fas.org/nuke/guide/usa/doctrine/dod/fm8-9/1ch5.htm.

7. http://w3.tue.nl/fileadmin/sbd/Documenten/Basiscursus/ALG/04-1170_Gezondheidseffecten.pdf.

8. Ho, S Lau, W Y Leung, T W Chan, M Johnson, P J Li,A K. Clinical evaluation of the partition model for estimating radiation doses from yttrium-90 microspheres in the treatment of hepatic cancer. *Eur. J. Nucl. Med.* 24, 293-298 (1997).

9. Vente, M A D Wondergem, M van der Tweel, I van den Bosch, M A A J Zonnenberg, B A Lam, M G E H van Het Schip, A D Nijsen,J F W. Yttrium-90 microsphere radioembolization for the treatment of liver malignancies: a structured meta-analysis. *Eur. Radiol.* 19, 951-959 (2009).

10. Tian, J H Xu, B X Zhang, J M Dong, B W Liang, P Wang,X D. Ultrasound-guided internal radiotherapy using yttrium-90-glass microspheres for liver malignancies. *The Journal of Nuclear Medicine* 37, 958-963 (1996).

11. Kao, Y. *et al*. Post-radioembolization yttrium-90 PET/CT - part 1: diagnostic reporting. *EJNMMI Research* 3, 56-56 (2013).

12. Carlier, T. *et al*. Assessment of acquisition protocols for routine imaging of Y-90 using PET/CT. *EJNMMI Research* 3, 11-11 (2013).

13. van Elmbt, L., Vandenberghe, S., Walrand, S., Pauwels, S. & Jamar, F. Comparison of yttrium-90 quantitative imaging by TOF and non-TOF PET in a phantom of liver selective internal radiotherapy. *Phys. Med. Biol.* 56, 6759-6777 (2011).

14. Lhommel, R. *et al*. Feasibility of 90Y TOF PET-based dosimetry in liver metastasis therapy using SIR-Spheres. *European journal of nuclear medicine and molecular imaging* 37, 1654-1662 (2010).

15. Kao, Yung-Hsiang Steinberg, Jeffrey Tay, Young-Soon Lim, Gabriel Yan, Jianhua Townsend, David Budgeon, Charley Boucek, Jan Francis, Roslyn St Cheo, Timothy Burgmans, Mark Irani, Farah Lo, Richard Tay, Kiang-Hiong Tan, Bien-Soo Chow, Pierce Satchithanantham, Somanesan Tan, Andrew Ng,David Goh, Anthony. Post-radioembolization yttrium-90 PET/CT - part 2: dose-response and tumor predictive dosimetry for resin microspheres. *EJNMMI Research* 3, 57-57 (2013).

16. Wang, S J Lin, W Y Lui, W Y Chen, M N Tsai,Z T Ting, G. Hepatic artery injection of Yttrium-90-lipiodol: biodistribution in rats with hepatoma. *The Journal of Nuclear Medicine* 37, 332-335 (1996).

17. Nijsen, J F W van het Schip, A D Hennink, W E Rook, D W van Rijk, P P de Klerk,J M H. Advances in nuclear oncology: microspheres for internal radionuclide therapy of liver tumours. *Curr. Med. Chem.* 9, 73-82 (2002).

18. Gao, Wen Liu, Lu Teng, Gao-Jun Feng, Guo-Sheng Tong,Guan-Sheng Gao, Nai-Rong. Internal radiotherapy using 32P colloid or microsphere for refractory solid tumors. *Ann. Nucl. Med.* 22, 653-660 (2008).

19. Lee, I. Enhanced tumor targeting by an intratumoral injection of colloidal chromic 32P in two human tumors (AsPC-1 pancreas and Ls174T colon) in nude mice. *J. Surg. Oncol.* 70, 161-166 (1999).

20. Gao, Wen Liu, Lu Liu, Zhi-Yong Wang, Yu Jiang,Bo Liu, Xin-Nong. Intratumoral injection of 32P-chromic phosphate in the treatment of implanted pancreatic carcinoma. *Cancer biotherapy and radiopharmaceuticals* 25, 215-224 (2010).

21. Junfeng, Y Ruping, Z Xinlan, D Xiaofeng, M Jianying, X Weiqing, H Duanzhi, Y Wei, Z Hong, X Yongxian, W Knapp,F F. Intratumoral injection with [(188)Re]rhenium sulfide suspension for treatment of transplanted human liver carcinoma in nude mice. *Nucl. Med. Biol.* 27, 347-352 (2000).

22. Wang, S J Lin, W Y Chen, M N Chi, C S Chen, J T Ho, W L Hsieh, B T Shen, L H Tsai, Z T Ting, G Mirzadeh, S Knapp,F F. Intratumoral injection of rhenium-188 microspheres into an animal model of hepatoma. *The Journal of Nuclear Medicine* 39, 1752-1757 (1998).

23. French, J T Goins, Beth Saenz, Marcela Li, Shihong Garcia Rojas, Xavier Phillips, William Otto,Randal Bao, Ande. Interventional therapy of head and neck cancer with lipid nanoparticle-carried rhenium 186 radionuclide. *Journal of vascular and interventional radiology* 21, 1271-1279 (2010).

24. Hrycushko, Brian Li, Shihong Goins, Beth Otto,Randal Bao, Ande. Direct intratumoral infusion of liposome encapsulated rhenium radionuclides for cancer therapy: effects of nonuniform intratumoral dose distribution. *Med. Phys.* 38, 1339-1347 (2011).

25. Li, Guiping Wang, Yongxian Huang, Kai Zhang, Hui Peng,Wuhe Zhang, Chunfu. The experimental study on the radioimmunotherapy of the nasopharyngeal carcinoma overexpressing HER2/neu in nude mice model with intratumoral injection of 188Re-herceptin. *Nucl. Med. Biol.* 32, 59-65 (2005).

26. Luo, Tsai-Yueh Shih, Ying-Hsia Chen, Chiung-Yu Tang, I-Chung Wu, Yu-Long Kung, Hong-Chang Lin,Wuu-Jyh Lin, Xi-Zhang. Evaluating the potential of (188)Re-ECD/lipiodol as a therapeutic radiopharmaceutical by intratumoral injection for hepatoma treatment. *Cancer biotherapy and radiopharmaceuticals* 24, 535-541 (2009).

27. Seevinck, Peter Seppenwoolde, Jan-Henry de Wit, Tim Nijsen, Johannes F W Beekman, Freek van Het Schip, Alfred D Bakker,Chris J G. Factors affecting the sensitivity and detection limits of MRI, CT, and SPECT for multimodal diagnostic and therapeutic agents. *Anti-cancer agents in medicinal chemistry* 7, 317-334 (2007).

28. Zielhuis, S W Nijsen, J F W Seppenwoolde, J H Zonnenberg, B A Bakker, C J G Hennink, W E van Rijk, P P van het Schip,A D. Lanthanide bearing microparticulate systems for multi-modality imaging and targeted therapy of cancer. *Current medicinal chemistry.Anti-cancer agents* 5, 303-313 (2005).

29. Lee, Jong Yang, Woo Lee, Min-Geol Ryu, Young Park, Jeon Shin, Kyoo-Ho Kim, Gwi Suh, Chang Seong, Jin Han, Byoung Choi, Chang Kim, Eun-Hee Kim,Kyung Park, Kyung. Effective local control of malignant melanoma by intratumoural injection of a beta-emitting radionuclide. *European journal of nuclear medicine and molecular imaging* 29, 221-230 (2002).

30. Lee, Tae-Hyung Cho, Young-Hun Lee, Jong Yang, Woo Shin,Jong Lee, Min-Geol. Enhanced antitumor effect of dendritic cell based immunotherapy after intratumoral injection of radionuclide Ho-166 against B16 melanoma. *Immunol. Lett.* 106, 19-26 (2006).

31. Kwak, Cheol Hong, Sung Seong, Seung Ryu, Jei Park,Moon Lee, Sang. Effective local control of prostate cancer by intratumoral injection of (166)Ho-chitosan complex (DW-166HC) in rats. *European journal of nuclear medicine and molecular imaging* 32, 1400-1405 (2005).

32. Kim, J. *et al*. Long-term clinical outcome of phase IIb clinical trial of percutaneous injection with holmium-166/chitosan complex (Milican) for the treatment of small hepatocellular carcinoma. *Clinical cancer research* 12, 543-548 (2006).

33. Suzuki, Y S Momose, Y Higashi, N Shigematsu, A Park, K B Kim, Y M Kim, J R Ryu,J M. Biodistribution and kinetics of holmium-166-chitosan complex (DW-166HC) in rats and mice. *The Journal of Nuclear Medicine* 39, 2161-2166 (1998).

34. Nijsen, J F Zonnenberg, B A Woittiez, J R Rook, D W Swildens-van Woudenberg, I A van Rijk, P P van het Schip,A D. Holmium-166 poly lactic acid microspheres applicable for intra-arterial radionuclide therapy of hepatic malignancies: effects of preparation and neutron activation techniques. *Eur. J. Nucl. Med.* 26, 699-704 (1999).

35. Bult, W Seevinck, P R Krijger, G C Visser, T Kroon-Batenburg, L M J Bakker, C J G Hennink, W E van het Schip, A D Nijsen,J F W. Microspheres with ultrahigh holmium content for radioablation of malignancies. *Pharm. Res.* 26, 1371-1378 (2009).

36. Bult, Wouter de Leeuw, Hendrik Steinebach, Olav van der Bom, Martijn J Wolterbeek, Hubert Heeren, Ron M A Bakker, Chris J G van Het Schip, Alfred D Hennink, Wim Nijsen,J Frank W. Radioactive holmium acetylacetonate microspheres for interstitial microbrachytherapy: an in vitro and in vivo stability study. *Pharm. Res.* 29, 827-836 (2012).

37. Zielhuis, Sander Nijsen, Johannes F W Krijger, Gerard van het Schip,Alfred D Hennink, Wim. Holmium-loaded poly(L-lactic acid) microspheres: in vitro degradation study. *Biomacromolecules* 7, 2217-2223 (2006).

38. Mumper, R J Ryo,U Y Jay, M. Neutron-activated holmium-166-poly (L-lactic acid) microspheres: a potential agent for the internal radiation therapy of hepatic tumors. *The Journal of Nuclear Medicine* 32, 2139-2143 (1991).

39. INGOLD, J A REED, G B KAPLAN, H S BAGSHAW,M A. RADIATION HEPATITIS. *Am. J. Roentgenol. Radium Ther. Nucl. Med.* 93, 200-208 (1965).

40. Smits, Maarten L J Nijsen, Johannes F W van den Bosch, Maurice A A J Lam, Marnix G E H Vente, Maarten A D Mali, Willem P T M van Het Schip,Alfred D Zonnenberg, Bernard. Holmium-166 radioembolisation in patients with unresectable, chemorefractory liver metastases (HEPAR trial): a phase 1, dose-escalation study. *Lancet oncology* 13, 1025-1034 (2012).

41. Bult, Wouter Kroeze, Stephanie G C Elschot, Mattijs Seevinck, Peter Beekman, Freek de Jong, Hugo W A M Uges, Donald R A Kosterink, Jos G W Luijten, Peter Hennink, Wim van het Schip, Alfred D Bosch, J L H Ruud Nijsen, J Frank W Jans,Judith J M. Intratumoral administration of holmium-166 acetylacetonate microspheres: antitumor efficacy and feasibility of multimodality imaging in renal cancer. *PLoS ONE* 8, e52178-e52178 (2013).

42. Bult, W. *et al*. Microbrachytherapy using holmium-166 acetylacetonate microspheres: A pilot study in a spontaneous cancer animal model. *Brachytherapy* 12, 171-177 (2013).

43. Van Nimwegen, S. A., Van Leeuwen, B. S., Nijsen, J. F. W. & Kirpensteijn, J. *Radioactive holmium (^{166}Ho) therapy for oral squamous cell carcinoma in cats & dogs* (WSAVA world congress, 2014).

44. http://www.nlm.nih.gov/cgi/mesh/2011/MB_cgi?mode=&term=SPECT.

45. Aarsvold, J. N. & Wernick, M. N. in *Emission Tomography : The Fundamentals of PET and SPECT* (Academic Press, Burlington, 2004).

46. Elschot, Mattijs Smits, Maarten L J Nijsen, Johannes F W Lam, Marnix G E H Zonnenberg, Bernard van den Bosch, Maurice A A J Viergever, Max de Jong,Hugo W A M. Quantitative Monte Carlo-based holmium-166 SPECT reconstruction. *Med. Phys.* 40, 112502-112502 (2013).

47. Nijsen, F Rook, D Brandt, C Meijer, R Dullens, H Zonnenberg, B de Klerk, J van Rijk, P Hennink,W van het Schip, F. Targeting of liver tumour in rats by selective delivery of holmium-166 loaded microspheres: a biodistribution study. *Eur. J. Nucl. Med.* 28, 743-749 (2001).

48. Gabor, T. H. in *Fundamentals of computerized tomography: Image reconstruction from projection, 2nd edition* 27-34 (Springer, London, 2009).

49. http://www.ncbi.nlm.nih.gov/mesh/68008279.

50. Seppenwoolde, Jan-Henry Nijsen, Johannes F W Bartels, Lambertus Zielhuis, Sander van Het Schip, Alfred D Bakker,Chris J G. Internal radiation therapy of liver tumors: qualitative and quantitative magnetic resonance imaging of the biodistribution of holmium-loaded microspheres in animal models. *Magnetic resonance in medicine* 53, 76-84 (2005).

51. Seevinck, P. R. *et al*. Magnetic Resonance Imaging-Based Radiation-Absorbed Dose Estimation of 166Ho Microspheres in Liver Radioembolization. *International Journal of Radiation Oncology*Biology*Physics* 83, e437-e444 (2012).

52. van de Maat, Gerrit H Seevinck, Peter Bos, Clemens Bakker,Chris J G. Quantification of holmium-166 loaded microspheres: estimating high local concentrations using a conventional multiple gradient echo sequence with Sâ,-fitting. *Journal of magnetic resonance imaging* 35, 1453-1461 (2012).

53. van de Maat, Gerrit H Seevinck, Peter Elschot, Mattijs Smits, Maarten L J de Leeuw, Hendrik van Het Schip, Alfred D Vente, Maarten A D Zonnenberg, Bernard de Jong, Hugo W A M Lam, Marnix G E H Viergever, Max van den Bosch, Maurice A A J Nijsen, Johannes F W Bakker,Chris J G. MRI-based biodistribution assessment of holmium-166 poly(L-lactic acid) microspheres after radioembolisation. *Eur. Radiol.* 23, 827-835 (2013).

54. van Es, R. J. J. The rabbit Vx2 auricle carcinoma. An animal model for development of new locoregional treatment strategies against squamous cell carcinoma of the head and neck. Chapter 1 General introduction and aim. , 1-16 (2001).

55. Kidd, J G Beard,J W Rous, P. SEROLOGICAL REACTIONS WITH A VIRUS CAUSING RABBIT PAPILLOMAS WHICH BECOME CANCEROUS : I. TESTS OF THE BLOOD OF ANIMALS CARRYING THE PAPILLOMA. *J. Exp. Med.* 64, 63-77 (1936).

56. Kidd, J. G. & Rous, P. A TRANSPLANTABLE RABBIT CARCINOMA ORIGINATING IN A VIRUS-INDUCED PAPILLOMA AND CONTAINING THE VIRUS IN MASKED OR ALTERED FORM. *J. Exp. Med.* 71, 813-838 (1940).

57. ROUS, P., KIDD, J. G. & SMITH, W. E. Experiments on the cause of the rabbit carcinomas derived from virus-induced papillomas. II. Loss by the Vx2 carcinoma of the power to immunize hosts against the papilloma virus. *J. Exp. Med.* 96, 159-174 (1952).

58. GREENE, H. S. The heterologous transplantation V-2 rabbit carcinoma. *Cancer Res.* 13, 610-612 (1953).

59. van Es, R J Dullens, H F van der Bilt, A Koole, R Slootweg,P J. Evaluation of the VX2 rabbit auricle carcinoma as a model for head and neck cancer in humans. *Journal of cranio-maxillo-facial surgery* 28, 300-307 (2000).

60. van Es, R J Franssen, O Dullens, H F Bernsen, M R Bosman, F Hennink, W E Slootweg,P J. The VX2 carcinoma in the rabbit auricle as an experimental model for intra-arterial embolization of head and neck squamous cell carcinoma with dextran microspheres. *Lab. Anim.* 33, 175-184 (1999).

61. van Es, R J Nijsen, J F van het Schip, A D Dullens, H F Slootweg,P J Koole, R. Intra-arterial embolization of head-and-neck cancer with radioactive holmium-166 poly(L-lactic acid) microspheres: an experimental study in rabbits. *International journal of oral & maxillofacial surgery* 30, 407-413 (2001).

62. van Es, R J Nijsen, J F Dullens, H F Kicken, M van der Bilt, A Hennink, W Koole, R Slootweg,P J. Tumour embolization of the Vx2 rabbit head and neck cancer model with Dextran hydrogel and Holmium-poly(L-lactic acid) microspheres: a radionuclide and histological pilot study. *Journal of cranio-maxillo-facial surgery* 29, 289-297 (2001).

63. Van Es, R J Baselmans, A H Koten, J W Van Dijk, J E Koole,R Den Otter, W. Perilesional IL-2 treatment of a VX2 head-and-neck cancer model can induce a systemic anti-tumour activity. *Anticancer Res.* 20, 4163-4170 (2000).

64. Nijsen, Johannes F W Seppenwoolde, Jan-Henry Havenith, Thomas Bos, Clemens Bakker, Chris J G van het Schip,Alfred D. Liver tumors: MR imaging of radioactive holmium microspheres--phantom and rabbit study. *Radiology* 231, 491-499 (2004).

65. Seevinck, P. R. *et al*. Quantitative 3D microCT imaging of holmium-166 microspheres in a rabbit liver tumor model after transarterial radioembolisation. , 82-100 (2009).

66. Bult, W Vente, M A D Zonnenberg, B A Van Het Schip, A D Nijsen,J F M. Microsphere radioembolization of liver malignancies: current developments. *The Quarterly journal of nuclear medicine and molecular imaging* 53, 325-335 (2009).

67. Van Nimwegen, S. A., Van Leeuwen, B. S., Reijniers, N. C. B., Nijsen, J. F. W. & Kirpensteijn, J. *Squamous cell carcinoma in cats & dogs: the multimodal approach* (ECVS/VSSO maxillofacial oncology session, 2014).

68. Brewster, S. Experimental studies on holmium therapy. Histological analysis of holmium treated tumors. (2012).

69. Zielhuis, S. W. *et al*. Surface characteristics of holmium-loaded poly(L-lactic acid) microspheres. *Biomaterials* 26, 925-932 (2005).

70. Molenbroek, W. J. Distribution of holmium-loaded microspheres after intra-tumoral injections in Vx2-tumor bearing rabbits: a pilot study. (2013).

71. Seevinck, P., Seppenwoolde, J., Zwanenburg, J. J. M., Nijsen, J. F. W. & Bakker, C. J. G. FID sampling superior to spin-echo sampling for T2*-based quantification of holmium-loaded microspheres: theory and experiment. *Magnetic resonance in medicine* 60, 1466-1476 (2008).

72. Seevinck, P. R., Bos, C. & Bakker, C. J. Ultrashort T2* relaxometry using conventional multiple gradient echo sampling with S0 fitting: validation with quantitative UTE (gUTE) imaging. (2008).

73. Konijnenberg, M. *et al*. Hepatic dosimetry for holmium-166 poly(L-lactic acid) microspheres: MIRD and beyond. *J NUCL MED MEETING ABSTRACTS* 50, 208 (2009).

74. Willems, D. Onderzoeksstage Holmiumtherapie. (2011).

75. Wasson, J., Amonoo Kuofi, K., Scrivens, J. & Pfleiderer, A. Caliper measurement to improve clinical assessment of palpable neck lumps. *Ann. R. Coll. Surg. Engl.* 94, 256-260 (2012).

76. Chen, C. *et al*. Shrinkage of head and neck cancer specimens after formalin fixation. *Journal of the Chinese Medical Association* 75, 109-113 (2012).

77. Johnson, R. E., Sigman, J. D., Funk, G. F., Robinson, R. A. & Hoffman, H. T. Quantification of surgical margin shrinkage in the oral cavity. *Head Neck* 19, 281-286 (1997).

78. Mistry, R., Qureshi, S. & Kumaran, C. Post-resection mucosal margin shrinkage in oral cancer: quantification and significance. *J. Surg. Oncol.* 91, 131-133 (2005).

79. Smits, M. L. J. *et al*. In vivo dosimetry based on SPECT and MR imaging of 166Ho-microspheres for treatment of liver malignancies. *The Journal of Nuclear Medicine* 54, 2093-2100 (2013).

80. Smits, M. L. J. *et al*. Holmium-166 radioembolization for the treatment of patients with liver metastases: design of the phase I HEPAR trial. *Journal of experimental & clinical cancer research* 29, 70-70 (2010).

81. Nakayama, Y. *et al*. Abdominal CT with low tube voltage: preliminary observations about radiation dose, contrast enhancement, image quality, and noise. *Radiology* 237, 945-951 (2005).

82. Haaga, J. R. *et al*. The effect of mAs variation upon computed tomography image quality as evaluated by in vivo and in vitro studies. *Radiology* 138, 449-454 (1981).

83. Vente, M. A. D. *et al*. Holmium-166 poly(L-lactic acid) microsphere radioembolisation of the liver: technical aspects studied in a large animal model. *Eur. Radiol.* 20, 862-869 (2010).

84. Stewart, H. in *Transplantable and transmissible tumors of animals /* , 1959).

85. http://www.pathologyatlas.ro/malignant-epithelial-tumors.php.

86. Huang, Y. *et al*. Large animal model for retroperitoneal lymphatic and lung metastasis. *Molecular Medicine Reports* 8, 1617-1622 (2013).

87. Chen, Y., Huang, A. & Lin, L. Sphere-forming-like cells (squamospheres) with cancer stem-like cell traits from VX2 rabbit buccal squamous cell carcinoma. *International journal of oral science* (2014).

88. LÃfrelius, L. E. & Stridbeck, H. Age related changes in tumor vascularity. Angiography and vascular casts of the VX2 tumor in the rabbit hind leg. *Acta radiologica.Diagnosis* 25, 529-533 (1984).

89. Qi, X., Liu, J., Burns, P. N. & Wright, G. A. The Characteristics of Vascular Growth in VX2 Tumor Measured by MRI and Micro-CT. *Journal of Oncology* 2012, 362096-362096 (2012).

90. Chauhan, V., Stylianopoulos, T., Boucher, Y. & Jain, R. Delivery of molecular and nanoscale medicine to tumors: transport barriers and strategies. *Annual review of chemical and biomolecular engineering* 2, 281-298 (2011).

91. Wang, Z. *et al*. Dynamical observation on biological progression of VX2 liver tumors to identify the optimal time for intervention in animal models. *PLoS ONE* 8, e74327-e74327 (2013).

92. Hoekstra, H. J. & Szabó, B. G. Chirurgie en intraoperatieve radiotherapie. *Ned Tijdschr Geneeskd* 135, nr 40, 1840-1844 (1991).

93. Van Dalsen, S. F. Intra-Tumoral MRI-Guided Injections With Radio-Active Holmium-166 (166HoPLLAMS). (2013).

94. Widmann, G., Schullian, P., Haidu, M., Fasser, M. & Bale, R. Targeting accuracy of CT-guided stereotaxy for radiofrequency ablation of liver tumours. *Minimally invasive therapy & allied technologies* 20, 218-225 (2011).

95. Bourrinet, P Dencausse, A Cochet, P Bromet Petit,M Chambon, C. Whole body quantitative autoradiographic study of the biodistribution of iobitridol in rats. *Invest. Radiol.* 29, 1057-1060 (1994).

96. Bourrinet, P Feldman, H Dencausse, A Chambon,C Bonnemain, B. High-performance liquid chromatographic determination of iobitridol in plasma, urine and bile. *Journal of Chromatography.B, Biomedical Applications* 670, 369-372 (1995).

97. Bourin, M Jolliet,P Ballereau, F. An overview of the clinical pharmacokinetics of x-ray contrast media. *Clin. Pharmacokinet.* 32, 180-193 (1997).

98. Holowka, S. D., Andrea. Scan-timed CT angiography in experimental arthritis: selective placement of regions of interest. *Pediatr. Radiol.* 35, 1271-1276 (2005).

99. Pannu, Harpreet Thompson, Richard Phelps, John Magee,Carolyn Fishman, Elliot. Optimal contrast agents for vascular imaging on computed tomography: iodixanol versus iohexol. *Acad. Radiol.* 12, 576-584 (2005).

100. Dencausse, A Violas, X Feldman, H Havard,P Chambon, C. Pharmacokinetic profile of iobitridol. *Acta radiologica.Supplementum* 400, 25-34 (1996).

101. Desser, T S Rubin, D L Muller, H McIntire, G L Bacon, E R Toner,J L. Blood pool and liver enhancement in CT with liposomal lodixanol: comparison with lohexol. *Acad. Radiol.* 6, 176-183 (1999).

102. Dean, P B Kivisaari,L Kormano, M. Contrast enhancement pharmacokinetics of six ionic and nonionic contrast media. *Invest. Radiol.* 18, 368-374 (1983).

103. Stewart, Errol Sun, Hongtao Chen, Xiaogang Schafer, Peter Chen, Yong Garcia,Bertha Lee, Ting-Yim. Effect of an angiogenesis inhibitor on hepatic tumor perfusion and the implications for adjuvant cytotoxic therapy. *Radiology* 264, 68-77 (2012).

104. Sun, Chang-Jin Li, Chao Yu, Jin-Ming Li, Tao Lv, Hai-Bo Luo, Yun-Xiu Huang, Jianming Wang, Guang-Hui Zhang,De-Kang Lang, Jin-Yi. Comparison of 64-slice CT perfusion imaging with contrast-enhanced CT for evaluating the target volume for three-dimensional conformal radiotherapy in the rabbit VX2 brain tumor model. *J. Radiat. Res.* 53, 454-461 (2012).

105. Morin, J P Boutelet, I Toutain, H Fillastre,J P. Pharmacokinetics and renal accumulation of three iodinated contrast agents. A comparative study of Telebrix, Hexabrix and Omnipaque in the rabbit. *Drugs Exp. Clin. Res.* 14, 679-686 (1988).

106. Dobson, J. M., Lascelles, B. D. X. & British Small Animal Veterinary Association. in *BSAVA manual of canine and feline oncology* (Gloucester British Small Animal Veterinary Association, Gloucester British Small Animal Veterinary Association 2011).

107. Stebbins, K. E., Morse, C. C. & Goldschmidt, M. H. Feline oral neoplasia: a ten-year survey. *Vet. Pathol.* 26, 121-128 (1989).

108. Northrup, N. *et al*. Outcomes of cats with oral tumors treated with mandibulectomy: 42 cases. *J. Am. Anim. Hosp. Assoc.* 42, 350-360 (2006).

109. Poirier, V., Kaser Hotz, B., Vail, D. & Straw, R. Efficacy and toxicity of an accelerated hypofractionated radiation therapy protocol in cats with oral squamous cell carcinoma. *Veterinary radiology & ultrasound* 54, 81-88 (2013).

110. Wagner, S. Benign lymph node hyperplasia and lymph node metastases in rabbits. Animal models for magnetic resonance lymphography. *Invest. Radiol.* 29, 364-371 (1994).

111. Steenbeek, I. Quantitative distribution assessment of HoAcAc microspheres and HoPLLA microspheres after direct injection. (2011).

112. Ning, S. *et al*. Intratumoral radioimmunotherapy of a human colon cancer xenograft using a sustained-release gel. *Radiotherapy and oncology* 39, 179-189 (1996).

113. Fang, F. *et al*. Mitochondrial modulation of apoptosis induced by low-dose radiation in mouse testicular cells. *Biomedical and environmental sciences* 26, 820-830 (2013).

114. Zhu, D. *et al*. Functional protection of pentoxifylline against spinal cord ischemia/reperfusion injury in rabbits: necrosis and apoptosis effects. *Chin. Med. J.* 121, 2444-2449 (2008).

115. Todd, D. *et al*. Apoptosis in renal cell carcinoma: detection by *in situ* end-labeling of fragmented DNA and correlation with other prognostic factors. *Hum. Pathol.* 27, 1012-1017 (1996).

116. https://cssportal.roche.com/LFR_PublicDocs/ras/11684795910_en_16.pdf.

117. http://www.questdiagnostics.com/testcenter/testguide.action?dc=TS_Ki-67&tabview=true.

118. Sato, M. *et al*. Optimal fixation for total preanalytic phase evaluation in pathology laboratories. A comprehensive study including immunohistochemistry, DNA, and mRNA assays. *Pathol. Int.* 64, 209-216 (2014).